Multimodal Bioinspired Artificial Skin Module for Tactile Sensing

Thiago Eustaquio Alves de Oliveira

Thesis submitted to the Faculty of Graduate and Postdoctoral Studies in partial fulfillment of the requirements for the degree of

Ph.D. in Electrical and Computer Engineering

Ottawa-Carleton Institute for Electrical and Computer Engineering

School of Electrical Engineering and Computer Science

University of Ottawa

Abstract

Tactile sensors are the last frontier to robots that can handle everyday objects and interact with humans through contact. Robots are expected to recognize the properties of objects in order to handle them safely and efficiently in a variety of applications, such as health- and elder care, manufacturing, or high-risk environments. To be effective, such sensors have to sense the geometry of touched surfaces and objects, as well as any other relevant information for their tasks, such as forces, vibrations, and temperature, that allow them to safely and securely interact within an environment. Given the capability of humans to easily capture and interpret tactile data, one promising direction in order to produce enhanced robotic tactile sensors is to explore and imitate human tactile sensing capabilities. In this context, this thesis presents the design and hardware implementation issues related to the construction of a novel multimodal bio-inspired skin module for dynamic and static tactile surface characterization. Drawing inspiration from the type, functionality, and organization of cutaneous tactile elements in the human skin, the proposed solution determines the placement of two shallow sensors (a tactile array and a nine DOF magnetic, angular rate, and gravity system) and a deep pressure sensor within a flexible compliant structure, similar to the receptive field of the Pacinian mechanoreceptor. The benefit of using a compliant structure is tri-folded. First, the module has the capability of performing touch tasks on unknown surfaces, tackling the tactile inversion problem. The compliant structure guides deforming forces from its surface to the deep pressure sensor, while keeping track of the deformation of the structure using advantageously placed shallow sensors. Second, the module's compliant structure and its embedded sensor placement provide useful data to overcome the problem of estimating non-normal forces, a significant challenge for the current generation of tactile sensing technologies. This capability allows accommodating sensing modalities essential for acquiring tactile images and classifying surfaces by vibrations and accelerations. Third, the compliant structure of the module also contributes to the relaxation of orientation constraints of end-effectors or other robotic parts carrying the module to contact surfaces of unknown objects. Issues related to the module calibration, its sensing capabilities and possible real-world applications are also presented.

Acknowledgements

First, I would like to thank God, the Almighty. I would like to address my very special thanks to my supervisors, Dr. Emil M. Petriu and Dr. Ana-Maria Cretu for their guidance and assistance throughout this research. I would like to thank my friends and colleagues from BioIn Robotics Lab for their support. Finally, I want to pay my gratitude to my parents and other family members for their priceless support and encouragement.

Table of Contents

ABSTRACT ..... **II**

ACKNOWLEDGEMENTS ..... **III**

TABLE OF CONTENTS ..... **IV**

LIST OF FIGURES ..... **VII**

LIST OF TABLES ..... **X**

LIST OF ACRONYMS ..... **XI**

CHAPTER 1 INTRODUCTION **1**

1.1 OBJECTIVES 4

1.2 RESEARCH APPROACH 7

1.3 THESIS ORGANIZATION 8

CHAPTER 2 LITERATURE REVIEW **10**

2.1 HISTORICAL PERSPECTIVE 10

2.2 USES OF TACTILE SENSORS AND TRANSDUCTION METHODS 12

2.2.1 Transduction methods and technologies for tactile sensors *13*

2.2.2 Sensors based on different physical/mechanical nature *17*

2.3 TACTILE SENSORS FROM THE POINT OF VIEW OF THE REPRESENTATION AND INTERPRETATION OF HAPTIC SIGNALS 18

2.3.1 Tactile sensing modalities *18*

2.3.2 Tactile perception *20*

2.3.3 The tactile inversion problem *20*

2.4 DYNAMIC TACTILE TASKS 22

2.4.1 Surface texture based tactile material recognition *22*

2.4.2 Object stiffness based tactile material recognition *24*

2.5 STATIC TACTILE TASKS 25

2.5.1 Local shape recognition *26*

2.5.2 Global shape perception *30*

2.6 POSE ESTIMATION VIA TOUCH SENSING 31

2.7 CONCLUDING REMARKS 33

CHAPTER 3 BIOINSPIRED ROBOTIC TOUCH SENSING **36**

3.1 PREAMBLE 36

3.2 INTRODUCTION 38

3.3 Human-Like Touch 39
3.4 Object Recognition by Static Touch 41
3.5 Surface Profile Recognition by Dynamic Touch 45
3.6 Conclusion 48

CHAPTER 4 TACTILE-ENABLED FINGERTIP FOR DYNAMIC EXPLORATION OF SURFACES 49

4.1 Preamble 49
4.2 Introduction 50
4.3 Literature Review 52
4.4 Bio-Inspired Tactile Sensor Module and Surface Characterization Experiments 56
4.4.1 Bio-Inspired MEMS Based Tactile Module 56
4.5 Experimental Setup 61
4.5.1 Experiment 1: Sensors Response to Ridged Surfaces (Grating Patterns) 62
4.5.2 Experiment 2: Surface Profile Classification 69
4.6 Conclusions 74

CHAPTER 5 BIOINSPIRED MULTIMODAL TACTILE SENSING MODULE 76

5.1 Preamble 76
5.2 Introduction 77
5.3 Literature Review 79
5.4 Bio-Inspired Tactile Sensing Module 83
5.4.1 Biological Tactile Sensing 83
5.4.2 Bio-Inspired Tactile Sensing Module Design 85
5.4.3 Study of the Compliant Structure Behavior 90
5.4.4 Comparison with Other Sensors from the Literature 93
5.5 Sensing Module fabrication (Prototyping) 94
5.6 System Components 96
5.6.1 Orientation Estimation 98
5.6.2 3D Force and Contact Points Estimation 100
5.7 Sensing Module Calibration 101
5.8 Module Characterization and Examples of Applications 103
5.9 Conclusions 106
5.10 Complementary results: End-effector approach flexibilization in a surface approximation task using a bioinspired tactile sensing module 108
5.10.1 Introduction 108
5.10.2 Experimental Apparatus and Procedure 109

5.10.3 Experimental Results and Discussion 112

5.10.4 Conclusion and Perspectives 119

CHAPTER 6 CONCLUSION 121

6.1 CONTRIBUTIONS 122

6.2 FUTURE WORK 125

REFERENCES 128

List of Figures

Figure 3-1 A dexterous humanoid robot in the BioIn Robotics laboratory at the University of Ottawa. 38
Figure 3-2 Human senses mapping on the sensory cortex (adapted from [236] and [237]). 40
Figure 3-3 Human senses mapping on the sensory cortex (adapted from [236] and [237]). 41
Figure 3-4 Cutaneous tactile sensor array and its functioning principle. 42
Figure 3-5 (a) Example of surface embossed 3D object and raw composite tactile image obtained while touch probing its surface and (b) Neural Network (NN) architecture used to recognize embossed symbols recovered in a tactile image. 42
Figure 3-6 (a) Robot finger exploring, (b) Various texture shape profiles. 46
Figure 3-7 Performance comparison for texture shape recognition with rigid versus soft finger. 48
Figure 4-1 Human skin mechanoreceptors, adapted from [6]; Pacinian corpuscle receptive field in blue; Merkel receptive field in red; and the Meissner receptive field in green. 57
Figure 4-2 (a) Tactile module: 1, pyramidal compliant structure; 2, MARG system on printed circuit board (PCB), the MARG system land grid array package is highlighted in yellow; 3, deep pressure sensor (barometer ventilation window); and 4, supporting collar. (b) Front view of the tactile probe: the MARG system is embedded under the red circle; the pressure sensor is under the yellow overlay in the black 3D printed collar. A side view of the module can be seen in Figure 4-3. 59
Figure 4-3 Sliding apparatus and gratings patterns: (a) side view of the tactile module in the beginning of the stimulation; and (b) grating patterns with a groove width varying from 2.0 mm to 3.5 mm; the depth of the grooves is 1 mm and the thickness of the ridges is 0.6 mm. 62
Figure 4-4 Robot finger composed of three motors: M1 is the “bottom” motor; M2 is the “middle” motor; and M3 is the “top” motor. The microcontroller is attached on top of Motors M1 and M2. 64
Figure 4-5 Pressure response for various groove widths of the gratings pattern: (a–c) 2 mm (31 ridges); (d–f) 2.5 mm (26 ridges); (g–i) 3.0 mm (23 ridges); and (j–m) 3.5 mm (20 ridges). 66

Figure 4-6 Frequency analysis: (a–c) deep pressure sensor data; (d–f) acceleration (x-axis); (g–i) angular velocity (y-axis); and (j–m) magnetic field (z-axis). 68
Figure 4-7 3D printed shapes: (a) Shape 2 on the top and Shape 1 on the bottom; and (b) list of shapes from Shape 1 on the top to Shape 7 on the bottom. 70
Figure 4-8 Normalized pressure samples collected over the Shapes 1 to 7; and (h) meaning of axes for the preceding plots. 71
Figure 4-9 Confusion tables for: (a) barometer, showing the misclassification of Shape 5 as Shape 4; and (b) accelerometer on x-axis, showing the misclassification between Shapes 1 and 2..... 73
Figure 5-1 Human skin mechanoreceptors, adapted from [6] and an illustration of Pacinian corpuscle receptive field. 83
Figure 5-2 Components of the tactile sensing module: 1 – Tactile array, 32 taxels; 2 – MARG (Magnetic, Angular Rate, and Gravity) system; 3 – compliant structure; 4 – barometer. 86
Figure 5-3 Force applied to the region on the center module's surface. 91
Figure 5-4 Force applied to the region out of the center module's surface. 92
Figure 5-5 Fabrication process: a) The barometer PCB is connected to a 3D printed mold (light blue); b) polyurethane (shown in orange) is cast into the mold; c) structure after degassing; d) MARG system is placed on the 3D printed mold; e) polyurethane is cast around MARG system; f) the barometer and the compliant structure are connected to the MARG system; g, h) the 3D printed mold is removed and positioning gaps are filled; i) tactile array added to the module. 95
Figure 5-6 a) Integration of the pressure sensor and MARG system; and b) tactile array added to the module. 96
Figure 5-7 System components and examples of applications. 97
Figure 5-8 Tactile module forces and orientation, fBz' denotes the scalar component of the force applied on the deep pressure sensor; LGq is the orientation estimation along the (compliance hemisphere) curvature path (dashed line); $f(ij)Az'$ is the force exerted on the taxel at row i column j. 100
Figure 5-9 Calibration setup, a) consisting of (1) a linear actuator; (2) a carriage; (3) a microcontroller; and (4) a computer. Module b) under compression and c) under tension..... 102
Figure 5-10 Force vs. sensor output. 102

Figure 5-11 Consecutive stimulations of the deep pressure sensor with different normal forces: a) intercalated sequence of 10 second stimulations; b) intercalated 0.5 second stimulations; c) increasing 3 second stimulations. 104
Figure 5-12 Deformation of the sensor module due to the contact of inclined planes with different slopes and its estimated slope angles: a) 45°; b) 30°; c) 20°; d) 10°; e) 5° and f) 2° 105
Figure 5-13 Left column shows the sensors response to tapping impact; the right column shows the sensors response when the module is in contact with the human skin over the carotid artery. 106
Figure 5-14 Experimental Setup: robotic manipulator, sensing module and explored surface. 111
Figure 5-15 End-effector and deformation of the tactile sensing module along the surface. zef and xef are the axis for the reference frame of the end effector, zsm and xsm are the axis for the reference frame of the sensing module; both relative to the base_link frame from Figure 5-14. 113
Figure 5-16 Normalized pressure output and corresponding surface and end-effector inclination. The letters from (a) – (k) represent the stimuli shown in Figure 5-15. 113
Figure 5-17 Position of the end effector during exploration. 114
Figure 5-18 Normal (in blue) and tangent (in red) vectors calculated from the pitch and contact points (green dots) at the timestamps shown in Figure 5-15 and Figure 5-16. The letters from (a) – (k) represent the stimuli shown in Figure 5-15. 116
Figure 5-19 Surface approximated using data from all 11 probing points. The green dashed line and orange segments show the cubic and linear interpolations respectively. The magenta line shows the Bézier curves that approximate the curve. 117
Figure 5-20 Surface approximated using data from 7 probing points, (points b, d, f and j were not considered in this scenario). The green dashed line and orange segments show the cubic and linear interpolations respectively. The magenta line shows the Bézier curves that approximate the curve. 118

List of Tables

Table 3-1 Performance evaluation for symbol recognition with the neural network architecture 45
Table 3-2 Performance evaluation for texture shape recognition with soft finger 47
Table 4-1 Human skin mechanoreceptors. 58
Table 4-2 LSM9DS0 and MPL115A2 frequency range and sensor resolution [257], [258], Selected M. range and Selected F. range, are the measurement range and frequency range the sensors are configured to operate at. 61
Table 4-3 Expected frequencies for different gratings and velocities. 63
Table 4-4 Root Mean Square (RMS) error for six runs of each grating. 69
Table 4-5 Classification results 72
Table 5-1 Properties and Functions of mechanoreceptors 85
Table 5-2 Sensing Modules comparison 93
Table 5-3 MARG Sensors Configuration 110
Table 5-4 Surface orientation by touch location 114

List of Acronyms

MEMS Micro-Electro-Mechanical Systems

MARG Magnetic, Angular Rate, and Gravity sensors

FEA Finite Element Analysis

FSR Force-Sensing Resistor

QTC quantum tunnelling composite

CCD Charge-coupled device

LED Light-emitting diode

FFT fast Fourier transform

PZT Lead zirconate titanate

PVDF polyvinylidene difluoride

PPS Pressure Profile Systems

MIS Minimally Invasive Surgery

LC Inductor Capacitor circuit

µMCA Maximum Covariance Analysis

WMCA Weakly paired MCA

SVM support vector machine

SOM Self-organizing map

SIFT Scale-invariant feature transform

SURF speeded up robust features

SHOT Signature of Histograms of OrienTations

LBP Local binary patterns

PCA Principal component analysis

kNN k-nearest neighbors

MLP Multilayer perceptron

RTCN Randomized Tiling Convolutional Network

ICP Iterative closest point

DOF Degrees of freedom

PCB Printed circuit board

TWI Two Wire Interface

ROS Robot Operating System

USB Universal Serial Bus

RMS Root mean square

ABS Acrylonitrile butadiene styrene

DWT Discrete wavelet transform

PVC Polyvinyl chloride

AMR Anisotropic magnetoresistance

RC resistor–capacitor circuit

MCU microcontroller unit

LSB least significant bit

Chapter 1 Introduction

In the first decades of the research on tactile sensors, industrial robots and automation were the main motivations for developments to the field. This motivation was overshadowed by the advance in the organization of factory lines and the design of structured environments favoring the use of vision-based algorithms, and thus reducing the need for tactile sensors in this context.

Nowadays robots are moving out of the factory lines and advancing towards collaborating activities, interacting with other robots and humans. There are robots emerging to work together with, or even replace, human operators performing complex dexterous manipulation operations in a variety of applications such as health- and elder-care, hazardous or high-risk environments, telemedicine, or manufacturing. In many of these new applications, there is no previous knowledge about the environment and the behavior of actors and objects within it. Constructing and validating models while actuating is a fundamental piece needed to expand the robot's role in these scenarios. Performing tasks in unstructured environments require robots to handle various types of objects, made of different materials, that can be situated out of the field of view of the robot or partially obstructed by the environment or by the robot itself.

In order to allow the construction of models for objects and environments, tactile sensing must be considered and integrated with vision and information derived from motor systems to enable robots to have more realistic and safe interactions. Tactile sensing is essential when handling objects while working on complex activities in unstructured environments. To stimulate the use of tactile sensors, improvements must be brought both to sensing technologies and to the capability of robots to make sense fast and use efficiently the sensed data.

The design of a general-purpose tactile sensing module has also to take into account the various tasks a robot may be required to perform using such a device. S*tatic tasks* may include grasping control, manipulation, and recognition of objects through one-touch exploratory movements. In this case, the transformation of the local frame of the sensing module to the frame of the object being manipulated or explored suffer little to no changes after the contact is established. In static tasks, tactile sensors can also acquire data about temperature or information about the local geometry of the object.

In *dynamic tasks*, tactile sensing differs from others sensing modalities due to the fact that it is an interactive sense. In human touch, finger movements explore objects and their surroundings, looking for tactile properties that may be close to the sensing apparatus but do not present themselves explicitly the way colors, sounds, and scents do. In such tasks, e.g., the exploration of surface profile and textures, the geometric transformation between the sensing module and an object changes after the contact is established. These changes excite the sensors and the interpretation of the resulting signals leads to a description of the contact. In dynamic touch tasks, the tactile apparatus collects data while the sensors slide over the object's surface, similar to human exploration of surfaces by lateral motion [1]. An efficient tactile sensing module must be able to perform both dynamic and static tasks.

Here we consider, following the definition of [2], tactile sensors as devices or systems that can measure objects or contact events' properties through physical contact between the sensor and the object. It is also important to explain the distinction between extrinsic and intrinsic tactile sensing. Extrinsic sensors are devices that are mounted at or near the contact interface and deal with localized regions, while intrinsic sensing refers to the derivation of contact data from force sensing within the mechanical structure of the system [2]. This thesis is centered on extrinsic tactile sensing, and while details of intrinsic designs or any other forms of force/torque sensors may be listed they are not the focus of this work. From here on, tactile sensors will refer to extrinsic sensors unless specified otherwise. It is interesting to note that the distinction between intrinsic and extrinsic tactile sensors also occurs in the human cognition system, with the part of the somatosensory and motor cortex being in charge of intrinsic sensors and another part of the same cortex being exclusively in charge of the extrinsic sensing [3], [4].

Inspired by the human tactile system and aiming at achieving similar results, the research in tactile sensors spread out the investigation over various sensor configurations with different transduction methods, materials and sensor structures. In biological tactile systems, properties of interest such as points of contact, pressure, torsion, normal and non-normal forces (stresses) are measured due to strain and changes in the topology of the network of cutaneous tactile elements (or adaptive mechanoreceptors) present in the skin and flesh of dexterous species, in particular, of human beings.

In human glabrous (hairless) skin, there are four main mechanoreceptors: Meissner corpuscles, Merkel disks, Ruffini and Pacinian corpuscles, organized in deep and shallow layers. These cells are sensitive to mechanical stimuli around the skin's surface on areas ranging from 9 to 60mm^2; these areas are named receptive fields. The receptive fields of such cells are combined and superimposed to achieve two-point discrimination of as low as 2mm on human hands [5].

All receptive fields present in the human skin are mapped (related) to the motor (i.e. skeletal), vision and balance (i.e. gravity frame – vestibular system) reference system frames [6]. Keeping track of these transformations is challenging in artificial tactile systems due to the fact that the mechanoreceptors in the human skin are embedded close to the skin surface over a highly compliant layer of flesh (muscles and fat).

The compliance provided by the flesh that supports the mechanoreceptors in the skin's tactile complex gives it the ability to deform and conform to objects. When the skin/flesh deforms, it brings more mechanoreceptors in contact with the object, gathering more data about the object's surface. Compliance also increases the overall dexterity; it relaxes control constraints, for example, tactile arrays on top of compliant structures would be able to adapt to surfaces and measure their characteristics even if the approach vector of the end-effector, or robotic limb, is not normal to the object's surface that it is approaching.

The multimodality, mechanoreceptor placement, compliance and kinematic structure of the human tactile system are a source of inspiration for this thesis. While the manner in which the biological tactile sensing data are acquired and processed might not always lead to best engineering solutions for tactile sensor design, it provides nevertheless a comprehensive, integrated framework for the design of sensors dedicated to robotic systems [5], [7], [8].

Although several efforts have been made on the development of robotic sense of touch and of related sensors that can detect multiple types of stimuli, the current generation of MEMS sensors has not yet been extensively explored while embedded in flexible materials, and in the context of multimodal sensing. Very few solutions in the literature use more than one type of sensor to collect tactile information. Moreover, the existing solutions fail to provide an integrated

approach for multimodal tactile module design, in particular for the placement of sensors within compliant structures. These are some of the issues that the current work attempts to tackle.

All the research in tactile sensing has not yet made it a “fundamental” component in robotics applications, despite the variety of commercial sensors available and the increasing number of publications reporting successful cases of tactile sensors’ use. By “fundamental” in this sentence, we mean the effective utilization of tactile sensing data in executing robot's tasks. This fact can be attributed to the challenges arising from the distributed nature of tactile sensing, from the varied spatiotemporal requirements in 3D space, and from the multiple contact parameters to be measured.

The ill-defined nature of tactile information makes tactile sensing the last frontier to robots that can handle everyday objects and interact with humans through contact. In order to ensure a safe and efficient interaction within real-world environments, tactile sensors have to sense various stimuli related to geometric properties, forces, and vibrations. To achieve such capabilities, several design aspects have to be considered [9], including sensor type, technology and placement, electronic and mechanical hardware, methods to access and acquire signals, calibration methods, algorithms to interpret sensed data in real-time and, in the case of multimodal sensors, solutions for the integration of signals from multiple sensing sources to ensure a robust interpretation of the acquired information.

1.1 Objectives

The goal of this research is to develop a general-purpose tactile sensing module capable of measuring forces, vibrations, and deformations due to contact. To do so, the module draws inspiration from the concept of the human mechanoreceptors, their functionality, the deep and shallow layers of the human skin and flesh as well as their compliance. The proposed module is thus *bioinspired*. According to Merriam-Webster dictionary [10], a “bioinspired” module is a module “inspired by or based on biological structures or processes”. It is important to state that this work doesn’t aim neither to understand in details the functionality of the human tactile systems, nor to blindly imitate the known behavior and functionality of the human skin; rather, this work aims at building an improved tactile sensing device while drawing inspiration from

known facts about the human tactile system, in particular about the placement and functionality of human tactile sensing elements (mechanoreceptors) and their compliant structure.

The term “bioinspired” is used instead of “biomimetic” or “bionic” because such terms evolved to represent devices that aim at mimicking organisms and their functions or replacing and enhancing a biological system.

The tactile sensing module design must determine the sensor placement within the compliant structure to tackle the tactile inversion problem and thus enable robots to identify and manipulate objects. The module has to be compliant so that the orientation of a robotic end-effector carrying the sensing apparatus can be relaxed when approaching unknown surfaces or obstructed objects. This is one major issue with the current generation of tactile sensors with rigid structure. In fact, most of the research in tactile sensing is focused on the implementation and use of such thin-film force sensitive arrays over rigid backing support. The field concentrated on the utilization of these sensors due to two reasons: a) force sensitive arrays can borrow many methods of image processing and apply these methods to the tactile image; and b) tactile arrays on a noncompliant structure mitigate the challenge of tracking changes on the surface of the membrane that serves as an interface between objects and transducers. Usually, the membrane that covers such transducers is thin and doesn’t over filter the tactile images collected. The advances in the use and implementation of tactile arrays did not however bring tactile sensing to the forefront of robotic applications. The main problem of these sensors is that they suffer from tight orientation constraints when approaching objects. In particular, the angles in which a robot carrying these devices approaches a surface has to be predetermined (i.e. usually normal to the surface in order to elicit maximum of tactile information possible), and tightly controlled to protect the robot itself and its surroundings. This limits the use of such sensors to structured environments and justify a continuous research effort on the development of novel sensing modules, as the one proposed in this thesis.

Similar to the mechanoreceptors in the human skin, the module can be replicated in a larger number of copies to create a “tactile surface” (artificial skin) that increases the coverage and the quantity of acquired tactile data and enabling to derive faster and more precisely surface/tasks

characteristics. Other robot parts could also be covered by similar tactile modules such that the robot can sense and react to unexpected contacts, in a similar manner to human skin. The module has to be of capable of performing both dynamic and static object exploration tasks.

Recently the field is focusing more on soft robotics where new sensing apparatus tends to prioritize flexible structures, disregarding the important advancements of tactile imaging technologies heavily used by the tactile sensor arrays. The tactile module proposed here tries to bridge this gap, by allowing for the addition of a tactile array on the surface of the module and tracking its orientation with the sensors embedded in the structure.

In this context, the work in this thesis has the following objectives:

1. The design and implementation of a novel bioinspired multimodal tactile sensing module capable of measuring forces and vibrations drawing inspiration from the mechanoreceptors present in the human skin, their placement, functionality, receptive fields, and synergetic collaboration. The sensing module must take into account the compliance of the flesh supporting the skin and its cushioning effect without disregarding the advances in the tactile sensing field when it comes to planar force sensitive arrays supported by rigid structures, i.e. it must consider the addition of a planar tactile array. The module must enable robots carrying it to perform dynamic and static tactile tasks relevant to practical applications in robotics.

2. Demonstrate the use of the tactile sensing module in dynamic tasks. In this context, we aim to demonstrate that sensors embedded deep in a compliant structure can match the performance of sensors in the literature in a grating task [11], [12] and that such sensors can be successfully used to classify tactile profiles while in movement and not constrained to fixed orientation and linear displacement.

3. Demonstrate the use of the tactile sensing module in static tasks. Regarding static tasks, In this context, we aim to illustrate the use of the module compliant structure and sensors to estimate surface orientation. The solution to the tactile inverse problem for a given sensing device should include the orientation of the surface of the sensing device, traditionally including pressure/forces and position. Surface orientation is often ignored due to the fact that most devices are rigid, or their compliant layers are not significant.

3.1. Demonstrate how a robot carrying a sensing module on its end-effector can approach a surface without significant orientation changes to its end-effector and detect the surface pitch around the contact point in one probing action.

3.2. Show how a sequence of normal and tangent vectors calculated from the pitch estimated by the module can be used to approximate a surface using Bézier curves with intermediate control points determined based on the intersection of tangent vectors. Demonstrate that the surface approximation using the orientation information is more robust with respect to the number of contact points considered when compared to the cubic and linear interpolations using only contact pressure and position. Fewer contact points lead to worse approximations in the latter case.

1.2 Research Approach

The investigation about the sensor placement, compliant structures, receptive fields, keeping track of the transformation between the surface of an elastic sensing module and a reference frame, as well as the use of a tactile sensing module with these features in static and dynamic tasks started with the work presented in [13]. In this paper, a standard *Magnetic, Angular Rate, Gravity* (MARG) MEMs system was used to identify profiles through the vibration of the kinematic chain of a robot while exploring objects with rigid and soft contact tips.

In [14] and [15], another MARG system and a barometer were embedded in a probe with a compliant structure and used in two dynamic tasks. The first experiment replicates the one used by [11], [12] to evaluate how tactile sensors in monkeys and artificial sensors perceive frequencies generated by gratings. The proposed sensing module is thus evaluated and demonstrated to be capable to perceive the gratings frequencies with errors comparable to those reported in [12]. The second experiment applied the new probe to the problem of classification of profiles using the same setup from [13]. The results show that the sensors in this probe can match the performance of other sensors in the literature, while using a much more compliant setup. The experiments in [13] were now reproduced with the sensors embedded in the elastic substrate and shown to achieve a similar performance.

In [16], the static tactile sensing task of classifying profiles and the dynamic classification of profiles using a soft tip were revisited. Feed forward neural networks were used to align and classify paterns from tactile images and to classify 3D-printed profiles from data collected during sligding motions by a robotic finger carrying the MARG system. This work helped to identify the need for a unified sensing device, capable of performing both static and dynamic tasks. One of the main challenges of combining these devices was the sensor placement, i.e. the inclusion of the force sensitive array used in the static task and the MARG and pressure sensors in a compliant structure without losing track of the array reference frame or over filtering the tactile data by placing the array under a thick compliant layer.

To accommodate the aforementioned tradeoffs, [17] presented a bioinspired design that takes into account the layers, compliance, sensor placement and the ability to perform dynamic and static tasks of the human skin. This layered design borrows the same sensing technology from [15] and [16], but solves the sensor placement problem, such that the module's shallow layers can conform to the surface of objects even if the angle of approach of an end-effector carrying the module is not normal to the target surface. The final design of the module, presented in the chapter 5 of this thesis, represents what can be thought of as a patch of artificial skin corresponding to the receptive field of the Pacinian corpuscle that encompasses the other mechanoreceptors and that can be used for the tactile characterization of surfaces. The multimodality of the patch is based not only on the presence of different sensors but also on its capability to sense pressure, surface inclination, and vibrations occurring from the interaction between module and the surface of objects. It does thus go beyond the current state of the art in tactile sensors.

1.3 Thesis Organization

This thesis is organized as follows: The second chapter provides a review of a wide range of research articles related to the work proposed in this thesis. The major focus of this chapter is to address the research problems in the current tactile sensing literature and describe the existing challenges.

Chapter 3 presents the paper [16]. It revisits works using force sensing resistor arrays and their contributions towards the resolution of the blurring effect of elastic layers and the orientation of the tactile features around the axis normal to the sensing plane. This chapter also includes the preliminary work with part of the sensors that would later be included in the module in a profile recognition task.

Chapter 4 presents the paper [15], demonstrating the use of MEMs barometer and MARG system embedded in a flexible substrate to perform the characterization of surfaces in a dynamic task and identifying tactile profiles.

The fifth chapter presents the papers [17] and [18]. It describes a novel tactile module design that attempts to combine bio-inspired concepts for receptive fields, mechanoreceptors placement and their organization in layers into a compliant structure with sensors embedded in it to tackle the tactile inversion problem with support for a force sensitive array. It also presents a demonstration of how the module can be used to estimate the angle of approach of an end-effector making contact with an unknown surface and how the surface can be approximated taking advantage of the surface orientation around contact points.

The last chapter presents a final discussion and future work that can arise from this thesis.

Chapter 2 Literature Review

2.1 Historical Perspective

Tactile sensors for robotic applications started to evolve in the 1970s, however, when compared to other sensory modalities, e.g., vision, the advances in the field had slower speed and lower inertia, with a smaller number of publications addressing the topic [19]. In its early days, the use of tactile sensors was mostly restricted to joint torques or intrinsic force sensors; such sensors were usually located within the body of robots. This was due to the fact that from the operational point of view, intrinsic tactile and vision sensors were sufficient for the structured industrial setups in which the robots where meant to operate.

Nicholls and Lee [20] show a spectrum of types of extrinsic sensing devices that appeared in the first half of the 1980s. Transduction techniques were the focus of the field during this period, and a large number of prototypes were reported in the literature. The main transduction methods utilized by these devices were resistive, capacitive, piezoelectric and pyroelectric, magnetic, and strain gauges.

The second half of the 1980s saw demonstrations of a range of sensors in laboratory setups to detect object shape, size, presence, position, forces, and temperature. Few examples of sensing of surface textures and hardness were reported. Most of the devices of this era were either of the scalar single-point contact variety or linear/rectangular arrays of sensing elements. During this period, a shift was noticed from transduction techniques to tactile applications and case studies. The design of tactile sensors and tactile sensor arrays for object recognition led the field in this period. The development of multi-fingered robotic hands increased the research interest in tactile sensors for fingertips, while the motion of arm manipulators in unstructured environments initiated the whole-body sensing efforts of the early 1990s.

During the 1990s, study cases and applications of tactile sensors continued to be developed with dynamic sensing emerging among the several tactile imaging publications. The importance of dynamic events was recognized by researchers, and many sensors were developed for detecting stress changes, slip and other temporal contact events.

The transition to the 2000s advanced the consolidation of tactile arrays technologies through the application of image processing techniques to static tactile images acquired by array sensors. Early works from the 2000s also show increasing concerns regarding practical aspects of tactile sensing, such as flexibility and conformability, stemming mainly in the field of soft robotics and the need for gentle manipulation and object exploration.

More recently, researchers started drawing inspiration from the human sense of touch [5] to build better sensing apparatus, balance its tradeoffs and create robots that can identify unknown objects and interact with their surroundings. The review presented in [5] brings design cues inspired by the human tactile sensing system to the development and enhancement of tactile arrays. Dahiya et al. [9] survey the field, analyzing devices with different transduction methods, smart materials and engineered structures, complex electronics, and the required data processing. This survey points out that the slow and elusive adoption of tactile sensors remains a contemporary reality. The authors also emphasize that, for the effective utilization of these sensors in robotic systems, the sensing units must be spread along the robot body with different 3D spatiotemporal characteristics, modular control, handling multiple simultaneous contacts. According to the authors, satisfying these requirements entails overcoming issues such as sensors placement, electronic/mechanical hardware, methods to access and acquire signals, calibration techniques, algorithms to process and interpret sensing data in real time, and above all system integration.

The advances in tactile sensors up to this point were not sufficient to make these sensors essential to industrial setups characterized by structured environments in which vision still and probably will continue to dominate. These advances may find applications in other scenarios such as rehabilitation, assistive, medical, and humanoid robots. The shift to everyday robotics also reinforces the need for whole-body tactile sensing, while manipulation tasks in unstructured environments boost the development of tactile sensors for the palm and fingertips of robots. While one design fits-all is probably not the approach that will dominate the field in the next decades, the quest for a general-purpose sensing system continues.

2.2 Uses of tactile sensors and transduction methods

Tactile sensing is vital in unstructured environment robotics. In tasks involving manipulation, tactile information is part of control parameters [21]–[24], typically involving contact point estimation, slip detection [25], surface normal and curvature estimations. The measurement of contact forces allows for grasp force control and is essential for establishing and maintaining stable grasps [26], [27]. The magnitude and direction of contact forces are critical in dexterous manipulation; they regulate the balance between normal and tangential forces allowing a manipulator to adjust its contact points to ensure grasp stability [28]. Shear information was also studied for tactile sensors in experimental setups [29], [30] and made use of Finite Element Analysis (FEA) [31], [32]. Some researchers used shear information for determining the coefficients of friction and the surface stress profile when sensors are covered by elastomers [33]. Even though most of the information about the environment and the objects being manipulated comes through the detection of normal and shear forces, e.g., shape [34]–[36], real-world interactions involving exploration in unstructured environments should also measure hardness [37], temperature [38], surface texture and surface profile [12], [39], [40].

Most sensing devices applied to the tasks referred above implemented some type of array of sensing elements usually designated as *tactels*. Arrays with *tactels* regularly distributed usually have their elements called *taxels* due to their similarities to picture elements, pixels. The authors of [5] present hints for the design of such sensing devices and identify several works that implemented sensors using these guidelines. According to the authors, the number and type of these sensors are still insufficient for complete humanoid robot applications. The authors also highlight that the interaction of robots with the environment through tactile sensors had been dominated by measurements of images representing normal static forces, while real-world interaction also involves non-normal static and dynamic forces. Most of these devices are designed in such a way that it is difficult to obtain information about friction, stickiness, texture, hardness and elasticity from the signals measured. On the other hand, these sensors achieve high applicability on classification tasks, static recognition of profiles and local features [12], [41]. Their implementation explored various modes of transduction, more specifically, resistive and piezoresistive, capacitive, optical, ultrasonic, magnetic, piezoelectric and tunnel effect. The

authors of [5], [19], [42] describe advantages and disadvantages of such transduction methods and their physical/mechanical nature, as described in the following sections.

2.2.1 Transduction methods and technologies for tactile sensors

1) *Resistive Sensors*: Tactile sensors based on resistive transducers are of two types: the ones where the resistance depends on the contact point and the others where the resistance varies according to applied forces. In many applications, these transducers are organized in arrays made of taxels. Resistive tactile sensors are sensitive and cheap but may present high power consumption depending on the materials and the area covered. The authors of [43] present a design that consists of a set of parallel continuous resistive sensing strips used to sample a sensor surface. The device is continuous in one direction and discrete in the other. The number of samples required to cover the sensor surface and connectors in the sensor circuitry is significantly reduced when compared to traditional 2D array approaches. The device can sense contact location and 2D shape. However, it cannot detect contact forces.

   A particular case of resistive sensors uses piezoresistive transducers. The resistance of these transducers changes according to force/pressure applied to the transducer. Piezoresistive sensors achieved a wide use in the form of FSRs (Force Sensing Resistors) [44], being applied to pointing and position devices such as joysticks. FSR sensors are appealing, because of their low cost, high sensitivity, low noise and simple electronics. The requirement for a rigid support and the large hysteresis are some of the drawbacks of FSRs. These transducers are usually used in 2D arrays to measure contact points and force amplitude at these points [41], [45], [46]. Tactile systems using this mode of transduction have been reported for use in anthropomorphic hands [47], [48] and are popular among the MEMS-based and silicon-based tactile sensors [49], [50].

   Commercial resistive tactile sensors can be illustrated by the products from Tekscan [51]. The company provides a wide range of gait measuring systems, including pressure mats and in-shoe foot pressure arrays. The sensing principle used in these products is based on $5mm^2$ resistive elements embedded in a large area flexible film with a thickness of 0.18mm. Tekscan's F-Scan sensing flexible sheet can be cut to fit into shoes for real-time

measurements. Donaghue and Veves [52] review other pedobarographs including some that use the same optical internal reflection principle as used in refractive index tactile sensors. FSRs are inexpensive off-the-shelf components found in many experimental tactile systems but suffer from the same issues as the F-Scan from Tekscan.

2) *Tunnel Effect Tactile Sensors*: Quantum Tunnel Composites (QTC) transducers are materials that change from a virtually perfect insulator to a metal-like conductor depending on the deformation they suffer due to compression, twist or stretch. Peratech [53], [54] developed a Quantum Tunneling Composite (QTC) material using an elastomeric matrix and nanostructured nickel powder. The particles in these powders have surfaces covered with sharp protrusions. In QTCs such particles never come into contact, they get so close that quantum tunneling (of electrons) takes place between the metal particles. A robot hand using QTC-based taxels is reported in [55]. Another highly sensitive sensor based on electron tunneling principle is reported in [39]. While effective in detecting deformations, QTC sensors by themselves cannot explain the contact event that provoked such deformations, i.e., compression, twist or stretch.
3) *Capacitive Sensors*: In robotic applications, capacitive sensors consist of two conductive plates with a dielectric layer between them. Forces applied to the sensor change the distance between the plates or their effective area and the capacitance of the transducer. Sensors based on capacitive transducers have been broadly used in robotics, from tactile arrays [56] to robotic grippers [57]. These transducers can be manufactured in small scale and allow the construction of dense arrays. An array of capacitive sensors which couples to the object through little brushes of fibers is described in [57]. The sensor taxels are reported to be very sensitive (5 mN) and robust enough not to be damaged during grasping. The authors of [56] present an 8x8 capacitive array with 1 mm^2 area and a spatial resolution at least 10 times better than the human limit of 1 mm. In [58], a capacitive sensor performs pressure measurements and collects 2D shape information about the contact between surfaces of a robot and the environment. Each sensor comprises 12 capacitive taxels in a triangular module and is supported by a flexible dielectric layer to conform to smooth curved surfaces. Capacitive sensing technology is also popular among the tactile sensors based on MEMS and

silicon micromachining [59], [56], [60], [57]. High sensitivity, stray capacity and hysteresis are the major characteristics of capacitive transducers.

The work of Gray and Fearing [56] exemplifies the level of resolution that can be achieved by tactile sensors. It reports on an 8 x 8 capacitive array that is $1mm^2$ in area. The authors claim that spatial resolution is at least 9 times better than the human limit. The sensor is intended for use in medical applications involving small manipulators, such as those employed in endoscopic surgery. The main drawback of this sensor is the presence of severe hysteresis. Even with such high resolution, these sensors did not find applications outside the medical domain.

4) *Optical Sensors*: Tactile sensors with optical transduction methods are usually of two types, namely refractive index-, and camera-based sensors. The former uses the properties of optical reflection between media of different refractive indices. Other sensors use traditional digital cameras to monitor changes in flexible structures that serve as an interface between the sensing apparatus and external objects. Reflective index sensors measure the change in light intensity when contact occurs and its relationship to contact pressure. An optical fiber-based sensor capable of measuring normal forces as low as 0.001N is reported in [61]; the sensor has a spatial resolution of 5 mm. An optical three axial sensor capable of measuring normal and shear forces is detailed in [62]. It uses a CCD camera to monitor the deformation of a cavity filled with LED (Light-Emitting Diodes) markers. Some cases of large area skin based on LEDs have also been reported in [63], [64]. Another example of an optical sensor is described in [65]; it has a 32 mm diameter, it is 60 mm long and weighs 100 g. Optical-based sensors are robust to electromagnetic interference, flexible, sensitive, and fast, but sometimes they are bulky due to the imaging equipment.
5) *Acoustic-based sensors*: Acoustic sensing is another technology used for the development of tactile sensors. In tactile setups, microphones are known to be useful for detecting contact and friction noise which are useful for the detection of slip, and texture. In [66], the authors present an array of microphones used to detect the contact point of a wooden brick falling from a manipulator into an operation bed. The authors of [67], present a microphone mounted on rod dragged by a mobile robot while it moves. The microphone is used to identify

textures of different terrains according to their acoustic signatures. In [68], a similar setup shows an artificial finger equipped with a microphone collecting frictional sound data and a system that maps the signals to the frequency domain through Fast Fourier Transform (FFT) to detect different textures.

The design presented by Shinoda and Ando [69], uses a set of ultrasonic transmitters and receivers to detect displacements as small as ten micrometers in sensing plates. In [70], the authors describe another ultrasonic sensor that uses a cross-field transmission in which the compression of an elastomer pad changes the transmission properties. The work presented in [71] uses microphones to detect variations in air pressure within cavities in a spherical silicone dome. In [67], a method for discriminating surface textures was used by a mobile robot that touched a boom-mounted microphone on the floor. The acoustic signatures from the impact allowed six-floor types to be classified with an accuracy of 98%.

6) *Magnetism-based Sensors:* Tactile sensors that use magnetic transducers measure the change in the magnetic flux caused by applied forces. These designs usually use magnets embedded in flexible substrates near sensing elements as markers. The flux measurements are performed by either Hall Effect [72], [73] or by magnetoresistive devices [74]. Tactile sensors based on magnetic phenomena have several advantages, including high sensitivity and dynamic range, linear response, and physical robustness. It is worth noting that such sensors have their usage limited to non-magnetic environments and objects.

   Li and Shida [75] present a sensor comprising of two interleaved planar spiral coils of 35mm in diameter. This multimodal structure is: 1) a capacitive sensor when external objects affect the capacitance between coils; 2) an inductor sensor when magnetic or non-magnetic materials change the frequency transfer function between the coils; and 3) a thermal sensor where one coil acts as a heater and the other as a temperature sensing resistor. The shortcomings of this sensor are the thermal time response of several seconds, the need to insulate metallic objects, and more importantly, the implicit assumption of constant applied contact pressure.

   Yamada et al. [76] deal with the problem of protecting joints of robot manipulators. In this case, a fixed skin is unsuitable since moving joints have a continuously changing surface.

Therefore, the authors used helical springs with 37 tactile sections; contact on a section causes an LC circuit to be activated, and by swept frequency scanning, all sensors can be read through a single pair of wires.

7) *Piezoelectric Sensors*: Piezoelectric materials like Lead Zirconate Titanate (PZT) and Polyvinylidene Fluoride (PVDF) generate charge/voltage proportional to the force applied to them. The use of PVDF for tactile sensing was first reported in [77], and after that, works based on PVDF or its copolymers have been proposed in the literature [78], [38]. In [79], [80], a 2×2 tactile array of (PVDF) is used to sense contact events. In this sensor, the PVDF polymer is used as a receiver to localize the contact point on a silicone rubber-sensing dome. The sensor is capable of detecting slip and surface roughness during movement. Temperature sensitivity of piezoelectric materials is the main concern for their use as tactile sensors.

Most of the sensors implemented using the transducers and technologies described above are specialized to measure one contact properties, being static pressure or forces, friction, stickiness, texture, hardness or elasticity. In these designs, the importance of dynamic contacts is acknowledged, and sensors developed for detecting stress changes, slip and other temporal contact events can be found in [57], [81]. A variety of sensors that can detect object 2D shape, size, position, and temperature are also found in the literature [2], [77], [82], [83]. According to [5], few examples of sensors that could detect surface texture [39], [40], hardness or consistency [84], [37] are reported in the literature; the same is true for sensors that can detect force and its direction [59], [72].

2.2.2 Sensors based on different physical/mechanical nature

The majority of tactile sensing devices present in the literature relies on moderately rigid materials for their construction or is covered by thin elastic layers. This is the natural development path for the field, since rigid systems are more straightforward to use and explain and have fewer variables to control and design. Observing studies about the human tactile system, some researchers have argued that softer materials may enable artificial tactile sensors able to perform closer to their biological counterparts despite their low-pass filtering behavior.

The authors of [85] examine a range of materials regarding strain energy dissipation and conformability and find that soft surfaces have more desirable properties for contact surfaces than hard materials. Touch sensors using conductive rubber as a transducer are found in [86], [87]. These sensors have compliance as one of their main advantages, and hysteresis and nonlinearity as drawbacks. In [88], the authors present a soft sensor based on a conductive gel showing a 20% change in impedance for pressure 0–400 kg/cm^2. A tactile sensor/actuator using an electrorheological gel is described in [89]; the gel changes from a fluid to a plastic solid through the application of a strong electric field. In [90], a polyelectrolyte gel is used to create a simple touch sensor based on the piezoelectric effect, capable of lighting a photodiode array according to the degree of the deformation experienced by the sensor. Despite being promising, the development of sensors using such materials is still primitive since tracking deformations on the surface of these highly compliant sensors is still challenging.

2.3 Tactile sensors from the point of view of the representation and interpretation of haptic signals

Throughout the literature, researchers approach the design of robotic tactile systems by trying to define: (1) what tactile perception consists of and (2) what implementations of general-purpose tactile sensing modules and more task-oriented tactile sensors should measure in such systems. Even though most tactile systems reported in the literature tackle the representation of touch events and tactile signals for specific experiments, sometimes with narrow applicability, the design of general-purpose tactile sensing modules can greatly benefit from the cues provided by these robotic systems. A general-purpose module can be thought as the combination of several approaches. It has to give users the possibility of representing contact events using already established methods (e.g. tactile imaging using pressure sensitive arrays) trying to enable as many representations as possible.

2.3.1 Tactile sensing modalities

Tactile perception is the process of interpreting and representing touch sensing data to examine properties of objects under mechanical interactions with the sensing apparatus. In a hierarchical view, perception is situated at a level above sensing, and provides useful, task-oriented

information for planning and control [19]. The way in which tactile sensing data is interpreted and represented is intimately associated with the kind of sensing devices used and with the tasks to be accomplished by the robot equipped with the sensors. The authors of [91], [92] and [93] categorize tactile sensors according to their coverage and spatial resolution in a similar manner to their appearance in the human body. The three types of tactile sensors are:

- **Single-point contact sensors, corresponding to single tactile cells:** This category of sensors is employed to confirm the object-sensor contact and detect forces or vibrations at the contact point. Force sensors for measuring contact forces, e.g., the ATI Nano 17 force-torque sensor and biomimetic whiskers, also known as dynamic tactile sensors, for measuring vibrations during contact are examples of this category [94]–[98].

- **High spatial resolution tactile arrays corresponding to human fingertips:** Most of the designs for tactile sensors and the related research focus on this category [9], [99]. An example of a 3×4 tactile array with sensing elements based on fiber optics can be found in [100]. More recently, the field has seen the use of MEMs barometers [101] and even embedded cameras being used as fingertip sensors [102]–[105]. There is also a number of commercial sensors available, such as: RoboTouch and DigiTacts from Pressure Profile Systems (PPS) [106], tactile arrays from Weiss Robotics [107], Tekscan tactile system [51], BioTac multimodal tactile sensors from SynTouch [108]. Most of these sensors are nonconformable planar array sensors.

- **Large-area tactile sensors corresponding to skin of human arms, back and other body parts:** Different from the high-resolution tactile arrays for fingertips, the spatial resolution is not the goal for such large-area sensors. According to [93], flexibility is one of the most important criteria for these sensors, since they may be attached to curved parts of robots. The attention to developing this category of sensors appeared in recent decades [109]–[111]. Researchers have developed this type of tactile sensors for hands [112], arms and legs [113], [114], front and back parts [115] of robots. A thorough review of large-area and flexible tactile skins can be found in [9], [116]–[118].

The tactile sensing module presented in this thesis incorporates elements from all three modalities. It makes use of a deep pressure sensor that can act as a single-point contact sensor in case of a failure of the other sensors, it considers the integration of a tactile array on the top of the compliant structure and several modules as the one proposed can be interconnected to cover a large area.

2.3.2 Tactile perception

Interpretation of tactile perception information as recuperated by tactile sensors is usually inspired by machine vision methods (where each tactile element from a regular distributed array is interpreted as an image pixel [119], [120]), inspired by biology [121], or resorts to dimensionality reduction [47], [122], [123] to render the large amount of information interpretable in a timely fashion. The interpretation of tactile data is tied to two aspects: the function of the robot and the sensor design itself. Shape, material properties, and object pose are among the main parameters that can be extracted from tactile sensing data.

Robot manipulation and grasp control [24], [124], slippage detection and prevention [125], grasp stability assessment [126], are some of the tasks where tactile information is fundamental. The applications for tactile perception systems range from Minimally Invasive Surgery (MIS) [127], to interfaces for interactive games [128], medical training simulators [129], and assisting underwater robotic operations [130]. But the advances in tactile perception still depend on the development of flexible tactile sensors, able to measure multiple modalities and to conform to external surfaces such that the sensor can acquire as much information about its surroundings as possible.

2.3.3 The tactile inversion problem

If considering sensors covered by a protective elastic layer, which provides compliance, assists in grasping tasks, and increases the robustness of the devices, the forward analysis consists of calculating the stress generated at the sensing points given the surface shape and the material properties of the elastic layer that touches the objects. On the other hand, inverse analysis

consists on the computation of changes on the surface of a compliant structure from the sensed data gathered through an elastic medium by sensing points.

Generally, the inverse analysis doesn't lead to a unique solution as there is no one-to-one correspondence between the stresses within an elastic material and those that are applied to the surface. Depending on the sensors and their arrangement, the same patterns of sensory values may be caused by many different patterns on the surface. Tactile inversion problem is a known ill-posed problem and, in many cases, cannot be solved by direct analysis. This particularly applies to form discrimination, because elastic materials act as a low pass filter, only transmitting large-scale spatial patterns and attenuating any fine detail. Nowlin [131] presents an example of the inversion problem and its ill-posed nature.

One way by which researchers try to overcome this limitation in tactile arrays is using stiff backing supports and thin elastic covers. These covers are usually engineered membranes featuring ribs, tabs or other forms of raised surface nodules, localized over the sensing elements. This technique is used by the authors of [45], to enhance the sharpness and resolution of tactile images from a 16 x 16 FSR sensing array. They also show the comparison between tabbed and uniform membrane surfaces. By keeping the nodules in the compliant overlay entirely separate, the compression of a tab is independent of the state of other tabs, thus reducing local crosstalk. It is also worth noting that in conventional FSR arrays, the sensing elements are placed to sense normal forces and cannot identify surface features more significant than a few millimeters.

Another design that uses an elastic covering with raised ribs with a force sensing array and a dynamic sensor is reported in [132]. Saad et al. [133] present a photoelastic tactile sensor that relies on the fact that the elastic layer becomes birefringent due to the stresses on its surface. The sensor recovers the phase-lead distribution and correlates it to the input force profile. The phase-lead represents how circularly-polarized input light is elliptically polarized at the output of the elastic layer. The linear relationship between force and phase-lead distribution is solved by an optimization function that may become computationally expensive depending on the size of the sensor and tasks where it is applied.

The tactile inversion problem is a major issue of compliant structures. Tactile arrays placed over flexible structures lose their coordinate frame related to the robot frame as the structure deforms, while arrays under compliant structures with stiff backing are affected by low filtering effects.

2.4 Dynamic Tactile Tasks

Contemporary and future robots require cues about the properties of objects surfaces for adequately interacting in various environments. Vision systems have been a popular tool to identify objects and materials [134]–[136]. Still, vision by itself cannot recognize or estimate mechanical parameters of a given surface material. Identifying mechanical properties of objects can only be fully accomplished through the utilization of sense of touch. Beyond shape, friction coefficients, roughness, texture, hardness, and stickiness, belong to the group of significant parameters for handling objects.

The human tactile sensing complex is highly effective in providing data and information to the somatosensory perception system. The information in this system is what enables humans to recognize objects materials properties [137]. A thorough review of the human perception of mechanical properties is presented in [138]. It is worth noting that the somatosensory system is a set of sensory neurons and pathways that react to changes at the surface of the skin and inside the human body.

In robotics, researchers have attempted to equip robots with systems that can mimic the performance of tactile sensors and of the somatosensory perception system present in humans. In dynamic tasks, these attempts can be categorized into two groups: the ones that try to identify texture-related features and the ones that focus on object stiffness.

2.4.1 Surface texture based tactile material recognition

In the literature, texture description by touch encompasses the study of friction coefficients, roughness, and microstructures of the surface of objects. These features can be extracted through a mix of sliding motions or through static contact, in the case of microstructures, between the tactile sensing device and the object being explored. One of the sensing methods

used in sliding motion procedures is the use of acoustic signals to estimate the friction of objects surfaces and recognize objects materials. This method is low-cost, since it can use traditional microphones and signal processing methods, and requires limited computational power [139]. In [94], the authors try to recognize textured surfaces through the use of Maximum Covariance Analysis (µMCA) and weakly paired MCA (WMCA) on acoustic data brought to the frequency domain by a Fourier transform. The authors of [140] classify textures from signals captured by a microphone using Self-Organizing Maps (SOMs). The use of microphones as tactile sensors has several advantages, but ambient and motor noise may depreciate the performance of such sensors.

In [141], an artificial silicone finger with embedded strain gauges and polyvinylidene fluoride films (PVDF) strips is used to collect vibration data from a sliding motion over a set of surfaces. Data collected over seven surfaces is classified in the frequency domain. The authors of [142], present a dynamic friction model, based on a 6-axis intrinsic force sensor, to determine surface physical properties while a robot finger slides along the objects surfaces with changing sliding velocities. In [143], tension sensitive conductive yarn is knitted into a fabric sensor in the form of a pile cloth. In this configuration, each yarn has many continuous loops that sense the traction between the sensor surface and external objects through the changes in its electrical resistance. The sensor is placed over a rigid aluminum fingertip and slid across three surfaces, denim, photo paper, and paper tape. The data collected is then classified from the detail components of a Discrete Wavelet Transform by an artificial neural network.

In [144] and [145], a three-axis accelerometer is attached to the end of an aluminum rod to measure the vibration originated from the interaction of the tip of the rod and surfaces. In [144] the rod is stationary, and the surfaces are placed on a turning table. In [145], the rod is attached to a mobile robot to touch the ground and identify surfaces. In [146], another three-axis accelerometer is used to classify surfaces. The sensor is attached to piece of plastic similar to a guitar pick to simulate a fingernail. The sensor is slid over a set of textures, and its data is classified by k-nearest neighbors (kNN) and support-vector machine (SVM) algorithms. Similarly, the paper [147] presents the association between contact forces and an accelerometer to classify different

surfaces. The authors of [148] add a proximity sensor to an accelerometer/normal force sensor module to enable a robot to discriminate different textures.

Some authors also refer to texture and microstructures in a surface as roughness. The authors of [149] approach object roughness estimation using a finger-pad-like sensor equipped with a strain gauge and a PVDF foil using discrete wavelet transformation. In [150], a microelectromechanical system (MEMS) tactile sensor is applied to discriminate the roughness of surfaces. In Xu et al. [151], the authors use a BioTac sensor to discriminate the roughness of 10 surfaces. The sensor measures vibrations in the skin using a liquid-filled cavity and a hydro-acoustic pressure sensor.

The microstructure present on surfaces of objects can also be used as a recognition parameter. Usually, these microstructures are measured by tactile arrays or camera-based sensors. In [104] and [152], the authors present the camera-based GelSight sensor to acquire height maps of surfaces. GelSight uses a camera on top of a piece of clear elastomer. The elastomer is coated with a reflective membrane that is pressed against surfaces and deforms assimilating surfaces nuances. The camera on the sensor records the deformation using LEDs that project different colors from different directions. These maps are treated as images to classify different surface features using visual texture analysis. TacTip, another camera-based tactile sensor, is also used to examine the surface textures in [153]. In [154] and [155], the authors use force sensitive arrays to discriminate simple textures like wood, carpet, clay, and grass.

2.4.2 Object stiffness based tactile material recognition

Stiffness or hardness is another critical object property in tactile systems and in manipulation tasks. In [156], a six-axis load cell is used to sense changes in stiffness in a balloon held between fingertips of a robotic hand. Some researchers try to estimate object softness by measuring the electrode impedance in the conductive fluid cavity of the BioTac sensor [157]–[159]. In more recent works [160], [161], the hardness of objects is also estimated by processing sequential images from a GelSight sensor. The authors of [162] also use tactile image sequences from a tactile array to classify objects into rigid and deformable. In [163], a load cell is used in a rolling probe to investigate the shear modulus, density, and stretch of silicone beds with embedded hard nodules simulating tumors. The load cell is far from the contact, and the system has no

information about the silicone beds surfaces and nodules. In [164], a set of plastic rods damped by springs are monitored by a camera and a set of markers. The system is used to examine the hardness of blocks of silicone.

In summary, the tactile systems for texture identification and hardness estimation found in the literature, with few exceptions, are implemented in such a way that requires the contact and the force driving the sensing apparatus to be normal to the surface of the object being explored. In experiments where a tactile sensor slides over a particular surface, the angle between sensor and texture is kept constant, and a linear carrier usually performs the motion. In tasks of recognition of microstructures or estimation of hardness, the sensors also approach and press the objects at a normal angle. This requirement is essential for these approaches to work, but no solution to the estimation of the approach angle can be found in the literature. Chapter 4 shows how the sensing module proposed in this thesis can be used for these tasks, and Chapter 5 presents the sensing module itself and the estimation of the approach angle as well as a surface approximation task.

2.5 Static Tactile Tasks

The concept of object shape perception is related to the capability to recognize or reconstruct the form of objects from sensors' input. The objectives of shape perception change depending on the task, from obtaining the exact contour of objects to the classification of shape components or overall profiles. The ability to achieve these goals is vital for robots to accomplish tasks such as in-hand manipulation and grasping. The skill level of a robot on planning and executing grasping trajectories, manipulation strategies and exploratory motions is directly linked to the tactile information the robot has at hand. The investigation about shape recognition has been ruled for several years by the computer vision methods [165], [166]. However, object features cannot be analyzed by cameras after manipulation starts due to occlusions by the end-effector or in scenarios where illumination is not favorable. On the other hand, shape perception through tactile sensing is not influenced by such factors; tactile sensors are meant to support robot-object interaction. The growing wave of sophisticated tactile sensors enables the fast expansion and development of algorithms to recognize object shapes via touch.

These algorithms usually focus on one of two scales, i.e., local or global. Local features can be explored by a single touch using image analysis from the data collected by tactile arrays, similar to the human cutaneous sense of touch. The global shape of an object is a contribution of both cutaneous and kinesthetic feedback; contours and curves extend beyond fingertip-size scales. In global shape perception, intrinsic sensors, i.e., joint effort and position, are used to calculate the position and orientation of a tactile equipped end-effector. The role of the tactile sensor in global shape perception tasks is to measure the forces and, if compliant, the deformations on its surface that explain that contact and help robots plan their next move.

2.5.1 Local shape recognition

Concerning the identification of local shapes, the increasing spatial resolution and temporal response of tactile arrays and the trend to interpret pressure patterns as images became more popular recently [120]. Notwithstanding the differences between camera and tactile images, several researchers have used feature descriptors from computer vision such as image moments [120], [167], to represent local geometry in tactile images. For cameras, the field of view (FoV) is open and global allowing multiple objects to be present in a single image. In cameras, several features can be extracted from a single image and collecting this image is a matter of exposing the sensor to light. On the other hand, the computational resources required to process such images are expensive, and several factors affect the extraction and description of features (i.e., scale, translation, rotation, illumination, resolution). Due to the fact that cameras are far-away sensors, scaling is produced by the distance of cameras to objects.

In tactile sensors, the FoV is local and closed since mechanical sensor-object interactions need to be made to stimulate the sensor. The tactile information carried in one reading is limited due to the resolution of such sensors. Usually, tactile sensors have low resolution when compared to conventional cameras. Furthermore, the appearance and geometry of objects cannot be expressed in a single tactile array reading. Compared to computer vision methods, it is costly to gather tactile data. Sensors, and in many cases redesigning robot components, are expensive, but on the other hand, processing tactile data requires fewer computations. In tactile images, there is no scaling effect as in computer vision, as the actual shape of an external object is

measured directly in the tactile sensor reference, whereas the impact of rotation, translation and "illumination" remains. For tactile imaging systems, the concept of illumination refers to the impressions of an object on the sensor caused by forces of different directions and magnitudes, similar to the effects of light conditions in vision systems. Tactile systems can extract object features that images cannot in many cases, e.g. surface texture [168], mechanical impedance [151] and local detailed shapes.

1) Shape descriptors for tactile object recognition: Most research works approach object shape perception by extracting features based on pressure distribution over tactile arrays and then feed these features into classifiers to recognize these objects. According to the descriptors presented in the literature, local shape recognition can be categorized as:

• Raw tactile readings as features: Raw tactile readings are used as features in [27], [169], [170]. This method is not robust against variations in positions, orientations, and contact forces. The authors of [119] concatenated the columns of a tactile array into a vector that is then used as a feature descriptor. This vector is susceptible to pose variations, and as a result, the same object may have different identities depending on its placement in the robotic gripper. The authors of [120] use a similar approach as a baseline and demonstrate that it has worse performance when compared to other methods. In [171], images of 12 taxels from iCub fingertip are taken to classify regions into edges, plane, and air.

• Statistical features: The authors of [172] used maximum, minimum and mean pressure values of each tactile reading and the position of the center of gravity in the image to form a 155-dimensional feature vector. The data from a tactile array is redundant, and an entropy-based method is used to evaluate the usefulness of features in the vector, but as a result, the system achieved a recognition rate of 60%. In [173], pressure intensity and area of contact are chosen as features to classify touch modalities. The authors of [174] estimate internal states of bottles and cans using the statistical features of the data collected by a tactile array.

• Descriptors adapted from computer vision: Image moments are used in several works as feature descriptors [120], [126], [162], [167], [175]. The image moment m_{pq} of order $p + q$ for a tactile image $f(x, y)$, can be calculated as $\mathrm{m_{pq}} = \sum_x \sum_y x^p y^q f(x, y)$; p and q indicate

the order of the moment; x and y are the horizontal and vertical positions of the taxels in the image. Usually moments of order up to 2 are used to compute descriptors like Hu's moments used in [120] and Zernike moments used in [167]. In [176], an ellipse encompassing the region of touch is approximated by the principal axis extracted from second order central moments of tactile readings. In [126], [177], image moments are used to perform stability analysis on tactile data acquired during grasp tasks. In [178], the pose of a cup handle is estimated using a Hough transform on the image collected by a tactile array mat. Hough transform and image moments are used to estimate the orientation of an edge with the goal of enabling tactile servoing in [179]. In [180], image moments, a 3D version of image moments and the average normal vector are used to assess grasp stability in manipulation tasks.

Other descriptors from computer vision and image processing also have been used on tactile images; regional descriptors are used in in [181]. The Scale Invariant Feature Transform (SIFT) was explored in [120], [182]–[184] for tactile recognition. Even though the scale invariance factor does not play a role in tactile applications, position and orientation invariance features extracted from algorithms like SIFT can be used to improve recognition performance as in the cases of applications employing Shape Context [185], SURF [186] and the 3D descriptor SHOT [187]. The authors of [188] explore the similarity between tactile and grey-scale images to generate histograms and discriminate human-robot touch patterns. The GelSight tactile sensor has a 320×240 pixels camera and enables the use of high level vision descriptors [189]. Using the GelSight sensor, the authors of [152], elaborate a multi-scale Local Binary Pattern (LBP) descriptor and use it to extract micro- and macro-structures of surfaces from tactile images.

• PCA-based features: Principal Component Analysis (PCA) can be utilized on tactile readings to find principal components (PCs) that can represent the data and be used as features. The authors of [122] project readings from a 16 x 16 resistive array onto a feature space formed by the largest eigenvectors to compute the principal components that best represent the data with lower dimensionality. In [123], the authors apply PCA to the vector $M = [x\ y\ p]^{\mathsf{T}}$ to calculate features based on the eigenvector lengths and principal axis direction to recognize local shapes. In this work, x and y represent the discrete position on the sensor plane, and p

is the pressure at x, y. In [190], kernel PCA-based features are fused to geometric features and Fourier coefficient descriptors to classify objects based on images collected by a piezoresistive tactile array. The authors of [191] apply PCA to reduce the dimensionality of the data collected by a BioTac sensor to asses grasp stability and adaptation, while in [192] and [193], PCA is applied to extract features from resistive tactile arrays to facilitate pose estimation.

• Self-organizing features: The features mentioned above are predefined to be fed into classifiers like neural networks, kNN, and SVM. Methods of this type might restrict the representativeness of the data to specific applications capturing features significant to a task, but not to others [194]. Multilayer/deep architectures methods to learn self-organizing features from sensory data have the advantage of not needing a priori set of features. In many cases, these systems can be applied to raw sensor data. The authors of [195] and [196] implemented an online generative Gaussian process model using recursive kernels to identify features in capacitive tactile arrays and classify objects. In [194] and [197], unsupervised hierarchical feature extraction using sparse coding is applied to sequences of raw, tactile images for object recognition tasks. The authors of [198] apply denoising autoencoders with a dropout function to a tactile object recognition task and observed an improvement of around 20% in the classification rate of 20 objects when compared to the performance of shallow neural networks and supervised learning. In [199], the Randomized Tiling Convolutional Network (RTCN) is used for the extraction of features for tactile recognition on datasets of tactile images collected using tactile arrays mounted on 3 robot hands. The authors of [200], propose a joint kernel sparse coding model for tactile image feature extraction and apply it to image sequences acquired using the tactile arrays mounted on a 3-finger Barrett hand. While the application of recently developed techniques in deep learning and unsupervised learning seems promising in the field of tactile sensing [201], the online application of computationally intensive processes is challenging in real-time scenarios. It is worth noting that the self-organizing features identified by these architectures not always translate to physical interpretations of the resulting model.

In the state-of-the-art literature, computer vision-based feature extractors and descriptors are broadly used for tactile object recognition, grasp stability [202], in-hand manipulation [203], contour following [171], and other tasks. More recently, the interest in applying unsupervised and deep learning architectures to extract features from raw data, especially images, has risen as demonstrated by the increasing number of algorithms and publications in the field. Different from the viewpoint in computer vision systems, the pose of the sensing apparatus in tactile sensors is critical since a small deviation in the angle between object and sensor may cause critical features to be left out of tactile images. In order to have the processing methods mentioned above applied with success in broader scenarios, the field needs advancements in compliant sensing devices capable of adapting themselves to object surfaces while tracking their orientation.

2.5.2 Global shape perception

Tactile sensing to reconstruct or recognize the global shape of objects can be categorized into two groups of methods based on: 1) contact points acquired by single-point contact force sensors; and 2) the pressure distributions in tactile arrays. “Global shape” in this context refers to contours that extend beyond the small fingertip-scale sensors. There are ainly two large categories of methods for global shape recognition:

- **Point based recognition**: Methods of this nature usually employ computer graphics techniques to fit clouds of contact points to geometric models and outline contours of the objects. In its early stages of development, researchers used this method to compensate the low resolution of tactile sensors and the dominance of single-point contact force sensors [204]–[206]. In [206], points from tactile readings are fit to super-quadric surfaces to reconstruct the sensed surface based on predefined models. Likewise, [207] presents simulations of a polyhedral model-based method for the recovery of object shapes based on the locations of contact points. The authors demonstrate the importance of surface normal estimation and its impact on the reconstruction of shapes. In [208]–[210], curvatures are described through polynomial fitting of contact points; in [211], estimation of nonparametric shapes is demonstrated using binary sensing (collision and no collision) and ergodic

exploration. These methods require a large number of points and estimate normals based on contact points that require remarkably precise robots. Some authors use the 3D spatial distribution of contact point clouds to classify objects; in [212] objects are classified through the application the Iterative Closest Point (ICP) algorithm on the 3D representations of objects from contact point clouds generated by Kalman filters. The utilization of contact only methods can be time-consuming due to the significant number of contacts required for recognizing or reconstructing the global object shape. In [213], the actuator positions of robot fingers and force values of embedded barometer sensors form the feature space to classify object classes using random forests with data acquired during a single and unplanned grasp.

• **Tactile patterns-based recognition**: Other methods use the pressure profile on tactile arrays to recognize global contact shapes based on tactile images from different contact locations. The most popular method in this category is to implement a codebook of tactile profiles and use it to classify objects similar to the Bag-of-Features (BoF) model found in [119], [120], [194]. In [119], Schneider et al. applied the BoF model to data collected by a parallel gripper equipped with two tactile arrays over a set of objects. Local features extracted from the tactile readings form a dictionary and cluster centroids are chosen as "codewords". The distance between codewords and tactile features is used to calculate a fixed length feature occurrence vector to represent an object. Implementations using this approach achieve high-performance, but the distribution of local patterns on 3D space is not taken into account. In [214], [215], series of local tactile images are concatenated to obtain a "global tactile image" using 2D correlation with the assistance of kinesthetic data. The authors of [216] expands this approach with an algorithm named Iterative Closest Labeled Point (iCLAP) that recognizes objects using both tactile and kinesthetic data.

2.6 Pose estimation via touch sensing

In-hand manipulation is the task of achieving and maintaining a specified object pose from an initial pose [217]. Computer vision methods are the most popular methods to estimate the pose of an object; but when a robot approaches an object, it may produce occlusions, rendering vision systems unreliable in close manipulation tasks. Tactile sensing methods, on the other hand, can

assist in the pose estimation in this scenario, determining the changes in the interface between the robot links and the object and its correlation to the object pose. Here, “object pose” represents the position and orientation of the object with respect to the robot end-effector or another global coordinate frame. It is worth noting that object pose perception is an essential part of object manipulation since the object's pose is the main feedback and set-point for such systems. Ideally, a robot must be able to grasp and estimate the pose of an object. Existing techniques can be categorized according to the sensing inputs as: single-point contact sensor and tactile sensing arrays.

• **Single-point contact based:** In [218], the authors present a simulation of a method for the estimation of the pose of an an object based on the angle and joint-torque of two kinematic chains that represent planar fingers. The authors of [219] propose the application of a particle filter to estimate the object pose and the hand-object configurations; simulation results are presented based on the position of seven contact sensors from the Robonaut hand. In [220], a similar approach is used to localize small buttons and snaps on fabrics and plastics that are subject to moving during manipulation. In [221]–[223], particle filters are employed to estimate the pose of objects using a 6DoF force/torque whisker and tactile arrays on parallel grippers and planar probes. The filters enable the localization, grasping and picking up of a rectangular box and a door handle.

• **Tactile sensing arrays**: Most methods for the estimation of object pose using tactile arrays assume that the object is normal to the sensing plane of the array. In [189], tactile images from the high-resolution GelSight sensor are used to build a height map using image registration to help localize objects held in a gripper. Initially, keypoints from individual images are used to build a map of the object's surface and later to estimate the rotation around the normal of the sensor plane and the translation from the center of the array. The authors of [224] used a Monte Carlo method to estimate the pose of an object from the local geometry sensed by joint position and sensors on the fingertips of a robotic hand. In [193], the authors present a method to estimate an object’s pose using pressure sensor arrays. The approach relies on PCA to calculate the covariances of the spatial and pressure data on the

sensors. Then, an optimization method is used to find a pose where the covariances of the local patches of the object's geometry match the principal components of the tactile data.

2.7 Concluding remarks

In one of the most advanced surveys of the field, the authors of [5] describe some of the characteristics of the human skin and how such features should inspire the development of tactile arrays. The authors describe the human skin as a medium in which indentations due to contact provoke stresses/strains and that are further coded as neural signals. This medium is a complex, non-homogeneous, multi-layered mechanical system supported by a deformable arrangement of muscles and fat [225].

The authors of [5] and [9] also revisit concepts from [2], [20], [77], [82], [226] to formulate basic design criteria for tactile (arrays) sensing devices of general robotic systems that can be employed in real-world environments. From these criteria for tactile arrays it is worth highlighting the following:

- Tactile sensing devices must be multimodal, thus being able to detect and measure both static and dynamic contact events. The authors point out that more than one mode of transduction may be required to meet such requirement.

- Taxels may be embedded in an elastic material similar to the manner in which mechanoreceptors of the human skin are placed in different layers of skin. The authors indicate that this criterion is a tradeoff between the blurring or filtering effects and the increase in contact resulting introduced by such materials. Flexible tactile modules have significant impact on robotic systems like prosthetics and surgical instruments where tactile skin can impact new functionalities.

- The elastic structure of the sensors should be designed to have structures that concentrate the stresses from the surface to sensing elements with the objective of lowering the blurring effect of the elastic medium. In the case of tactile arrays, textured patterns like papillary ridges on the surface of elastic layers may increase detectability [227], [228], [229]. Thin film

sensors are only a component of a complete tactile sensing system since they are usually restricted to the measurement of normal forces.

• Robotic taxels should be robust, flexible, stretchable and soft so that they can gather data about contours of objects in a way similar to the compliant human skin [63], [86], [230], [231]. In the whole-body skin context, the sensing elements should not significantly increase the diameter/thickness of robot link/parts.

• The spatial resolution for taxels should vary depending on the placement of the sensor on the robot, [3]–[5], [232]. The authors recommend a resolution of about 1mm for fingertips and 5mm for other parts of the body of the robot.

The authors of [5] consider that the requirements above are also subject to the specific robot application and should not be viewed as absolute. Manufacturing issues like the number of interconnections, hysteresis from elastic layers and the difficulties of fabricating high-resolution compliant arrays are some of the challenges that affect the implementation of such design criteria. Surface sensing over large tactile envelopes or skins is also an important research issue in the field. Dynamic envelopes are one of the central challenges in the field, as tactile sensors in these envelopes have to sense not only forces, but also changes in the envelope itself.

The authors of [9] expand the survey found in [5] by analyzing directions towards the effective design and utilization of tactile sensors. Identifying the number, placement and distribution of sensors is considered as one of the main issues to be addressed in order to assure the quality and flexibility of measurements and eventually the effectiveness of tactile data utilization. While it is quantitatively impractical to reproduce the spatial concentration of sensors of the human skin in artificial system, it is possible to approximate their performance through the implementation of algorithms like the “super–resolution” algorithm found in [233]. This method can mitigate the low resolution of low cost resistive or capacitive sensors, large size sensors, or smaller sensors placed far apart from each other by geometrically aligning, into a common reference frame images, taken from slightly different orientations obtained by actively touching the object [234]. The alignment of this method consists on applying rotation and translation operators between the data collected on overlapping locations.

It is worth noting that while the main surveys of the field [2], [5], [9], [77], [82], [226] present directions towards the placement of sensors on the surface of robots and the importance of compliant structures, they lack the description of how sensors should be placed and embedded in such compliant layers. Thus, this is one of the aspects that is studied in this thesis.

Chapter 3 Bioinspired Robotic Touch Sensing

3.1 Preamble

This chapter contains the paper “Touch Sensing for Humanoid Robots” [16]. The paper starts with a review on the human tactile sensing and perception systems and continues revisiting the development and use of a planar tactile array probe built in the *Sensing and Modeling Research Laboratory* (SMRLab) at the University of Ottawa [41], [45], [46] for an object recognition task by static touch. The application of such an array in the recognition of symbols embossed on the faces of cubes demonstrates the effectiveness of the approaches to mitigate the tactile inversion problem with two aspects worth noting here. The first one is the adoption of an elastic overlay consisting of a relatively thin membrane with protruding round tabs sitting on top of each node of the FSR matrix to provide a de facto spatial sampling. The adoption of this specially designed tabbed layer reduces the blurring effect on the sensing nodes and enables the measurement of local stresses normal to the array in each tab. The second one is the use of a neural network to align the input of the tactile array around the normal to the sensing plane. The results show that these two techniques combined can achieve high recognition rates for symbols oriented from -90° to 90° around the axis normal to the sensing plane.

These developments advanced two important factors in the application of such sensors, namely the increase in resolution for the local geometry and the alignment of tactile features around the axis normal to the sensing plane. On the other hand, the rigid structure supporting the sensing apparatus had a negative effect on the overall compliance of the system and small inclinations between array surfaces may cause sensing elements not establish contact. The tactile array cannot be used to determine the approach angles of an end-effector or a robotic link carrying it to make contact with a surface. Solving this problem requires a compliant structure serving the same conformability functionality of the flesh and fat that support the human skin while keeping track of the geometric transformation between surface and base of the structure when deformed. This is one of the aspects considered in the design of artificial skin module presented in Chapter 5.

The second part of the paper presents the initial effort of using the kinesthetic and tactile data to classify a set of profiles in a dynamic tactile sensing task. Soft and rigid fingertips were slid against 3D printed profiles using a pre-set movement and the data of sensors present in the actuators of a robotic finger and an inertial measurement unit (IMU) mounted on the fingertip was collected and fed to a neural network. The movement performed by the robot had to be prerecorded due to the fact that with intrinsic sensors there was no direct method to probe the surface and acquire its position and inclination, task usually performed in a static manner (and that will be the subject of Chapter 5 of this current thesis). The results indicated that the sensors in the IMU could achieve satisfactory results even in the case of a soft fingertip. These results inspired the placement of the sensors in the compliant structure presented in Chapter 4 and Chapter 5.

3.2 Introduction

A new generation of humanoid robots is emerging to work together with, or even replace, human operators performing complex dextrous manipulation operations in a variety of applications such as health and elder care, hazardous or high-risk environments, telemedicine, or manufacturing. To meet the challenging operational requirements of such applications, this new generation of humanoid robots should not only look as humans, but should also behave like them, being able to sense and perceive the external world and perform tasks as humans do.

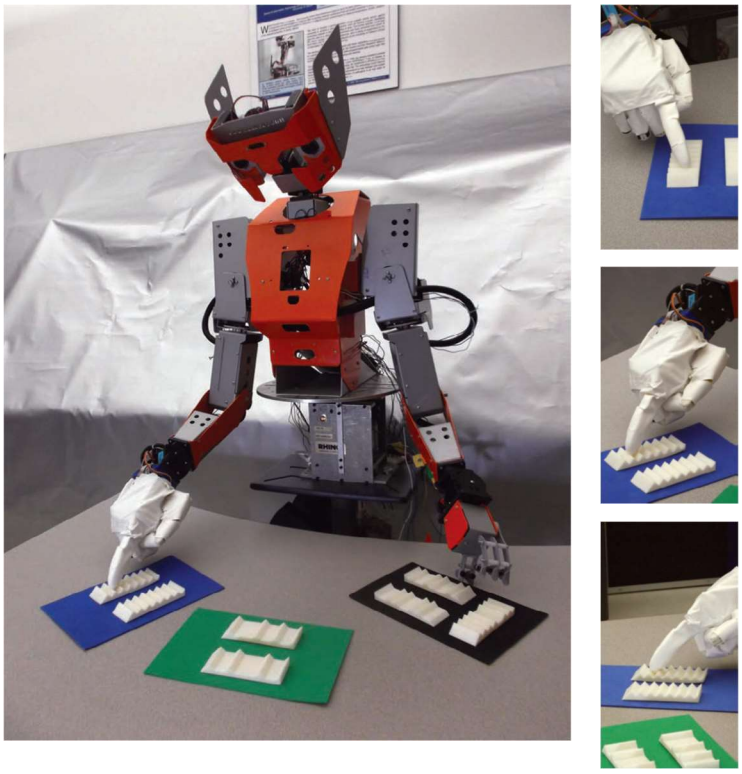

Figure 3-1 A dexterous humanoid robot in the BioIn Robotics laboratory at the University of Ottawa.

Touch sensing and perception is essential when handling objects while working on such complex activities in unstructured environments. The major challenges encountered when replicating the human touch sensing mechanisms are due to the inherently low resolution of the tactile images produced by the artificial sensors, to the complexity of interpreting the sensor data, and to the fact that robot hand technology is still clumsy when compared with the nimble dexterity of the

human hand and fingers. This paper presents practical touch sensing solutions for humanoid robots (Figure 3-1) that mimic the complex sensing mechanisms occurring in a human hand while exploring by touch 3D objects.

3.3 Human-Like Touch

It is traditionally accepted that humans have five basic senses: sight, hearing, touch, smell and taste providing sensory information about the world around them. While remarkable progress has recently been made in the development of human-like robot vision and audio sensors, as well as in that of chemical analysis instruments capable of performance similar to the human smell and taste, there is still much left to explore for the development of a robot touch sensing capability able to match that of humans.

While the cutaneous field of perception of the fingertip is quite restricted compared to vision, the human touch plays a major role, as "touch can be constructed as the most reliable of the sensor modalities. When senses conflict, touch is usually the ultimate arbiter" [235]. The main importance of the touch sensing among the five fundamental human senses is demonstrated by the large area dedicated to it on the human sensory cortex [236], as Figure 3-2 illustrates.

The development of truly performant human-like tactile sensing capability for dexterous robotic hands requires mimicking the complicated human hand's touch sensing mechanisms during the dexterous manipulation of objects. Human touch sensing and perception is the result of complex investigatory handling involving two distinct sensing components:

- cutaneous information from tactile sensors about the topology, texture, contact force, and elasticity of the touched object's surface, and
- kinaesthetic information about the position and velocity of the kinematic structure of the hand [225], [5].

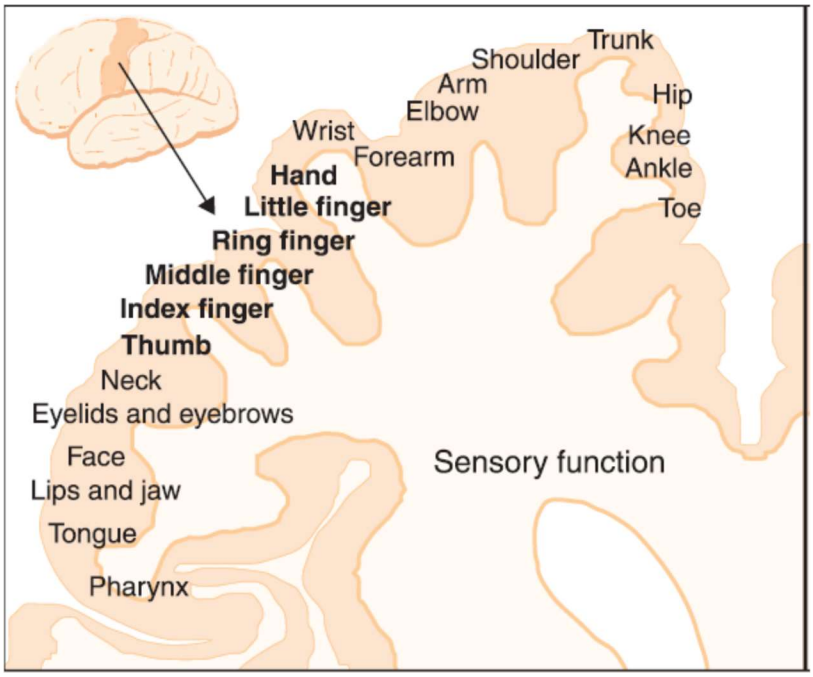

Figure 3-2 Human senses mapping on the sensory cortex (adapted from [236] *and* [237]*).*

The human hand contains four types of cutaneous sensing elements (or adaptive mechanoceptors) distributed within the skin [235]:

- Meissner's corpuscles for sensing velocity and movement across the skin and are involved in two-point discrimination;
- Merkel's disks for sensing textures and shapes during light touch or with superficial pressure application;
- Pacinian corpuscles for sensing deep pressure, pressure changes and vibrations of about 250 Hz; and
- Ruffini corpuscles for detecting skin stretch and slip during continuous touch or pressure (Figure 3-3).

Touch provides information about 3D object properties that cannot be estimated by any alternative means. Static tactile exploration predominantly consists of pressing tactile sensors against the object being explored. Temperature, hardness, and profile are some of the features that can be detected by static touch.

Beyond the tactile data provided by the sensors in the skin, the movements performed while gathering tactile data also play a significant role in the haptic object exploration. Dynamic tactile information is obtained by slipping the skin ridges on the surface of the explored objects.

Properties such as friction, smoothness, roughness, slippery, or stickiness can be hardly estimated without it [238]. It is important to note that even if the static and dynamic approaches are explored separately in what follows, they are not mutually exclusive.

3.4 Object Recognition by Static Touch

In order to improve the efficiency of robot-based manufacturing operations we have developed in the past high-accuracy tactile sensor systems for industrial robots [41], [45]. This tactile sensor array mounted on the two opposing fingers of the robot's gripper allows identifying the geometric shape of the object surface that is actually grasped and the pressure exerted by the robot gripper.

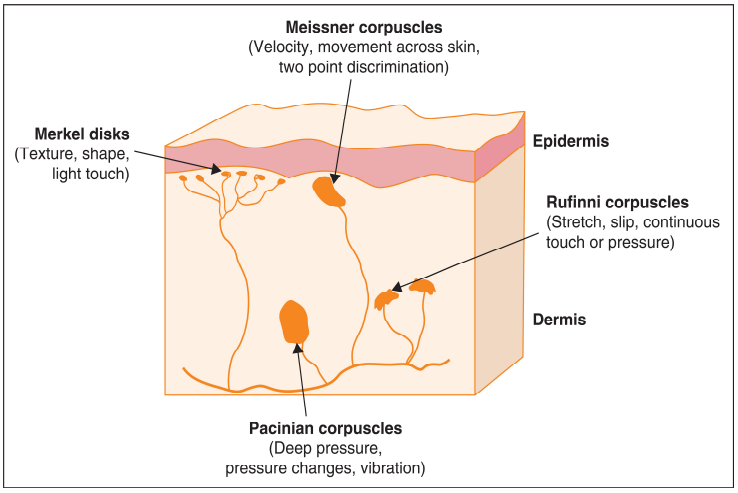

Figure 3-3 Mechanoceptors in human skin (adapted from [237].*).*

The tactile sensor array consists of a 16-by-16 matrix of force sensing resistor (FSR) piezoresistive transducers covering a 1 sq. inch area, shown in Figure 3-4a. An elastic tab-shaped "skin" covers the FSR array as illustrated in Figure 3-4b. Under the pressure exerted by an external force, the elastic skin deforms by indentation capturing the local geometric profile of the explored object surface. The applied force must be strong enough to ensure the necessary contact between the tactile probe and the explored object surface. The induced contact forces are transmitted through the elastic tabs to the FSR transducers placed on a rigid backing as shown in Figure 3-4c. As a result, the measurement data provide a tactile image of the local geometric profile of the touched object surface. The elastic overlay acts as a low-pass filter and at the same time ensures the displacement-to-force conversion that enables the tactile sensor array to quantify the profile

of the object surface being touched as shown in Figure 3-4d. Furthermore, the particular construction of this skin as a thin membrane with protruding round tabs sitting on top of each node of the matrix of FSR elements allows the elastic skin material to expand laterally without stress in the x and y directions and compress in the z direction. This special skin design significantly reduces the blurring effect inherent in one-piece monolithic elastic pads.

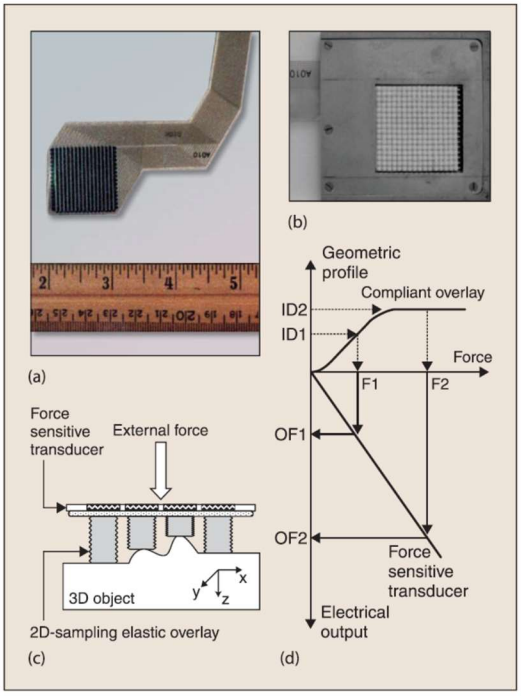

Figure 3-4 Cutaneous tactile sensor array and its functioning principle.

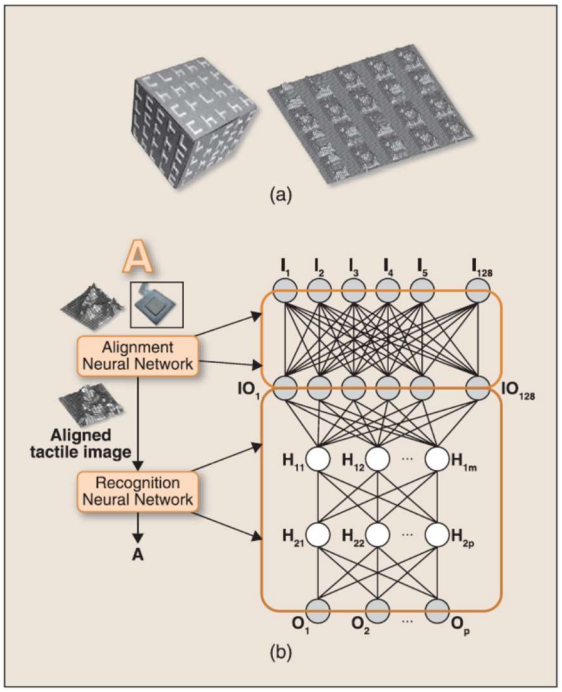

Figure 3-5 (a) Example of surface embossed 3D object and raw composite tactile image obtained while touch probing its surface and (b) Neural Network (NN) architecture used to recognize embossed symbols recovered in a tactile image.

A special 16-bit microcontroller-based interface was designed to collect and preprocess the data captured by the tactile sensor system [41]. The primary design goals were the ability to deal with the sensor's large resistance range and to avoid electrical cross-talk between the FSR matrix nodes. The interface contains two analog multiplexers; one that selects the row address and the other one the column address. The multiplexers provide random access to each individual FSR node within the tactile sensor array. The resistance of each selected node is measured by an A/D converter onboard the PIC microcontroller. The microcontroller also provides several control functions including the FSR address selection, the storage of data in memory and the serial data

communication to a computer. The tactile system output, as provided by the interface, is a 16x16 matrix of data that represents normal-displacement components of the 3D geometric profile of the surface of an object under investigation. These data can then be further used to characterize the touched object 3D profile or to blindly recognize the touched object identity.

The object surface area explored during each touch is relatively small when compared to the entire surface that has to be investigated. In view of gathering sufficient information, the robot hand equipped with the tactile array sensor has to sequentially probe the object's surface. This procedure allows to incrementally recover sufficient meaningful features for the subsequent model-based recognition of object's identity [45]. The reconstruction of the entire object shape takes then the form of a composite tactile image obtained by overlapping successive tactile images collected at each touch using a 2D cross-correlation technique.

As an example of object recognition by static touch, Figure 3-5a illustrates a 3D object having its surfaces embossed, Braille style, with four types of pseudo-random encoded symbols [46], and on the right-hand side of the figure it shows the raw composite tactile image obtained by incrementally probing the surface of the cube using the FSR array. After fusing the collected static tactile data, relevant object features can be recovered by performing basic image processing operations that will clarify the embedded shape, such as filtering and edge enhancement [45].

Neural Network (NN) clustering [41], [239], bag-of-features [120], or winged-edge model-based recognition [45] techniques are a few of the solutions employed to recognize the 3D objects based on such kind of tactile information. Among these techniques, NNs are the most compatible with the biological perception. Their inherent parallel structure and the potential for hardware implementation provide an efficient way to deal with the real-time constraint while still using real, raw noisy data as those collected by the sensors. They provide efficient solutions to recognize complex geometric profile features in composite tactile images of the touched surface of objects. NN architectures [239] as the one illustrated in Figure 3-5b allow model-based invariant recognition of various embossed symbols, such as characters (e.g., letters and numbers) or any other tactile primitive (e.g., edges) in tactile images obtained by the tactile sensor array. In order to reduce the NN complexity, the 16x16 tactile images are reduced to an 8x16 matrix (128 element vectors) by eliminating every other row in the matrix. Due to the size of the embossed

symbols with respect to the one of the round tabs on the tactile sensor array, no important information is lost because of this operation. The architecture is based on a cascade of two NNs, in which the alignment NN ensures position-invariant symbol recognition. As the symbol embedded in the raw data can be rotated, due to the positioning of the tactile sensor over its surface, the role of this bidirectional associative memory with an input and an output layer of size 128 each, is to map a possibly misaligned symbol to its aligned counterpart by scanning through the database that contains the set of possible symbols until a suitable match is found. This aligned symbol is then used as input to the symbol recognition NN whose role is to recognize it. The network has a three-layer feed-forward architecture and acts a classifier for the tactile data representing various symbols. The input layer has a size of 128, while the size of the hidden layer and the output layers can be varied to adapt to the specific datasets of symbols to be recognized. The scaled conjugate gradient back-propagation algorithm is used to train the network over tactile images representing various symbols in their raw, noisy format obtained by measurement, but also a variety of tactile images obtained from this raw data by processing it with different filters as well as by removing noise and enhancing edges. For the recognition of the four embossed symbols, the three-layer feedforward architecture contains 6 and 4 hidden neurons respectively in the first and second layer, and 4 neurons in the output layer.

Table 3-1 shows in the first row the performance of the network to recognize the four symbols with variations from -90° to 90° with respect to the straight position. In order to classify the 10 digits, the feed-forward architecture is based on 15 neurons in the first hidden layer, 10 in the second one and 10 outputs, each corresponding to one identified digit. The second row illustrates the recognition rate for the digits, for rotation variations between -90° to 90°. The related misclassifications are justified because when comparing a rotated 6 with a 9 or an 8 with a 9, the difference between them is not clear, especially if data is noisy. Finally, the third row of the table shows the results obtained for the recognition of the letters of the alphabet using a similar architecture to the one for the recognition of digits, but with 50 neurons in the first layer and 25 in the second one. Data is not available for the letter W, therefore the results are presented for the other 25 letters, for rotation variations between -90° to 90°. The misclassification affects

solely the letters X and V. An overall recognition rate of 94.9% is obtained over these three datasets.

Table 3-1 Performance evaluation for symbol recognition with the neural network architecture

Dataset	Average recognition rate	Comments
Embossed cube symbols (4 symbols)	96%	The symbol "reverse T" is misclassified as an "h" in 2 of 14 cases
Digits from 0 to 9 (10 symbols)	92.9%	The digit 8 is misclassified as a 6 in 2 out of 14 cases
Embossed alphabet letters A to Z (25 symbols)	96%	The letter "V" is misclassified as an "X" in 4 cases

These experimental scenarios illustrate quite convincingly the efficiency of the discussed tactile sensor array and Neural Network techniques for the recovery of meaningful geometric features on the 3D object surfaces explored by the robot hand. These features are then further used as primitives for model-based recognition of the explored objects.

Several issues remain nevertheless open for further research, such as the impact of the number of sensors to be used on the robot hand, their placement, and specific sensor data integration in view of a more reliable collection of only relevant data instead of proceeding by an exhaustive exploration of a surface.

3.5 Surface Profile Recognition by Dynamic Touch

While previously unused by the industrial robots, the dynamic touch is nevertheless an essential feature for multi-finger hands of the new generation humanoid robots. This function emulates the human hand's sliding motion, a repetitive rubbing movement that is most often associated with friction, slippery, adherent, texture or profile identification. In such exploration, it is important to consider both movements and sensors response.

In order to study the dynamic tactile sensing while a fingertip slides over the object surface, we used the experimental set-up, shown in Figure 3-6. This experiment serves as basis for a data-driven analysis of the sensor selection for the contour following for shape discrimination task. Looking for solutions that are better suited for different applications we studied the effect of different profile shapes, as shown in Figure 3-6b, and of using soft and rigid fingertips, on the

dynamic response of the sensors that equip the finger's actuators [13]. The rigid fingertip was made entirely from ABS while the soft one has an ABS base and a smooth core and tip. A pre-set finger-movement pattern was repeated 100 times for the tactile exploration of each texture shape. Sensor data were continuously collected from all finger's motors while the finger dynamically explored these shapes. The data analyzed comprised accelerations, velocities, positions and loads from the motors, data from an inertial measurement unit (IMU), consisting of an accelerometer and a gyroscope, and a magnetometer. From all these sensor data, 25 sets were then randomly chosen for each of the 7 texture profiles and further processed. Principal Component Analysis (PCA) is used in order to reduce the dimensionality of the multimodal sensor data. The resulting feature vectors are then presented to a two-layer perceptron feed-forward NN with 10 neurons in the hidden layer and 7 at output and trained with scaled gradient backpropagation which performs the pattern recognition on these sensor data. Table 3-2 shows classification results for the 175 sets of data collected from the four motor torque sensors when the NN classifier uses 90% of PCA information.

The misclassification of Shape 1 and 2 is not difficult to understand as the textures resemble quite a lot as shown in Figure 3-6b, Shape 2 is a little sharper than Shape 1.

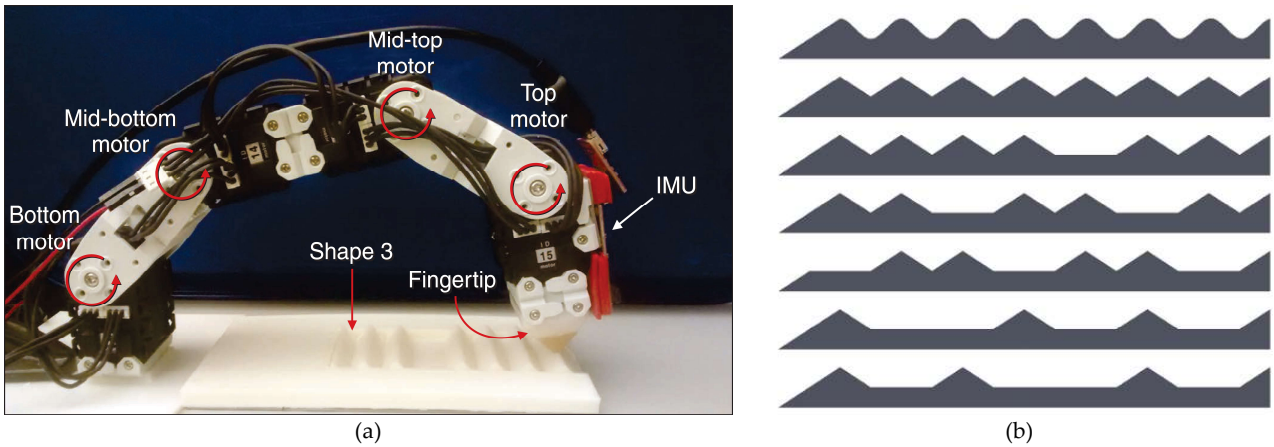

(a) (b)

Figure 3-6 (a) Robot finger exploring, (b) Various texture shape profiles.

Figure 3-7 considers a scenario where sensors are prone to noise. In this case, PCA information is reduced to 60%, the less important principal components are eliminated and only the most representative are considered. Results provided in this figure illustrate the variation of classification rate as function of the fingertip material (e.g., soft versus rigid) as well as on the

type of sensor considered. The difference in performance for soft and rigid fingertips, as well as the change in the sensor's response, is due to the compliance difference between the two fingertips. When compared to rigid fingertips, soft ones have higher compliance, leading to amplitude attenuation in most signals.

The sharper features that arise from the rigid tip touch affect the bottom motor so that the recognition rate for all motors achieves 96.6%, the highest when compared to the other sensor combinations. The compliance of the soft fingertip increases the importance of the motors closer to the interaction (e.g. closer to the top motor showm in Figure 3-6a) with recognition rates from 85.1% for rigid tip to 99.1% for soft fingertip.

Table 3-2 Performance evaluation for texture shape recognition with soft finger

Data Source	**Average recognition rate**	**Comments**
Four motor sensors	96%	• Shape 2 is misclassified as Shape 1 in 1 out of 25 cases • Shape 2 is misclassified as Shape 6 in 1 case • Shape 2 is misclassified as Shape 6 in 2 cases • Shape 2 is misclassified as Shape 1 in 2 cases
Magnetometer (x, y, z)	98.9%	• Shape 5 is misclassified as Shape 4 in 1 case out of 25 • Shape 7 is misclassified as Shape 6 in 1 case
Load on top motor	93.1%	• Shape 1 is misclassified as Shape 2 in 2 cases, as Shape 3 in 2 cases and as Shape 4 in 2 cases • Shape 3 is misclassified as Shape 1 in 1 case • Shape 7 is misclassified as Shape 5 in 1 case and as Shape 6 in 4 cases

Regarding the performance of the IMU sensors, it has been noted that the gyroscope performed poorly because of the vibrations caused by the other motors, the accelerometer was consistent in both cases, and the magnetometer follows the load variations, specifically of the load in the last actuator. This is an interesting case where the magnetometer measures the intensity and direction of the magnetic field generated by the actuation of the top motor and outperforms other IMU sensors.

This experiment shows that tactile and kinaesthetic information can also be used to recognize shapes from dynamic movements. Several aspects that remain to be studied in this context are related to the dynamic movement are the sensors' placement, the impact of active motor compliance over tactile data and the response of the system to softer fingertips. Recurrent NN architectures, such as the Long Short-Term Memory (LSTM), could also be a viable recognition

tool in dynamic touch tasks since they are particularly well suited for sequential data learning, the main challenge for this approach being the multi-modality nature inherent to tactile data.

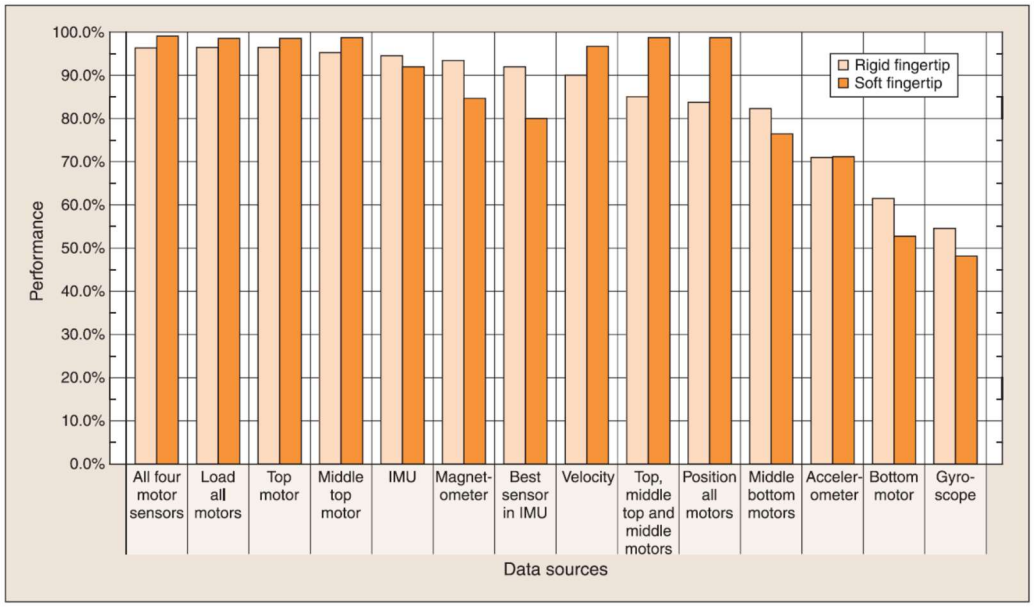

Figure 3-7 Performance comparison for texture shape recognition with rigid versus soft finger.

3.6 Conclusion

A human-like touch and feel ability is still a major challenge yet to be solved in order to accelerate robot's transition from performing routine, preplanned, tasks in structured industrial environments to creatively performing tasks in unstructured environments such as nuclear stations, war zones, underwater, outer space, health- and elder-care, or telemedicine. Due to those unsolved challenges encountered in the development of a truly human-like touch sensing and perception capability for humanoid robot hands, considerable effort is still required before achieving the point of replicating the human hand's abilities by a multi-finger robot hand able to efficiently carry on dexterous robotic manipulation operations. All these challenges provide a strong incentive for using the bio-inspired approaches to develop efficient static and dynamic touch sensing technologies for the new generation of humanoid robots.

Chapter 4 Tactile-enabled fingertip for dynamic exploration of surfaces

4.1 Preamble

This chapter presents the contents of the paper “Multimodal Bio-Inspired Tactile Sensing Module for Surface Characterization” [15]. The work presented in this paper expands previous works [13], [14], [16] by presenting a bio-inspired tactile sensing module for the dynamic exploration of surfaces. The paper includes a detailed description of the novel module, accompanied by an evaluation on tasks related to dynamic surface characterization. The evaluation aims at analyzing the module’s response on a standard gratings exploration tasks, from [11], in ideal conditions (i.e. constant orientation and linear velocity as encountered in most of the work in the literature) and in real conditions, where the sensor is attached to a robotic finger and no constraints are imposed apart from the continuous contact throughout the interaction. In this setup, the module achieves the same performance as the sensors presented in [12], [150], [240]. The module is also used in a second experiment, for a classification task of seven synthetic shapes using the same robotic finger. This task shows that the data collected by the module can be used to distinguish the shape profiles by applying multiscale principal components analysis prior to the classification with a multilayer neural network.

4.2 Introduction

Recognition of objects by touch is one of the first steps to enable robots to help humans in their everyday activities. Many applications such as health and elder care, manufacturing, and high-risk environments involve tasks in unstructured environments that require robots to handle various types of objects, made of different materials, that can be situated out of the field of view of the robot or partially obstructed. In order to cope with these situations, improvements must be made both in sensing technologies enabling the robot touch and in the capability of robots to make sense fast and efficiently of perceived data.

Similar to humans that recognize the properties of an object by touching it, in order to manipulate objects efficiently, robots need to first be able to identify them based on their properties. Object identification by touch can be divided into the identification through static or dynamic touch. In static touch, the tactile sensing apparatus establishes contact with an object and collects data while the object is in touch with the probe; the apparatus and explored object are not moving during the sensing process. This approach can, for instance, gather data on temperature or information on the local geometry of the object. In dynamic touch, the tactile apparatus gathers data while the sensors slide over the object's surface, similar to human exploration of surfaces by lateral motion. Klatzky [1] observed that people use a lateral motion with one or more fingers, that may move more quickly or more slowly, using either a rubbing in circle or a short sweep in order to detect an object's roughness. The invariant aspect of this exploratory movement is the fact that the skin moves tangentially across the local of the surface. Similarly, a sliding movement over an object executed by a robot finger can enable robots equipped with appropriate sensors to collect information about the roughness of its surface and help identify its properties.

Although several efforts have been made on the development of robotic touch and related sensors that can detect multiple types of stimuli, the current generation of MEMS sensors have not yet been extensively explored while embedded in flexible materials, and in the context of multimodal sensing. Very few solutions in the literature use more than one type of sensor to collect tactile information. Moreover, the existing solutions fail to provide an integrated

approach for multimodal tactile module design, in particular for the placement of sensors within compliant structures. These are some of the issues that the current work attempts to tackle.

This paper focuses on the issue of surface characterization through sliding motions, performed by a linear motion carriage and by a robot finger composed of three motors, both equipped with a bio-inspired multimodal tactile module. Taking inspiration from the function and the organization of mechanoreceptors in the human skin on one side and from the hardness of human skin, on the other side a novel tactile module is built, comprising a 9-DOF MEMS MARG (Magnetic, Angular Rate, and Gravity) system and a deep MEMS pressure (barometer) sensor, both embedded in a compliant structure that mimics the hardness of human skin. When the module's tip slides over a surface, the MARG unit vibrates and the deep pressure sensor captures the overall normal force exerted.

The module is evaluated in two experiments. The first experiment compares the frequency content of the data collected in two setups: in the first setup, the module is mounted over a linear motion carriage that slides four grating patterns at constant sliding velocities. In this setup, the orientation of the module with respect to the grating patterns is also kept constant. This is an ideal setup that evaluates the basic capabilities of the tactile module and that is similar to the testing conditions in most of the current work in the literature. In the second setup, the module is carried by a robotic finger that keeps contact with the same grating patterns while performing a sliding motion similar to the exploratory motion employed by humans to detect object roughness. In this setup, the orientation, velocity and pressure exerted by the module are not kept constant. This sort of setup that characterizes real-world applications, in which the robot needs to deal with unknown objects and in which a constant orientation, velocity and pressure are almost impossible to achieve, allows evaluating the capabilities of the tactile module in realistic conditions. The second experiment shows how localized features extracted from the data collected by the robotic finger over seven synthetic shapes can be used to classify them and therefore enabling the robot to characterize them. The method employed to distinguish them consists on applying multiscale principal components analysis prior to the classification with a multilayer neural network.

This paper builds on our previous work in [14]. The paper now includes a detailed description of a novel bio-inspired tactile module, accompanied by a thorough evaluation on tasks related to dynamic surface characterization. The additional evaluation aims at analyzing the module's response on gratings exploration tasks both in ideal conditions (constant orientation as encountered in most of the work in the literature) and in real conditions, where the sensor is attached to a robotic finger and no constraints are imposed. The contributions of this paper are: (1) the design of a tactile module inspired from biology, mimicking the mechanoreceptors' placement, function and the hardness of skin within the compliant structure that embeds the sensors; (2) the comparison of data collected in frequency and time domains on an orientation-constrained linear setup to the one sensed while performing the exploration by a 3-DOF robotic finger; and (3) the classification of data collected by the robotic finger over synthetic shapes with localized features.

The paper is organized as follows: The next section discusses relevant work in the literature. The material and methods employed in the experimental setup are detailed in Section 4.3. This is followed by a presentation of our approach for the problem of shape discrimination from multi-sensory data collected during a sliding motion of a robot finger in Section 4.4. The experimental results are presented in Section 4.5. Finally, insights on future work and final considerations are described in Section 4.6.

4.3 Literature Review

The design of tactile sensors and the interpretation of the data gathered by such sensors is the subject of vast literature. Most of the solutions in the literature propose a single sensing technology, such as pressure/normal forces sensors, accelerometers, fiber optic and other optical sensors, and microphones to dynamically acquire tactile data for texture identification [9].

The most explored sensing modality in tactile sensing is pressure or force sensing. In [12], [150], a tactile sensor array based on MEMS sensors embedded in a polymeric packaging and inspired from the SA1 innervation density in humans, is investigated for roughness encoding. A time-frequency analysis on pairs of tactile array outputs yields 97.6% discrimination accuracy with a k-nearest-neighbor (k-NN) classifier. The authors of [241] perform tactile texture recognition with

a 3-axial force MEMS integrated in artificial finger that slides on a surface. Supervised classification methods are used to discriminate fine textures over 10 kinds of paper.

In [141], Jammali and Sammut present a system where textures are distinguished by the presence of different frequencies in a signal collected from a fingertip equipped with randomly distributed strain gauges and polyvinylidene fluoride (PVDF) films embedded in silicone. The Fourier coefficients of the signal are used to train a series of classifiers (i.e., naive Bayes, decision trees, and naive Bayes trees). The classifiers achieved an accuracy 95 ± 4% on materials such as carpet, flooring vinyl, tiles, sponge, wood, and woven mesh.

Another category of solutions to collect tactile information for surface identification is based on the use of accelerometers. Dynamic exploration tasks such as the identification of shapes and textures benefit from the data collected by such sensors, both in the cases where the sensor is static and the object is moving [144] and in the scenarios where the sensor is moving and the object is static [16]. A tactile probe in form of a small metallic rod with a single-axis accelerometer attached to its tip is employed to classify surfaces based on their mean, variance, and higher order moments using a support vector machine in [242]. A training data set is collected over 28 different indoor and outdoor surfaces while the test surface is rotated by a turntable, and a neural network achieves a surface recognition rate of 96.7% based on 1 s of data. The authors demonstrate as well that similar results can be achieved without the need for ground truth or the actual number of surfaces using Dirichlet process mixture models, a Bayesian nonparametric approach. Due to the use of a turntable, such a solution cannot be readily applied in interactions between a robot and an object. Considerations about the changes in orientation, position, and velocity of the sensor relative to the object are obstacles to the direct application of such a setup in active sensing applications. The same idea of a metallic rod dragged along a surface to be identified is also explored in [243]. In [243], eight features in time and frequency domains are used for classification using a neural network and a recognition rate of 90.0–94.6% for a 1- and 4-s time-window is achieved for ten types of indoor and outdoor surfaces. An unsupervised classification recognition rate of 74.1% for 1-s time windows of terrain data is achieved in [145]. A three-axis accelerometer captures vibro-tactile feedback as a robot is performing a scratching

motion in [146] and the collected data over 20 surfaces is used to recognize the surface material using machine learning approaches.

Another category of tactile sensing solutions uses optical and fiber optical sensors. The tactile sensor of De Maria et al. [244] is based on a matrix of LED-phototransistor couples embedded in a deformable elastic layer in the form of a hemisphere. The deformable layer transduces external forces and torques into local deformations which produce a variation of reflected light intensity and of the photo-current flowing in the photodetectors. A model of the same sensor based on extended Kalman filter allows to reconstruct the position and orientation of the surface in contact with a rigid object [245]. The friction coefficient is then estimated based on the contact plane position and orientation information together with the contact force vector measured by the sensor. A slippage control algorithm for the same sensor is proposed for manipulation tasks in [246]. Chorley and coworkers' sensor [102], based on the morphology of the fingertip skin in encoding tactile edge information, comprises a thin flexible rubber skin with structural details and encases a clear, compliant polymer melt blend. Markers on the internal structural details of the rubber skin are tracked by an embedded CCD, illuminated by four infrared LEDs and enable detection of surface deflections. The same sensor is used to detect object edges in the context of a robotic contour following task in [247]. The authors of [248] detect contact and control forces during fine manipulation with the help of four fiber optical sensors embedded in an exoskeletal robot finger. Fiber Bragg gratings ensure a high strain sensitivity and immunity to electromagnetic interference.

In [68], an artificial finger equipped with a microphone to detect frictional sound is employed to quantify texture. Recordings of a series of artificial surfaces were made to create a library of frictional sounds for data analysis and were mapped to the frequency domain using fast Fourier transforms. Features such as modal frequency and average value were calculated to analyze the data and compared with attributes generated from principal component analysis. Classification of the recordings using k-nearest neighbors obtained a high accuracy for PCA data. The idea of using a microphone is also exploited in [140], [249]. The authors developed a microphone-based texture sensor and a hardness sensor that measures the compression of the material at a

constant pressure. Raw-sensor output is conveyed to a self-organizing map that represents after training the textural properties of the explored materials.

All standalone sensing technologies are associated with specific drawbacks. Magnetic sensors can only be used within environments with low magnetic field variations. Fiber optic sensors are expensive and difficult to integrate in tactile modules due to the bending losses in the fiber routing [244]. CCD camera solutions involve generally a high cost and weight, while the loss of light due to microbending or chirping causes distortion is the measured data [5]. To alleviate the drawbacks associated to any one single technology, a possible solution is to capitalize on the use of multiple sensor technologies for recuperating tactile information [13], [94], [144], [250]. A biomimetic fingertip containing three accelerometers and seven force sensors in two layers of polyurethane [251], is employed to discriminate six fabrics and an aluminum plate by comparing the differences in their surface texture in [252]. An input signal is computed by calculating the covariance of two adjacent accelerometers and a neural-network classifier using as features the variance and power of the accelerometer signal is used to discriminate the seven textures. The same fingertip distinguishes seven wood samples in [250], by training a neural-network based on three features calculated from the covariance signal of two adjacent accelerometers in the fingertip, namely the mean and variance of the approximate signal, and the energies of the detailed signal. The covariance signal is transformed using Discrete Wavelet Transform and a 65% success rate is reported for classifying the wood samples. The authors of [151] use multimodal tactile sensing (force, vibration and temperature) and program a robot hand to make exploratory movements similar to those humans make when identifying objects by their compliance, texture, and thermal properties. The proposed Bayesian exploration algorithm is augmented with reinforcement learning to enable the evolution of internal representations of objects according to cumulative experience. The robot is able to correctly identify 10 different objects on 99 out of 100 presentations. A data-driven analysis to the problem of sensor selection in the contour following for shape discrimination task is presented in [13]. Data collected from the motors, an inertial measurement unit, and a magnetometer attached to a 4-DOF robotic finger, during the exploration of seven synthetic shapes are analyzed using principal component analysis and a multilayer perceptron neural network is trained to classify the shapes. Kroemer and coworkers'

[94] tactile sensor consists of a compliant pin that makes contact with a surface and a capacitor microphone that detects the vibrations of the pin. A multisensory data fusion algorithm combines readings from the pin with vision data collected with a camera to classify rich-textured surfaces. This paper tackles the dynamic tactile surface characterization problem using a novel bio-inspired tactile module that uses traditional MEMS sensors embedded in a compliant substrate mimicking the function and placement of mechanoreceptors as well as the hardness of the human skin. In particular, a 9-DOF MEMs MARG (Magnetic, Angular Rate, and Gravity) module and a MEMs pressure (barometer) sensor are positioned so that when the tip of the module is rubbed over a surface, the MARG unit vibrates and the deep pressure sensor captures the overall normal force exerted. The experiments show that the traditional MEMS sensor can detect the stimuli generated by grating patterns used in other sensors' validation [12], even when the sensors are embedded in a truly compliant structure. This paper also shows the performance of the module in realistic interaction scenarios between a robotic finger and an unknown surface in which the orientation, velocities and forces are not kept constant. As it is demonstrated in the experimental part of this paper, the signals measured in such conditions can be used to classify surface profiles.

4.4 Bio-Inspired Tactile Sensor Module and Surface Characterization Experiments

4.4.1 Bio-Inspired MEMS Based Tactile Module

The tactile module presented in this work draws inspiration from the human tactile system. According to Loomis and Lederman [253], tactile perception refers to sensing capabilities mediated by cutaneous stimulation, involving a physical contact between an object and the surface of the skin that encases the mechanoreceptors [5]. The cutaneous stimuli sensed by tactile receptors embedded in the skin are interpreted into information about topology, texture, contact force, elasticity of the touched object's surface, and other features. The skin on the human hands contains four types of cutaneous mechanoreceptors [6], [235], Meissner's corpuscles, Merkel disks, Pacinian and Ruffini corpuscles, as illustrated in Figure 4-1.

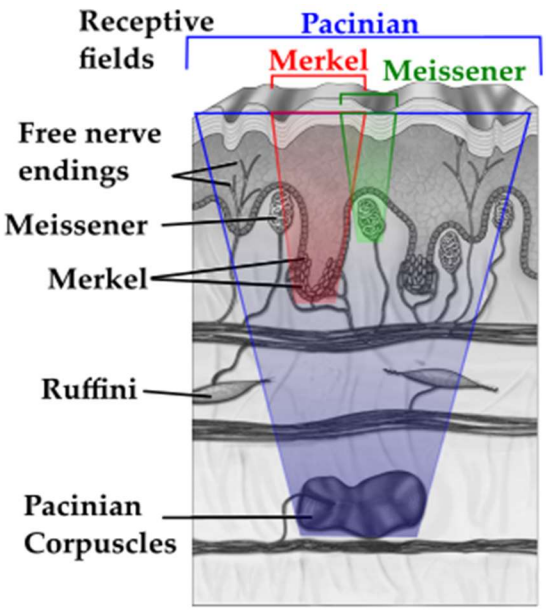

Figure 4-1 *Human skin mechanoreceptors, adapted from [6]; Pacinian corpuscle receptive field in blue; Merkel receptive field in red; and the Meissner receptive field in green.*

Merkel disks and Ruffini corpuscles are slow adapting, i.e., detect constant stimuli (e.g., constant pressure or skin stretch). Merkel disks can also detect initial contact. Meissner and Pacinian are fast adapting receptors able to detect short pulses, such as the initial contact. Meissner and Merkel are located in shallow levels, close to the skin surface, while Pacinian and Ruffini are present in deeper levels of the human skin. While the exact role, function and properties of each of these receptors are not yet completely understood, Table 4-1 summarizes aspects accepted in the current literature from neuroscience and experimental psychology [5], [6], [254].

Mechanoreceptors in the human skin work in synergy to enable the correct perception of different stimuli that emerge from manipulation of objects or from haptic exploration. For example, in the context of edge detection, Meissner's corpuscles sense small sharp borders in dynamic touch tasks, while Merkel disks sense the same information during static touch. Larger surface features are sensed by Pacinian and Ruffini corpuscles due to their large receptive fields. Mechanoreceptors are sensitive to mechanical stimuli around the skin's surfaces on areas ranging from 9 to 60 mm2. The receptive fields of such cells are combined and superimposed to achieve two-point discrimination of as low as 2 mm on human hands [5]. Some mechanoreceptors are more specialized in static exploration, while others in dynamic scenarios. Dynamic tactile data are gathered when skin ridges on the surface slide in contact with explored

objects. Properties such as stickiness, smoothness, friction, roughness, slippery can be hardly estimated by static probing [238].

Table 4-1 Human skin mechanoreceptors.

Receptor	Properties and Functions
Merkel disks	Location: Shallow Receptive field: small (2–3 mm)—Frequency Range: 0–100 Hz (Peak at 5 Hz) Functions: form/shape detection; texture detection, fine details discrimination, constant pressure, presence, location and static deformation at points and edges; curvature detection; tactile flow perception.
Ruffini corpuscles	Location: Deep Receptive field: large (larger than 10 mm)—Frequency range: 0–? Hz (Peak at 0.5 Hz) Functions: directional (lateral) skin stretch; direction of object motion; position of hand and fingers; slip detection; stable grasp; tangential force estimation; tension (continuous touch or pressure).
Meissner's corpuscles	Location: Shallow Receptive field: small (3–5 mm)—Frequency range: 1–300 Hz (Peak at 50 Hz) Functions: motion detection; velocity; slippage; low frequency vibration; local skin deformation; tactile flow perception; grip control; flutter; dynamic deformation; two-point discrimination; encode normal (horizontal) strain forces.
Pacinian corpuscles	Location: Deep Receptive field: large (larger than 20 mm)—Frequency range: 5–1000 Hz (Peak at 200 Hz) Functions: deep pressure; pressure change; un-localized high frequency vibration; body contact when grasping an object (tool use).

The focus of the bio-inspired tactile module developed in this article is to gather dynamic tactile data. It integrates and organizes conventional MEMS sensors embedded in a compliant structure in a manner similar to the mechanoreceptors in the human skin, while focusing on the study of dynamic tasks. It takes inspiration from the type of mechanoreceptors present in glabrous skin, from their two-layered organization (Figure 4-1) and from their functional relationships. Therefore, it consists of a shallow 9-DOF MARG (Magnetic, Angular Rate, and Gravity) sensor, a flexible compliant structure and a deep pressure sensor, as shown in Figure 4-2. It implements the deep pressure sensing functionality by using a MEMS barometer embedded in bottom of the pyramidal compliant structure. This component of the tactile module reproduces the functions of Pacinian corpuscles in sensing deep pressure and pressure changes (Table 4-1). The compliant pyramidal structure conducts forces applied to the shallow sensors in the tip of the structure to the barometer ventilation window (Figure 4-2a(3)). The shallow sensors implemented by a MARG system measure vibrations (accelerations, angular velocities and changes in the magnetic field

surrounding the module) (Figure 4-2a(2)) on the higher levels of the module and emulate the functionalities of Merkel cells and Meissner's corpuscles.

The module in this article does not focus on the tactile imaging that is usually performed by pressure sensitive tactile arrays in static tactile exploration, but some of the sensors embedded in the module could play the role of mechanoreceptors specialized in static tactile functions, for example the gravity and magnetic field sensors.

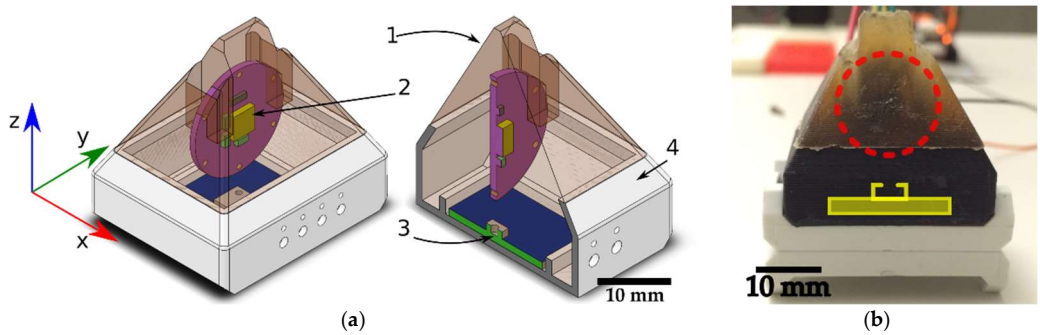

Figure 4-2 *(**a**) Tactile module: 1, pyramidal compliant structure; 2, MARG system on printed circuit board (PCB), the MARG system land grid array package is highlighted in yellow; 3, deep pressure sensor (barometer ventilation window); and 4, supporting collar. (**b**) Front view of the tactile probe: the MARG system is embedded under the red circle; the pressure sensor is under the yellow overlay in the black 3D printed collar. A side view of the module can be seen in Figure 4-3.*

The compliant structure connects the shallow and deep sensors (Figure 4-2a(1)). This structure performs the role of the receptive field, refining the spatial resolution of the shallow sensors and conducting the forces applied on the tip of the pyramidal structure to the deep pressure sensor. The pyramidal structure tries to mimic the area corresponding to the intersection between the receptive fields of one Pacinian (deep pressure sensor), one Merkel cell, one Meissner's corpuscle and one Ruffini nerve ending. The PCB on which the MARG system is mounted helps guiding pressures in the fingertip to the deep pressure sensor. The compliant structure deformation makes the shallow sensors vibrate when the module's tip slides on external surfaces. The compliant structure in the prototype has shore 20 A hardness, similar to the human skin in the index fingertip pad [255]. Structures with hardness lower than shore 20 A tend to degrade fast and would need to be repaired often, harder structures (e.g., hardness shore 70 A) would limit the deformability of the module vibration of the MARG system. The flexible structure also adds compliance to the module. The authors of [256] state that compliance makes sensing more

efficient by reducing the control precision required to maintain gentle contact with an object, avoiding sharp forces during exploration, and increasing the robustness of the sensors.

The proposed bio-inspired tactile module capitalizes therefore on a combination of various sensors: The accelerometer provides information on the orientation of the shallow sensors relative to a gravity frame. It is also useful to detect light touch and deformation on the tip of the compliant structure. Dynamic exploration tasks such as the identification of shapes and textures benefit from the data collected by accelerometers. This component of the tactile module emulates a behavior resembling the one of Merkel cells within human skin. The 3-DOF angular rate sensor (gyroscope) embedded in the same integrated circuit (MARG unit) of the accelerometer collects data about the rate of vibrations onto the shallow sensors (angular velocities). The rate of deformation that occurs on the tip of the module is related to the angular rate of the shallow sensors. The measured data acquired by this sensor simulate the one recuperated by Meissner's corpuscles within the glabrous skin. The 3-DOF magnetometer measures the orientation of the shallow sensors, thus the deformation of the module's tip, relative to a reference magnetic field that can be either the earth's magnetic field or a local magnetic field induced by permanent magnets. Permanent magnets can be employed as local reference frames while measuring stretch or deformation of flexible substrates. However, relying solely on magnetic measurements is not an ideal scenario for tactile sensing due to the magnetic interference when touching ferrous objects or when working in ferrous environments. Machine learning systems and other algorithms applied only on magnetic measurements could be misled by the presence of the unexpected ferrous object. This is one of the reasons why it is desirable to use complementary sensors, for example accelerometer, gyroscope and magnetometer in the same integrated circuit, as in the current work. The capability of this component of our tactile module to provide form and stretch information mimics the functionality of Ruffini endings. Finally, the role of the Pacinian corpuscles is performed by the deep pressure sensor realized by a MEMS barometer encased in polyurethane on the bottom of the compliant structure. The height of the compliant structure from the tip to the ventilation window Figure 4-2a(3) of the barometer is 28 mm. This sensor collects data on the pressure of un-localized touch around the tip area of the module and high frequency changes in pressure.

The 9-DOF MARG system used for the experimentation is the STMicroelectronics© LSM9DS0 (manufacturer, location) composed of a triple-axis accelerometer, a triple-axis gyroscope, and a triple-axis magnetometer. The pressure sensor (i.e., MPL115A2 from Freescale Semiconductor©, manufacturer, location) sits on the bottom of the black 3D printed collar that holds the compliant structure. The flexible rubber from the compliant structure is made of VytaFlex© Shore 20 A hardness. The microcontroller serving as an interface between the computer that collects and analyzes the data from the sensors is a Freescale Semiconductor© MK20DX256VLH7 Cortex-M4 at 72M Hz. It is connected to the sensors through a two-wire interface (TWI) at 400 K Hz. The microcontroller connects to the computer through a USB Serial interface. The data acquisition software is developed using the Robotic Operating System (ROS). The computer running ROS accesses the data from the sensors through the interface microcontroller at 440 Hz. Table 4-2 shows the details (measurements range, frequency range, and sensors resolution) for the MARG system and the deep pressure sensor used in this work.

Table 4-2 LSM9DS0 and MPL115A2 frequency range and sensor resolution [257], [258]*, Selected M. range and Selected F. range, are the measurement range and frequency range the sensors are configured to operate at.*

	Magnetic Sensor	**Gravity Sensor**	**Angular Velocity**	**Pressure Sensor**
Measurement range	±2 – ±12 Gs	±2 – ±16 g	±245 – ±2000 dps	50 – 115 kPa
Selected measurement range	±2 Gs	±2 g	±245 dps	*Not applicable*
Frequency range	3.125 Hz – 100 Hz	3.125 Hz – 1600 Hz	3.125 Hz – 1600 Hz	333.3 Hz (max)
Selected frequency range	100 Hz	800 Hz	800 Hz	333.3 Hz
Resolution	0.08 mG	0.061 mg	8.75 mdps	0.15 kPa

4.5 Experimental Setup

Two experiments were performed with the tactile module introduced above, the first one exploring the capability of the sensor to sense gratings on surfaces in a linear motion setup and when it is attached to the tip of a robotic finger. The grating patterns are inspired by the experiments in [11] and employ the same dimensions as in [12], namely the same ridge width and height and groove width (i.e., distance between ridges). The second experiment focuses on the application of the module to the exploration and identification of coarser tactile profiles.

4.5.1 Experiment 1: Sensors Response to Ridged Surfaces (Grating Patterns)

During this experiment, the tactile module is tested in two setups to evaluate its capability to detecting ridges on surfaces and their spatial distribution.

In the first setup, the module is fixed over a linear motion setup. The purpose of this setup is to evaluate the sensors and compliant structure's response to regularly spaced ridges on a surface while keeping the module in a steady orientation relative to the grating pattern surface. The tactile module is mounted above a linear motion actuator carriage where gratings with different patterns are fixed to stimulate the tactile module deforming its fingertip while sliding under it. Figure 4-3a shows a close-up view of the tactile module and the 2.5 mm groove width grating pattern in the beginning of the stimulation. The sliding motion occurs along the sensor's x-axis. The fingertip is slightly deformed due to the contact with the first ridge. Figure 4-3b shows the grating patterns with a groove width varying from 3.5 mm to 2.0 mm. The depth of the grooves is 1 mm and the thickness of the ridges is 0.6 mm. The grating pattern with 3.5 mm groove width has 20 ridges; the ones with 3.0 mm, 2.5 mm, and 2.0 mm groove have 23, 26 and 31 ridges, respectively. The length of the 3D printed grating patterns is 100 mm. The height of the layers in the 3D printed patterns is 0.1 mm. To minimize the impact on measurements, the layers were deposited such that the module did not cross layers during the exploratory movement.

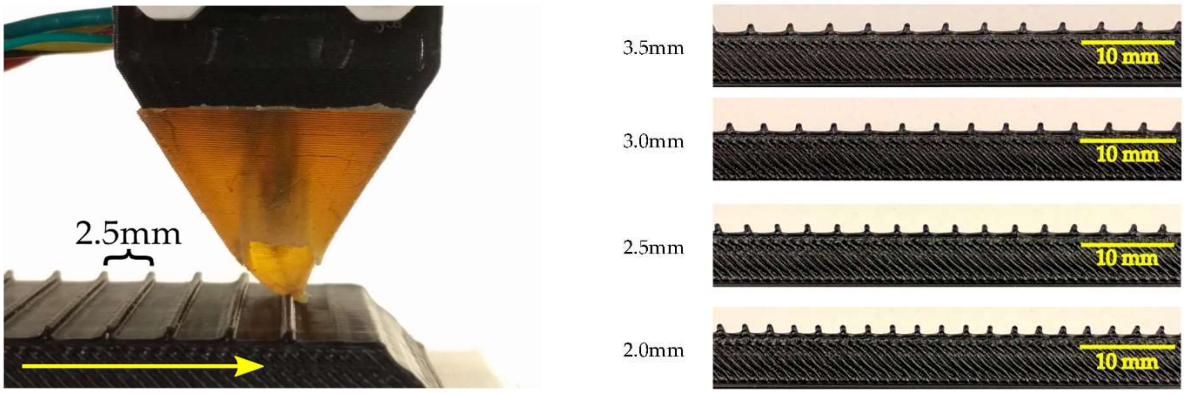

*Figure 4-3 Sliding apparatus and gratings patterns: (**a**) side view of the tactile module in the beginning of the stimulation; and (**b**) grating patterns with a groove width varying from 2.0 mm to 3.5 mm; the depth of the grooves is 1 mm and the thickness of the ridges is 0.6 mm.*

During experimentation, the patterns were approximately aligned to the x-y plane of the sensor. This was done on purpose, since keeping a steady pressure should not be an obstacle to

identifying the frequencies induced by the patterns. For instance, monkeys do not keep a steady pressure while performing surfaces exploration [11].

The experiment and data acquisition started with the module unloaded, i.e., not in contact with the grating pattern, and then the linear platform carrying the grating pattern brought it to contact the tip of the module. The contact of the pattern and tip generates a small load that is detected by the sensors embedded in the compliant structure. When the sensing module encounters the ridges of the grating pattern, larger loads are driven into the structure of the module and exerted on the sensors.

The sliding stimulus occurred with two translational velocities (15 mm/s and 30 mm/s, respectively), and were chosen in accordance to the ones used in [12]. The velocities, directions and starting position of the gratings related to the module were the same for all gratings. The travel distance for the linear carriage was 130 mm, ensuring that the entire length of the grating pattern passed under the modules tip. The dynamic stimulations from the first to last ridge lasted from 5.6 s to 2.8 s depending on the velocity employed. By the end of the sliding motion the module was unloaded since the entire grating pattern slid under the tip and the contact was interrupted.

The authors of [259] suggest that human beings perceive roughness sensation as the change of frequency detected by Meissner's corpuscles in relationship with their hand movements and the physical properties of roughness of materials. According to the same authors, given velocity v, the frequency of stimuli f, which are generated in a point of finger, can be expressed by $f = v/\Delta p$, where f is the frequency in Hz, v is velocity measured in mm/s and Δp is the groove width plus the ridge width. Assuming the velocities of 15 mm/s and 30 mm/s, the expected frequencies generated in a point of the tip of the tactile module for the different grating patterns are defined in Table 4-3. The information in this table will be used later to validate the response of our tactile module.

Table 4-3 Expected frequencies for different gratings and velocities.

$f = v/\Delta p$	$\Delta p = 4.1$ mm	$\Delta p = 3.6$ mm	$\Delta p = 3.1$ mm	$\Delta p = 2.6$ mm
$v = 15$ mm/s	3.66 Hz	4.17 Hz	4.84 Hz	5.77 Hz
$v = 30$ mm/s	7.32 Hz	8.33 Hz	9.68 Hz	11.54 Hz

In the second setup, the module was mounted on the tip of a 3-DOF robotic finger as an end effector. The finger prototype used to perform the sliding motions can be seen in Figure 4-4. It contains three Robotis Dynamixel AX-12A robot actuators labeled M1 (bottom), M2 (middle) and M3 (top). The motors are controlled by a ROS node joint position controller. Each joint adjusts its position to minimize the difference between its current position and the one in the prerecorded movement. The prerecorded movement started with the finger extended and the tactile module touching the ramp on the beginning of a shape without gratings (a blank pattern). The finger carried the module through the extension of the grating patterns keeping contact between module and pattern with unconstrained fingertip orientation and pressure. The average velocity along grating pattern was 33 mm/s.

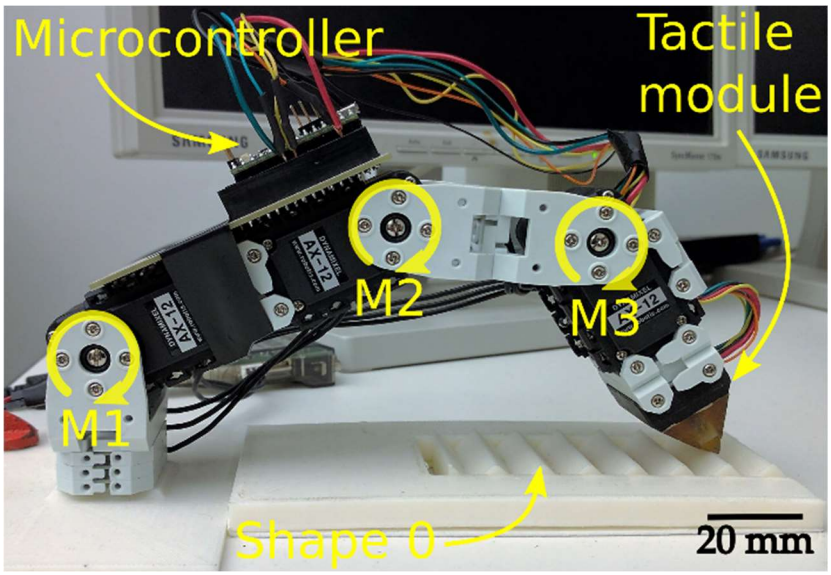

Figure 4-4 Robot finger composed of three motors: M1 is the "bottom" motor; M2 is the "middle" motor; and M3 is the "top" motor. The microcontroller is attached on top of Motors M1 and M2.

Figure 4-5 shows the pressure response captured by the module for the grating patterns explored by the linear motion setup for various speeds and by the robotic finger. The first two columns show the data gathered under a velocity of 15 and 30 mm/s, respectively. The last column shows the pressure response for the exploration performed by the robotic finger using an average velocity of 33 mm/s. The rows of graphs show the data collected for the gratings from the 2 mm groove width in the first row to the 3.5 mm in the bottom row. The graphs from the first two columns show clear valleys in the raw output of the pressure sensor corresponding to the ridges

in the grating pattern; as the pressure inside the collar increases, the digital output of the pressure sensor decreases. The deformation of the fingertip increases the pressure inside the collar sensed by the deep pressure sensor. The deformation and the rate at which the deformation occur are sensed by the gravity and angular velocity MARG system. These measurements are independent of pressure. The patterns were slightly inclined relative to the module, i.e., the z-axis from the module was not perfectly normal to the grating pattern plane; this aspect is more noticeable on the 3.5 mm plots. These small misalignments are not an issue when detecting the number of ridges in the patterns and should not affect the frequency of the stimuli detected by the various sensors.

The first two columns show the data gathered under a velocity of 15 and 30 mm/s, respectively. The last column shows the pressure response for the exploration performed by the robotic finger using an average velocity of 33 mm/s. The rows of graphs show the data collected for the gratings from the 2 mm groove width in the first row to the 3.5 mm in the bottom row. The graphs from the first two columns show clear valleys in the raw output of the pressure sensor corresponding to the ridges in the grating pattern; as the pressure inside the collar increases, the digital output of the pressure sensor decreases. The deformation of the fingertip increases the pressure inside the collar sensed by the deep pressure sensor. The deformation and the rate at which the deformation occurs are sensed by the gravity and angular velocity MARG system. These measurements are independent of pressure. The patterns were slightly inclined relative to the module (within ±2 degrees), i.e., the z-axis from the module was not perfectly normal to the grating pattern plane; this aspect is more noticeable on the 3.5 mm plots. This small misalignment is not an issue when detecting the number of ridges in the patterns and should not affect the frequency of the stimuli detected by the various sensors. Well-structured setups as the linear motion presented here and in [11], [12] are useful to validate and analyze the feasibility of application for tactile sensors, but the assumptions of constant velocity, of constant pressure (or regular increments in pressure) as well as of constant orientation of the sensing apparatus limit the applicability of such sensors in more elaborated robotic applications. The third column of Figure 4-5 illustrates a scenario closer to real-world applications. The last link of the 3-DOF robotic finger was not constrained to have constant orientation, velocity or pressure. This is the case of

almost all real situations involving the exploration of unknown surfaces by autonomous robots. The only constrain in the prerecorded trajectory was the uninterrupted contact between fingertip and grating pattern. As one can notice in the last column of Figure 4-5, different from the linear motion setup, the data collected by the 3-DOF finger did not present noticeable valleys in pressure. This is due to the changes in orientation and velocity of the fingertip as well as to the variations in force exerted by the fingertip along the movement.

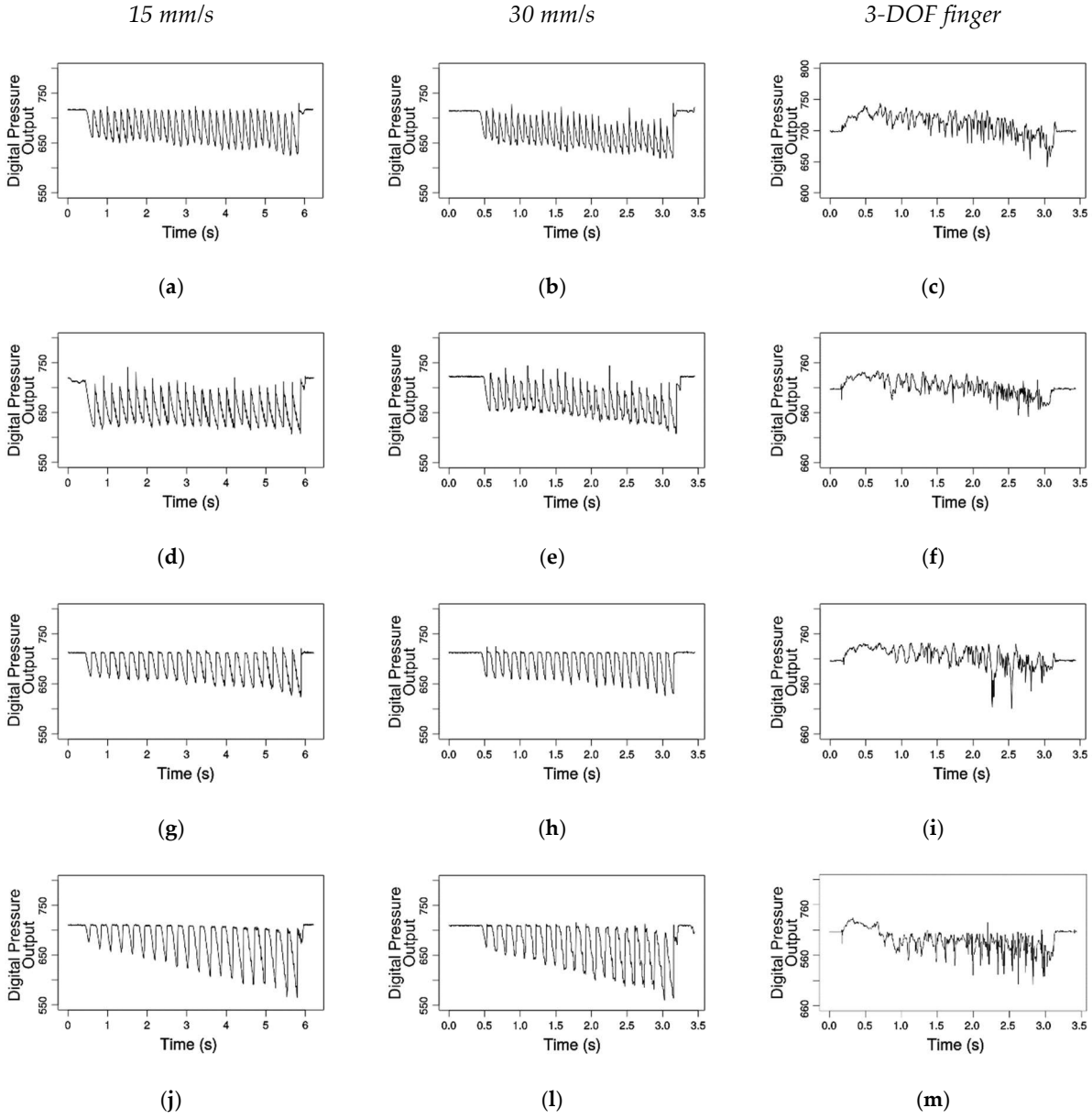

*Figure 4-5 Pressure response for various groove widths of the gratings pattern: **(a–c)** 2 mm (31 ridges); **(d–f)** 2.5 mm (26 ridges); **(g–i)** 3.0 mm (23 ridges); and **(j–m)** 3.5 mm (20 ridges).*

Localized features in the collected signals can still be used as discriminative inputs for classification systems. In order to analyze the frequency content of the signals collected by the sensors in each setup, the raw discrete signals z were subject to a non-normalized discrete Fourier transform [260]:

$$y[h] = \sum_{k=1}^{n} z[k] e^{-2\pi i(k-1)(h-1)/n} \quad (1)$$

for $h = 1, \ldots, n$ where n is the length of the signal z.

Figure 4-6 shows the frequency content of the signals collected by each sensor while exploring the 4 grating patterns in the linear motion and in the robotic finger setup. The first two columns of graphs show the magnitude spectrum in dB of data gathered under 15 and 30 mm/s, respectively. The last column shows the magnitude spectrum in dB for the exploration performed by the robotic finger. The graphs concentrate in frequencies up to 30 Hz, close to the expected frequencies for the grating (Table 4-3). In all graphs from Figure 6, black lines represent the frequencies of the signals collected over the grating pattern with 2.0 mm groove width; red, blue and green represent the frequencies related to the patterns with a groove width of 2.5 mm, 3.0 mm and 3.5 mm, respectively. The first row of Figure 4-6 shows the frequencies corresponding to the changes in pressure. The second row shows the frequencies for the changes in acceleration. Third and fourth rows show the frequencies for the data collected by the gyroscope and magnetometer respectively. Regarding the linear motion setup, as expected, the pressure frequencies show peaks (as pointed by the vertical arrows in Figure 4-6a,b) around 5 Hz for 15 mm/s; the 30 mm/s graph shows that the frequencies are shifted to 10 Hz. The frequencies present in the data gathered by the accelerometer do not present high amplitude differences, but a similar frequency profile can be seen, for example, in the red line with fundamental frequencies and harmonics following the same periods of the pressure changes in Figure 4-6a,b.

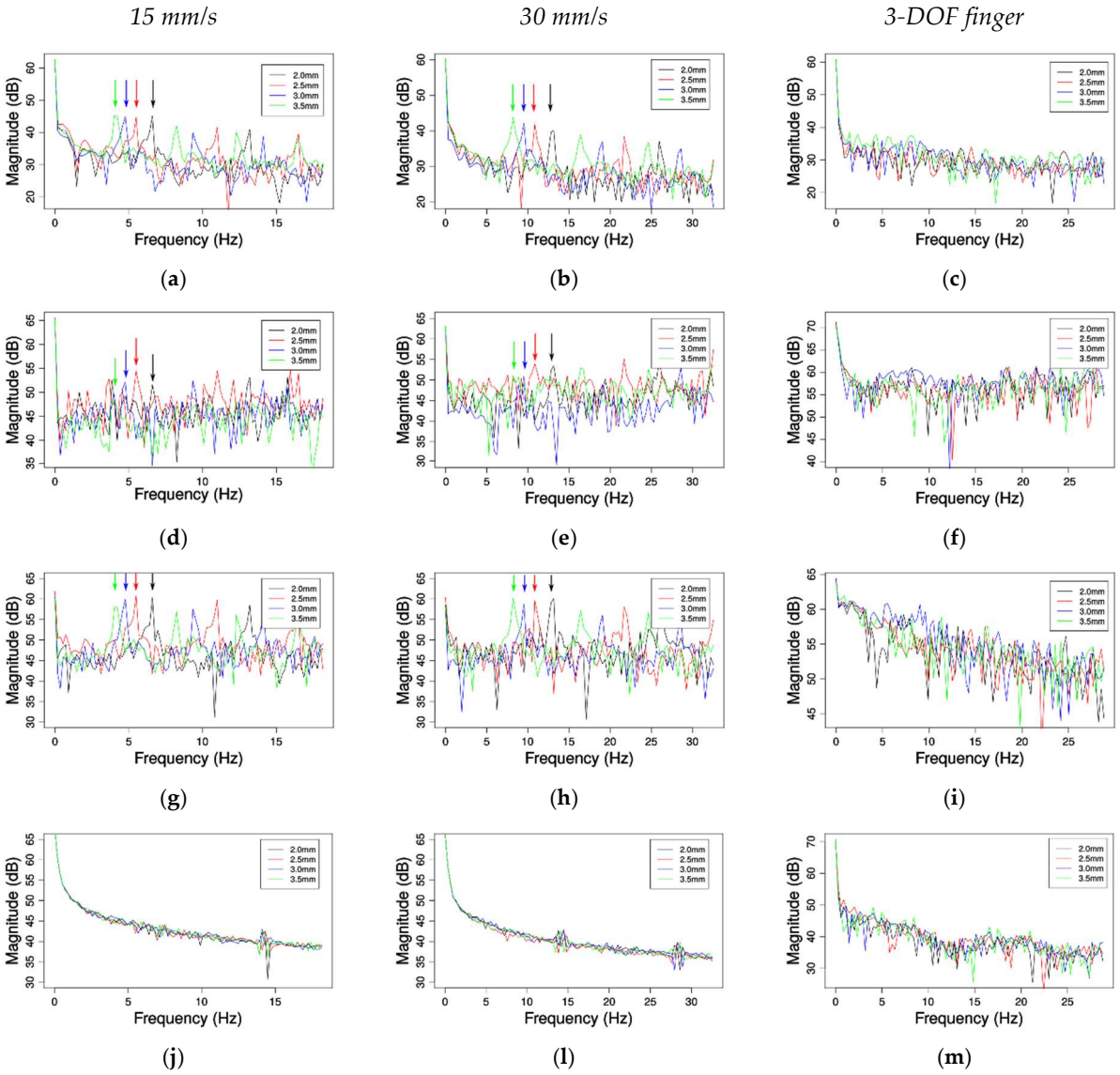

*Figure 4-6 Frequency analysis: (**a**–**c**) deep pressure sensor data; (**d**–**f**) acceleration (x-axis); (**g**–**i**) angular veloci (y-axis); and (**j**–**m**) magnetic field (z-axis).*

The angular velocity frequencies have the same behavior as the pressure sensed by the deep pressure sensor; the pronounced peaks around 5 Hz in Figure 4-6g are shifted to around 10 Hz in Figure 4-6h. The frequencies seen in Figure 4-6j–l shows that there are no significant changes in the magnetic field orientation and amplitude, except when the metallic linear motion carriage passes under the module and disturbs the magnetic field. As expected the 3.5 mm groove width grating yields the lowest frequencies; the frequencies detected for the 3.0 mm, 2.5 mm and 2.0

mm groove width are ordered from low to high as shown in peaks identified by the arrows in the Figure 4-6a,b,g,h. The last column of Figure 4-6 shows that the frequency content of the data collected on the finger setup does not contain peaks around the frequencies expected for each pattern, but localized features on frequency/time domain can be detected by the use of wavelets to characterize surfaces as demonstrated by the experiment in the next section.

Finally, Table 4-4 compares the expected frequencies for different gratings and velocities from Table 4-3 (in the row "Expected") with the detected frequencies by the module ("Mean detected"). The Root Mean Squared (RMS) error is computed as the difference between the expected and detected frequencies while using the linear motion setup, over six passes for each grating pattern and using linear velocity.

Table 4-4 Root Mean Square (RMS) error for six runs of each grating.

$f = v/\Delta p$		$\Delta p = 4.1$ mm	$\Delta p = 3.6$ mm	$\Delta p = 3.1$ mm	$\Delta p = 2.6$ mm
$v = 15$ mm/s	Expected	3.66 Hz	4.17 Hz	4.84 Hz	5.77 Hz
	Mean detected	3.66 Hz	4.10 Hz	4.83 Hz	5.86 Hz
	RMS error	0	0.07	0.01	−0.09
$v = 30$ mm/s	Expected	7.32 Hz	8.33 Hz	9.68 Hz	11.54 Hz
	Mean detected	7.32 Hz	8.35 Hz	9.67 Hz	11.44 Hz
	RMS error	0	−0.02	0.01	0.10

The results are close to the expected ones, with a maximum difference of ±0.1 Hz. These errors could be due to small imperfections in the 3D printed gratings patterns, small deviations on the speed controller, and/or to the small variations of the sampling rates.

4.5.2 Experiment 2: Surface Profile Classification

This experiment expands the previous one by using localized features to distinguish shapes from the data collected throughout an exploratory movement using the same robotic finger from the second setup of the previous experiment. The shapes used in this experiment are coarser than the gratings from the previous experiment.

These shapes increase the degree of complexity of the task due to the fact the module may lose contact with their surface. The ABS 3D-printed shapes are fixed in front of the robotic finger (as

seen in Figure 4-4) that establishes contact and slides the tactile tip over them. Shapes 1 and 2 can be seen in Figure 4-7a, while the seven profiles used for testing are shown in Figure 4-7b.

(**a**) (**b**)

*Figure 4-7 3D printed shapes: (**a**) Shape 2 on the top and Shape 1 on the bottom; and (**b**) list of shapes from Shape 1 on the top to Shape 7 on the bottom.*

A standard recorded movement is executed over each of the shapes and the data representing acceleration, angular velocity, magnetic field intensity and direction, is saved in a database. The database contains 100 runs for each shape, 700 samples in total. From these, 175 samples (25 for each class) are randomly chosen for training, in order to accommodate for tip abrasion, temperature variance, and other possible outliers. Over the time, the tip could become worn and the temperature due to friction could affect the collected data. This process of sampling avoids as well overtraining and increases the generalization capability of the classifier trained to distinguish between patterns.

The graphs in Figure 4-8 show for example the normalized pressure data for each shape. The vertical axes represent the pressure level (Figure 4-8h), the horizontal axis the discrete time, varying for 0 to 3800 and the number of sample varying from 0 to 100 is shown over the depth dimension. Figure 4-8d is presented under a slightly different viewpoint to emphasize the number of runs collected.

The data collected pass by three stages to discriminate the surfaces: (a) wavelet decomposition; (b) principal component analysis; and (c) classification by a multilayer perceptron (MLP) neural network.

Initially, the signals of each axis collected by the MARG system and barometer were subjected to a Discrete Wavelet Transform (DWT) decomposition [261] in order to reduce the noise and detect

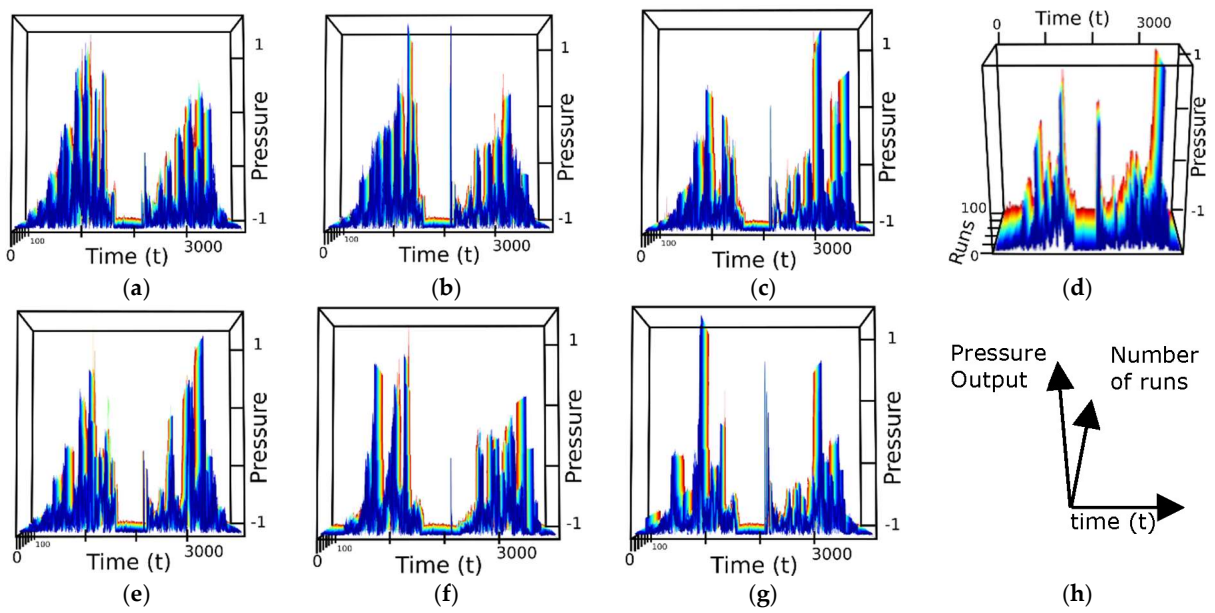

*Figure 4-8 Normalized pressure samples collected over the Shapes 1 to 7; and (**h**) meaning of axes for the preceding plots.*

discriminative features of interest. The DWT decomposition consists on the simultaneous filtering of the signals by a low-pass filter, to generate the approximation coefficients, cA1, and by a high-pass to produce the detail coefficients, cD1. The same operation is iteratively applied to the previous approximation signal producing new levels of approximation cAi and detail cDi (i is the level of the decomposition). In this paper, the low-pass and high-pass filters applied to the sensors signals are based on the fifth order of Symlets wavelet (sym5) and the decomposition level is set to 5. The frequencies for the low pass and high pass filters for each level are determined by $\left[\frac{\pi}{2^i} \sim \frac{\pi}{2^{i-1}}\right]$ for the high pass filter and $\left[0 \sim \frac{\pi}{2^i}\right]$ for the low pass filters, where i is the decomposition level.

The data resulting from the wavelet decomposition are then subject to principal component analysis (PCA). PCA [262] is a multivariate method of analysis widely applied on multidimensional data sets for dimensionality reduction. This approach reduces the number of variables in a dataset retaining as much as possible of its variances. PCA achieves the retention of variance by projecting the original correlated variables into a new set of uncorrelated variables. This reduction is carried out by taking a dataset consisting of p variables $X_1 ... X_p$ and finding the combinations of these to produce uncorrelated orthogonal principal components (PCs) $PC_1 ... PC_p$.

There are many ways to find PCs; according to the eigenvalue decomposition, PCs are eigenvectors basis for transformation from data space to feature space. The eigenvalues related to these eigenvectors are a measure of each PC representativeness. Organizing the eigenvalues and eigenvectors enables the selection of the most important principal components. The projection of the original data onto a subset of PCs reduces the dataset dimensionality maintaining the variance proportional to the eigenvalues of the number of PCs used. In this paper, original data of each sensor are reduced to the number of components corresponding to 90% of the total variance.

After PCA is performed on the wavelet decomposition data, we apply a multilayer perceptron neural network to classify the signals into their corresponding profiles. The feature vectors resulting from the PCA are the input to a two-layer feed forward neural network with ten nodes in the hidden layer, and seven neurons in the output layer, the latter corresponding to the number of shapes. The activation functions of all neurons are hyperbolic tangents. The network is trained using the scaled conjugate gradient backpropagation algorithm [263].

The results for the classification of data representing the 5th-wavelet approximation level of each sensor axis are shown in Table 4-5.

Table 4-5 Classification results.

Sensor	Accuracy (%)
Accelerometer X	92
Accelerometer Y	92.6
Accelerometer Z	85.1
Gyroscope X	98.3
Gyroscope Y	93.3
Gyroscope Z	98.9
Magnetometer X	88
Magnetometer Y	86.9
Magnetometer Z	91.4
Barometer	98.9
Acc. Y—Gyro. Z—Magn. Z—Barometer	100

Each DOF of the MARG sensor is classified individually. The accelerometer group obtains a classification accuracy between 85.1% and 92.6%. The accuracy when considering the gyroscope

group is between 93.3% and 98.9%. When considering the magnetic field variations along the trajectory, the results range is 86.9% and 91.4%. The pressure profile measured by the barometer yields an accuracy of 98.9%. The results from the acceleration suggest that the z-axis is the least aligned of the three. Because the angular velocity sensor is sensitive to shock/vibration even when the direction of the event is not aligned with its axis, it obtains high accuracy rates in all axes. The low variations of the magnetic field lead to classification rates not as high as those obtained by the inertial sensors. The classification using the data measured by the barometer achieved one of the highest accuracy rates due to the variation of pressure over time and discontinuity of the contact between tactile tip and shapes while the movement was performed. As expected, the best axis of each sensor combined show the highest accuracy. We consider that in a larger dataset with more shapes and complex movements the system would require more components to achieve satisfactory rates of classification. Removing more than 10% of the principal components could narrow data representativeness and generalization. Having redundant measurements may make the system more robust in case of a failure of one of such axes, or in environments and tasks that are not favorable to one or more of such axes (e.g., in the presence of unexpected ferromagnetic objects).

*Figure 4-9 Confusion tables for: (**a**) barometer, showing the misclassification of Shape 5 as Shape 4; and (**b**) accelerometer on x-axis, showing the misclassification between Shapes 1 and 2.*

Most of the classification errors for the inertial sensors happened between Shapes 1 and 2 due to their similarity, as shown in Figure 4-9b and in the confusion table in Figure 4-9b. This is not the case when the sensor considered is the barometer, as shown in Figure 4-9a where the misclassification mainly affects Shape 5.

4.6 Conclusions

This paper presented a novel bio-inspired design for a tactile module considering the mechanoreceptors' placement and function and the skin hardness. The compliant structure embedding the sensor allows for vibration of the MARG unit and guides forces acting on the tip area to the deep pressure sensor.

The module is tested in two experiments to study the sensors response to ridged surfaces and coarser shapes. The first experiment showed the traditional sensors in the module can detect fundamental frequencies, varying from 3.66 Hz to 11.54 Hz with an overall maximum error of ±0.1 Hz, over grating patterns sliding under the module at a velocity of 15 mm/s and 30 mm/s, respectively. This experiment also shows that such frequencies are dependent on constant orientation, velocity and pressures that are not detected in a 3-DOF robotic finger setup where such variables are not kept constant. The second experiment showed how localized features in the data collected over seven coarser shapes by sensing module while it was attached to the end of the robotic finger can be classified. The measurements were subject to wavelet decomposition and the 5th level approximation had its dimensionality reduced by 10% before the classification by a neural network. Classification accuracies from 85.1% to 98.9% for the various sensor types demonstrate the usefulness of traditional MEMS as tactile sensors embedded into flexible substrates.

The placement of sensors in the design presented in this paper focuses on dynamic simulation tasks. In future works, the module's structure should be modified to accommodate the study of static stimulation tasks as well. The future work will also concentrate on the evaluation of the proposed approach over a larger dataset, including fabrics and plastics for texture classification and on how different wavelet decomposition levels can be employed to discriminate finer texture.

The placement of sensors in the design presented in this paper focuses on dynamic simulation tasks. In future works, the module's structure should be modified to accommodate the study of static stimulation tasks as well. The future work will also concentrate on the evaluation of the proposed approach over a larger dataset, including fabrics and plastics for texture classification and on how different wavelet decomposition levels can be employed to discriminate finer texture.

Chapter 5 Bioinspired Multimodal Tactile Sensing Module

5.1 Preamble

This chapter contains the paper “Multimodal Bio-Inspired Tactile Sensing Module” [17]. This paper expands the work from paper [15] presented in the previous chapter, by presenting a novel bioinspired tactile sensing module. The novel design follows recommendations present in the main surveys of the field [5], [9] and still important as of today, as pointed out in another recent survey [93]. The design considers the relationship between mechanoreceptors, their receptive fields, their organization in layers and the compliance of the human flesh/skin to enable the module to adapt and estimate the inclination of a surface in relation to base of the module. Conforming to surfaces and estimating such angles is essential to the recognition of shape and geometry of objects as well as planning dynamic exploratory trajectories. The structure of the module satisfies requirements related to static tasks but can also be used in dynamic tasks with the advantage that the orientation of the module in relation to the surface can be estimated in an initial static probing stage and based on that kept constant. The article in this chapter contributes to the tactile sensing field with an approach that proposes a bio-inspired design of a multimodal tactile sensing module, defining sensor type and placement to mimic the function and organization of mechanoreceptors within human skin not found in the literature. The proposed module also addresses the estimation of 3D forces using a highly flexible structure an aspect that is not widely explored in the literature. The conformability of the module is also connected to the relaxation of the orientation constraint of an eventual end-effector approaching an object surface, as shown by the complementary article “End-effector approach flexibilization in a surface approximation task using a bioinspired tactile sensing module” [18] in Section 5.10.

Abstract

Tactile sensors are the last frontier to robots that can handle everyday objects and interact with humans through contact. To be effective, such sensors have to sense the geometry of touched surfaces and objects, as well as any other relevant information for their tasks such as forces, vibrations, and temperature that allow them to safely and securely interact within an environment. Given the capability of humans to easily capture and interpret tactile data, one promising direction in order to produce enhanced robotic tactile sensors is to explore and imitate human tactile sensing capabilities. In this context, this paper presents design and hardware implementation issues related to the construction a novel bio-inspired tactile sensing module. Drawing inspiration from the type, functionality and organization of cutaneous tactile elements, the proposed solution comprises two shallow sensors, namely a 32–taxel–tactile array and a 9 DOF MARG (Magnetic, Angular Rate, and Gravity) sensor, a flexible compliant structure, and a deep pressure sensor placed in a structure similar to human skin. The module's compliant structure and sensor placement provides useful data to overcome the problem of estimating non-normal forces accommodating sensing modalities essential for acquiring tactile images and classifying surfaces by vibrations and accelerations. Issues related to the module calibration, its sensing capabilities and possible real-world applications are also presented.

5.2 Introduction

The development of tactile sensors has attracted a lot of research interest over the last decades, in particular in the areas of transduction methods, materials, electronics, and intelligent data processing techniques. While very successful on various research scenarios, the adoption of such sensors in real-world robotic applications is still challenging, slow and limited to a few use cases. The ill-defined nature of tactile information turns these sensors into the last frontier to robots that can handle everyday objects and interact with humans through contact. In order to ensure a safe and efficient interaction within real-world environments, tactile sensors have to sense various stimuli related to geometric properties, forces, vibrations, and temperature. To achieve such capabilities, several design aspects have to be considered [9], including sensor type, technology and placement, electronic and mechanical hardware, methods to access and acquire

signals, calibration methods, algorithms to interpret sensed data in real-time and, in the case of multimodal sensors, solutions for the integration of signals from multiple sensing sources to ensure a robust interpretation of the acquired information.

In biological tactile systems, properties of interest such as points of contact, pressure, torsion, normal and non-normal forces (stresses) are measured due to strain and changes in the topology of the network of cutaneous tactile elements (or adaptive mechanoreceptors) present in the skin and flesh of dexterous species, in particular, human beings. In human glabrous (hairless) skin, there are four main mechanoreceptors: Meissner corpuscles, Merkel disks, Ruffini and Pacinian corpuscles, organized in deep and shallow layers. These cells are sensitive to mechanical stimuli around the skin's surfaces on areas ranging from 9 to 60mm^2. The receptive fields of such cells are combined and superimposed to achieve two point discrimination of as low as 2mm on human hands [5]. While as stated in [264], the manner in which the biological tactile sensing is acquired and processed might not always lead to best engineering solutions for tactile sensor design, it provides nevertheless a comprehensive, integrated framework for the design of sensors dedicated to robotic systems.

Drawing inspiration from the type of mechanoreceptors, their function and their organization in the human skin, this paper presents a novel bio-inspired tactile module that comprises two shallow sensors, a 32-taxel-tactile array and a 9 DOF MARG (Magnetic, Angular Rate, and Gravity) sensor, a flexible compliant structure and a deep pressure sensor. Making use of a complementary filter, the orientation of the shallow sensors can be estimated, and the force applied on these sensors is conducted through the compliant structure to the deep pressure sensor. The module's configuration expands the use of tactile sensors providing data to estimate non-normal forces without excluding modalities well developed in the literature and essential for tactile profiling and classifying surfaces by vibrations and accelerations. To further enhance sensing and obtain richer tactile information, multiple modules can be networked both physically and logically, as in the skin. It is important to state that in spite of its bio-inspiration, the tactile module is not designed to blindly mimic the distribution and function of mechanoreceptors in glabrous skin. It also takes into account practical sensor issues, such as the need to be low-cost and technology independent in order to accommodate the developments (e.g. of tactile sensing

arrays and MEMs sensors) present in the literature and the future developments within these areas.

Although there have been several efforts on developing robotic touch and related sensors that can detect multiple types of stimuli [9], the current generation of MEMs sensors have not been explored while embedded in flexible materials, and in the context of multimodal sensing. Very few solutions in the literature use more than one type of sensor to collect tactile information. Moreover, the existing solutions fail to provide an integrated approach for multimodal tactile module design, in particular for the placement of sensors within compliant structures. Finally, the majority of publications considers only normal forces and is not able to deal with non-normal forces.

To the best of our knowledge, this is the first approach to propose a bio-inspired design of a multimodal tactile sensing module, defining sensor type and placement to mimic the function and organization of mechanoreceptors within human skin. The proposed module also addresses the estimation of 3D forces and torsion, two aspects that are not widely explored in the literature.

The following section presents an overview of the relevant literature on tactile sensing and its interpretation from software and hardware points of view. Section 5.4 presents biological aspects that inspired this work, the tactile sensing module design and the behavior of its compliant structure when subject to external forces. The fabrication process of the module is presented in Section 5.5. The system components and its capabilities are detailed in Section 5.6, while module calibration is discussed in Section 5.7. The module sensing capabilities are validated in section 5.8 that also presents possible applications. Finally, insights on future work and final considerations are described in section 5.9.

5.3 Literature Review

Over the last decades, a large number of tactile sensors using various materials, structures, electronics and data processing techniques have been proposed in the literature, varying from tactile modules based on a single sensor to tactile skin comprising of grids of tactile sensing elements. A brief overview of standalone tactile sensing technologies is presented in this paper,

concentrating on the issues related to this work, while a comprehensive description of various tactile sensing aspects is available for the interested readers in [1,3].

Most of the solutions in the literature propose a single sensing technology, such as Hall effect sensors [264]–[266], barometers [101], [267], tactile sensor arrays [12], [41], [119], [120], [162], [200], [239], [268], fiber optic sensors [248], [269], other optical sensors [102], [244]–[247], and accelerometers [94], [144], [146] to acquire tactile data.

Yousefian et al. [264] design a compliant tactile sensor with a dome-like shell geometry. A magnet on the tip of the structure and 4 Hall-effect sensors allows estimating the normal and shear contact forces applied on the sensor. The authors of [265], [266] also explore the use of magnets and Hall-effect sensors in tactile setups. In [265] a small magnet immersed in a silicone body over a 1-axis Hall-effect sensor measures the magnetic field generated by the magnet, which changes when the magnet is displaced due to an applied external force. An application is presented in which the information from the sensors is combined with proprioceptive data to identify two objects: a plastic bottle and a woolen scarf wrapped in a cylindrical shape. In [266], the authors expand the initial design substituting the 1-axis Hall-effect sensor by a 3-axis one (MLX90393). The new sensory apparatus allows for the measurement of the magnet displacement and the correlated force in 3D. The authors observe the sensor output when a force is applied over a 45° angle plane and present the footprint for a printed circuit board (PCB) containing a 4x4 array of MLX90393 sensors. Being based on magnetic field measurements, is expected that the output of such sensors is affected when the sensor is used in the proximity of ferrous objects or electrical appliances.

The multimodal sensor system developed in [41] uses a 16x16 force sensing resistors array to refine 3-D shape measurements in selected areas previously monitored with a laser range finder. The system is able to recognize small-size objects that cannot be accurately differentiated through range measurements and provides an estimate of the objects' shape and orientation. In [239], the authors tackle the issues of recognition of objects from tactile displacement profiles obtained by force sensing transducers and of the recognition of textures using a rubbing motion executed by a robotic finger equipped with a dynamic tactile fingertip. Pezzementi et al. [120]

simulate the blind collection of tactile images as they would have been returned by a pressure profile tactile sensor and a bag-of-feature solution is proposed to estimate the probability of the object identity. Schneider et al. [119] use a similar approach, based on tactile images collected using a tactile sensor array of 6×14 sensing elements attached to the finger of a robot to classify industrial objects. In [200], tactile data recuperated by a 3×8 tactile array attached on each of the 3 fingers of a robot hand is viewed as time sequences, and employed to classify a set of objects, whether in a fixed or a movable position. In [101], the tactile sensor array comprises 3 barometric pressure sensor chips encapsulated within soft polymers. The authors of [162] present a tactile sensor array based on flexible piezoresistive rubber sandwiched between two substrates of PVC rubber and two substrates of conductive threads. A robotic gripper with two sensors mounted on its fingers performs a palpation procedure to acquire tactile information and to classify the palpated objects. In [12], the change in the resistance of 4 piezoresistors is proportional to longitudinal stress applied on the body of a sensor dedicated to roughness estimation.

Another category of tactile sensing solutions employs fiber optic and optical sensors. Park et al. [248] embed 4 fiber optical sensors in an exoskeletal robot finger to detect contact and control forces during fine manipulation. Fiber Bragg gratings ensure a high strain sensitivity and immunity to electromagnetic interference. De Maria et al.'s tactile sensor [244] contains a matrix of LED-phototransistor couples embedded in a hemisphere-shaped deformable elastic layer. The deformable layer transduces external forces and torques into local deformations and these, in turn, produce a variation of reflected light intensity and of the photo-current flowing in the photodetectors. In [245], an model of the same sensor based on an extended Kalman filter allows to reconstruct the position and orientation of the surface in contact with a rigid object. The friction coefficient is then estimated based on the contact plane position and orientation information together with the contact force vector measured by the sensor. A slippage control algorithm is proposed for manipulation tasks [246].

The authors of [102] develop a sensor based on the morphology of the fingertip skin features and on the role of Meissner's corpuscles in encoding tactile edge information. The sensor comprises a thin flexible rubber skin with structural details and encases a clear, compliant polymer melt blend. An embedded CCD camera tracks markers on the internal structural details of the rubber

skin, illuminated by 4 infrared LEDs enabling detection of surface deflections. The sensor is employed in [247] to detect object edges in the context of a robotic contour following task.

Dallaire et al. [144] use a steel stylus attached to a triple axis digital MEMs accelerometer to gather information about a surface through a rubbing action, while the surface is rotated by a turntable. An unsupervised learning scheme is then proposed for surface identification (i.e. linoleum, leatherette, grass carpet, etc.). Sinapov et al. [146] use a three-axis accelerometer to capture vibrotactile feedback as a robot is performing a scratching motion over 20 surfaces in order to recognize the material using machine learning approaches.

All standalone sensing technologies are subject to specific drawbacks. The use of magnetic sensors is limited to nonmagnetic environments. Tactile sensors array are in general associated with the lack of contact force measurement [5] and their stiff backing impedes the collection of data over arbitrarily curved surfaces. Fiber optic sensors are expensive and difficult to integrate in tactile modules due to the bending losses in the fiber routing [244]. CCD camera solutions involve generally a high cost and weight, while the loss of light due to microbending or chirping causes distortion is the measured data [5]. To partly eliminate the drawbacks associated to one single technology, a few solutions capitalize on the use of multiple sensor technologies for recuperating tactile information [13], [94], [144], [250]. Chathuranga et al. [250] develop a fingertip sensor equipped with 7 flexible force sensors and 5 accelerometers embedded in polyurethane rubber and wrapped in a ridged rubber layer. Its proposed use is for the classification of wood samples by rubbing over their surface. A data-driven analysis to the problem of sensor selection in the contour following for shape discrimination tasks is presented in [13]. Data collected from the motors, an inertial measurement unit, and a magnetometer attached to a 4-DOF robotic finger, during the exploration of 7 synthetic shapes are analyzed using principal component analysis and a multilayer perceptron neural network is trained to classify the shapes. Kroemer et al.'s [94] tactile sensor consists of a compliant pin that makes contact with a surface and a capacitor microphone that detects the vibrations of the pin. A multisensory data fusion algorithm combines readings from the pin with vision data collected with a camera to classify rich-textured surfaces.

While multimodal systems allow acquiring a more complete description of tactile information, they come with various challenges including: the choice of sensor types to be employed, the placement of sensors within compliant structures, the data preprocessing procedure required to make sense of the collected data and the integration of signals from multiple sensing sources for a robust interpretation. Following a series of papers available in the literature [12], [102], [246], [247], [250], [264], a novel bio-inspired approach is proposed in this paper to tackle some of the above-mentioned challenges. To the best of the authors' knowledge, the proposed multimodal module is the only one that defines the sensor type and placement to mimic the function and organization of mechanoreceptors within human skin, as further described in the following section.

5.4 Bio-Inspired Tactile Sensing Module

5.4.1 Biological Tactile Sensing

Human touch sensing and perception is the result of complex investigatory handling involving two distinct sensing components: *cutaneous information*, retrieved by tactile receptors embedded in the skin, regarding the topology, texture, contact force, and elasticity of the touched object's surface, and *kinesthetic information* about the position and velocity of the

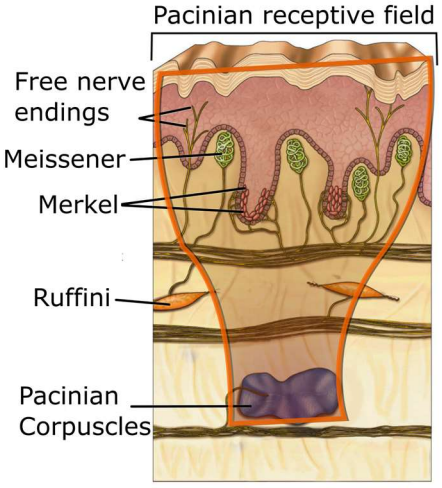

Figure 5-1 Human skin mechanoreceptors, adapted from [6] and an illustration of Pacinian corpuscle receptive field.

kinematic structure of the hand retrieved by receptors within muscle, tendons and joints [5], [225].

According to Loomis and Lederman [253], tactile perception is referring to sensing capabilities mediated by cutaneous stimulation, involving a physical contact with the stimuli [225]. The human hand contains four types of cutaneous sensing elements, or adaptive mechanoreceptors, distributed within the skin [6], [235], namely Meissner's corpuscles, Merkel's disks, Pacinian corpuscles and Ruffini corpuscles, as illustrated in Figure 5-1.

Based on their localization, they can be characterized as: shallow (Meissner and Merkel) or deep (Pacinian and Ruffini). According to their speed of adaptation, they can be classified as slow adapting – meaning they can detect constant stimuli, such as constant pressure or skin stretch (Merkel and Ruffini belong to this category), or fast adapting – meaning that they are able to detect only short pulses, such as initial contact (Meissner and Pacinian are fast adapting receptors). While their exact role, function and properties are not yet completely known and understood, Table 5-1 summarizes aspects presented in neuroscience and experimental psychology [5], [6], [254], that contain relevant information on the mechanoreceptors for the design of the proposed tactile sensing module. It is worth noting that these mechanoreceptors are not working independently to ensure the perception of stimuli, but they work together to achieve this task. For example, in the context of edge detection, small and sharp borders are perceived by Meissner and Merkel corpuscles, while large, vague borders are sensed by Pacinian and Ruffini. Both slow adaptive and fast adaptive receptors respond simultaneously at edges and borders, but at other points, fast adaptive receptors do not fire. Moreover, the response of slow adaptive receptors is higher at edges than on uniform surfaces. The sensitivity of the receptors not only to the curvature, but to the rate of change of curvature, implies that robotic tactile sensors should be able to detect and measure both static and dynamic stimuli [5].

Some mechanoreceptors are more specialized in static exploration, while others in dynamic scenarios. Static tactile exploration predominantly consists of pressing the hand, and hence the tactile sensing elements against the surface or object being explored. Temperature, hardness, and profile are some of the features that can be detected by static touch. On the other hand, the movements performed while gathering tactile data also play a significant role in the haptic object exploration. Dynamic tactile information is obtained by sliding the skin ridges on the surface of

the explored objects. Properties such as friction, smoothness, roughness, slipperiness, or stickiness can be hardly estimated without it [238].

Table 5-1 Properties and Functions of mechanoreceptors

Receptor	Properties and functions
Merkel disks	• *Location*: Shallow • *Receptive field*: small (2-3mm) • *Functions*: form/shape detection; texture detection, fine details discrimination, constant pressure, presence, location and static deformation at points and edges; curvature detection; tactile flow perception;
Ruffini corpuscles	• *Location*: Deep • *Receptive field*: large (larger than 10 mm) • *Functions*: directional (lateral) skin stretch; direction of object motion; position of hand and fingers; slip detection; stable grasp; tangential force estimation; tension (continuous touch or pressure)
Meissner corpuscles	• *Location*: Shallow • *Receptive field*: small (3-5 mm) • *Functions*: motion detection; velocity; slippage; low frequency vibration; local skin deformation; tactile flow perception; grip control; flutter; dynamic deformation; two-point discrimination; encode normal (horizontal) strain forces
Pacinian corpuscles	• *Location*: Deep • *Receptive field*: large (larger than 20 mm) • *Functions*: deep pressure; pressure change; un-localized high frequency vibration; body contact when grasping an object (tool use)

5.4.2 Bio-Inspired Tactile Sensing Module Design

The design of the tactile sensing module rose from the need to measure touch properties going beyond normal forces (stress) that are sensed by most current tactile sensing technologies. To do so, we did not simply apply concepts from the mechanoreceptors present in glabrous skin, but we also explored its layered organization and the functional relationships. Our tactile module consists of two shallow sensors, a 32-taxels array and a 9-DOF MARG (Magnetic, Angular Rate,

and Gravity) sensor, a flexible compliant structure and a deep pressure sensor, as shown in Figure 5-2.

The shallow sensors (Figure 5-2.1 and Figure 5-2.2) emulate the functionalities of Merkel cells and Meissner's corpuscles. The tactile array and the gravity field sensor measure together contact points, force magnitudes, and provide a rough orientation of the surface of the "skin", as Merkel cells do. The angular rate sensor, part of the MARG unit (Figure 5-2.2), measures vibrations on the higher levels of the module. Ruffini endings have the function of providing form and stretch information emulated by the magnetic field sensor (part of the MARG unit as well). The deep pressure sensor (Figure 5-2.4) reproduces the Pacinian corpuscles functions of sensing pressure on the lower levels of the module.

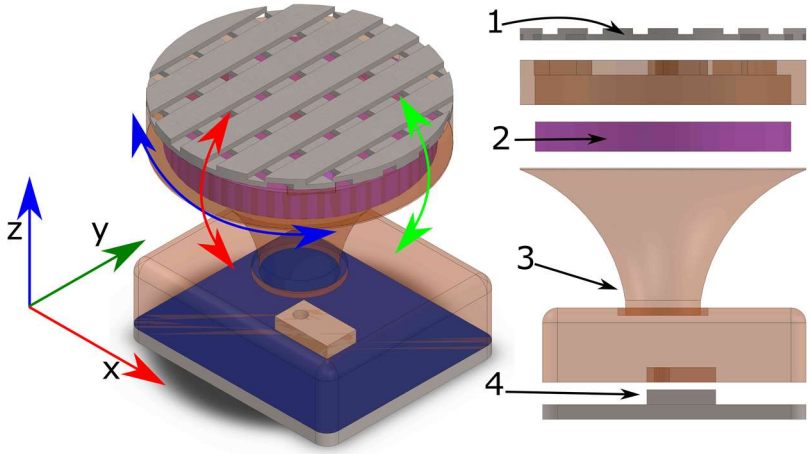

Figure 5-2 Components of the tactile sensing module: 1 – Tactile array, 32 taxels; 2 – MARG (Magnetic, Angular Rate, and Gravity) system; 3 – compliant structure; 4 – barometer.

The compliant structure connects the shallow and deep sensors (Figure 5-2.3). This structure performs the role of the receptive field (Figure 5-1) defining the spatial resolution of the deep pressure sensor and conducts the forces applied on the surface of the module to the deep pressure sensor. It also allows upper level sensors of the module to rotate when torque or shear forces are applied on the shallow levels of the sensor.

This layered structure also emphasizes the various spatial resolution levels present in human skin, where Pacinian corpuscles have the largest receptive field area, while Merkel cells have the finest resolution (Table 5-1). In humans, this is important while encoding multi-resolution tactile

information [270]. This contrasts with many works that only partially reproduce the functionality of Merkel cells by means of thin tactile arrays supported on top of rigid surfaces [2], [9].

The following paragraphs discuss briefly the working principle of the sensors included in our tactile module:

5.4.2.1 Piezo-resistive Tactile Array:

Tactile arrays are the most developed and explored category of tactile sensors in the literature. Multimodal approaches cannot ignore the past advances in the applications such sensors. The sensing principle of tactile arrays is simple. Tactile arrays are formed from groups of tactile sensing elements called taxels, each taxel being a region where two sensing electrodes superimpose. When electrodes placed on both sides of a pressure-sensitive conductive material move closer to each other due to a force being applied in one of the sensing planes, the electrical resistance across the intersection of the electrodes decreases. This change in resistance is proportional to the normal force being applied to each sensing element. Tactile arrays are traditionally used in static tactile profiling (static sensing) [41] and more recently in dynamic sensing [162], [200] for object classification while performing a palpation-like motion.

The tactile array used in our module consists of conductive threads and a piezoresistive polymeric foil (polyolefins) impregnated with carbon black. This component of the module is similar to the one presented in [162], but it could be replaced by any alternative solution, for example, the ones presented in [41], [200] or [271]. The essential requirement for a tactile array is to have an electrical resistance or capacitance between opposing electrodes varying due to strain on the sensing plane.

The piezo-resistive tactile array chosen in our design is sufficient to measure changes in resistance at each taxel. Furthermore, as demonstrated in [272], such sensors can be characterized by a high sensitivity, a high repeatability, can achieve a high spatial resolution and can be easily integrated. Moreover, [162] and [200] show that such sensors can be extremely useful when classifying objects by touch, one of the desired characteristics that will enhance the sensing capabilities of the proposed bio-inspired module. It is also worth mentioning that even in those cases when this layer gets damaged during the interaction with a surface, contact with

objects can still be detected by the deep pressure sensor, from where stems the interest of building multimodal sensing modules.

5.4.2.2 Gravity (field) sensor – Accelerometer:

Tactile arrays provide data about contact points and normal forces but, when placed on a compliant support, they lack the means to track topological changes, such as when taxels change their position or orientation with respect to other taxels. To partially tackle this issue, we add an accelerometer to observe how the shallow sensors are oriented with respect to the gravity field.

The proposed module encompasses a 3DOF accelerometer placed right below the tactile array (Figure 5-2.2). The accelerometer provides information beyond the (static) orientation of the shallow sensors relative to a gravity frame. It is also useful to detect light touch and vibrations. Dynamic exploration tasks such as the identification of shapes and textures benefit from the data collected by accelerometers, both in the cases where the sensor is still and the object is moving [144] and in the scenarios where the sensor is moving and the object is static [16].

The combination of the tactile array and the accelerometer ensures a behavior of the tactile module resembling the one of Merkel cells within human skin.

5.4.2.3 Angular rate sensor – Gyroscope:

While accelerometers measure the orientation of shallow sensors related to a gravity field, the angular rate sensor measures the angular velocity related to the sensor itself. MEMs rate gyroscopes (or Type II gyroscopes according to [273]) use the Coriolis effect that appears in rotating reference frames to measure rotation. A vibrating proof mass suspended above the substrate by anchored compliant flexures is free to oscillate in two orthogonal directions: the drive direction and the sense direction. The drive is usually excited by electrostatic forces to a constant amplitude of oscillation, while the rotation-induced Coriolis force triggers the sense direction.

The proposed module encompasses a 3DOF gyroscope embedded in the same integrated circuit (MARG unit) of the accelerometer placed below the tactile array. The gyroscope collects data

about the rate of vibrations onto the shallow sensors, and is useful in detecting light touch, shape and textures classification [16], slippage and even speech [274]. The measured data acquired by this sensor simulates the one recuperated by Meissner cells within the glabrous skin.

5.4.2.4 Magnetic (field) sensor – Magnetometer:

Hall effect sensors are the basic tool for sensing magnitude and direction of magnetic fields enabling proximity switching, current sensing and positioning applications. MEMs magnetometers were initially based on Hall effect sensors, but nowadays most MEMs magnetometers are based on anisotropic magnetoresistance (AMR) [275].

The proposed tactile module uses a 3DOF magnetometer to sense the orientation of the shallow sensors according to a reference magnetic field that can be earth's magnetic field or a local magnetic field induced by permanent magnets. Small permanent magnets can be used as local reference frames while measuring stretch or deformation of flexible substrates. Magnetometers can also be used as proprioception sensors measuring joint effort due to motor torque [13]. The authors of [264], [276] show how Hall effect sensors can be employed to sense deformations in a hollow sphere or flexure of a joint in a compliant finger. Relying solely on magnetic measurements is not an ideal scenario for tactile sensing due to the magnetic interference when touching ferrous objects or when working in ferrous environments. This is one of the reasons we use an accelerometer, gyroscope and magnetometer in the same integrated circuit. The capability of this component of our tactile module to provide form and stretch information mimics the functionality of Ruffini endings.

5.4.2.5 Deep pressure sensor – Barometer:

Pressure is one of the essential properties of interest on tasks involving tactile sensing. Recently, barometric pressure sensors made their appearance in the tactile sensing field [101], [267]. Initially conceived to measure atmospheric pressure, these sensors were encompassed in the tactile sensing domain by the substitution of the atmosphere by rubber or an envelope surrounding the transducer. The authors of [101] introduced the idea of casting the barometric pressure sensors in rubber, isolating the transducer from the atmosphere, sensing pressure due to deformations in rubber. The authors of [267] encapsulate barometers in an air tight cushion

made of a foam core coated with rubber. Both approaches are affected by the tactile inversion problem [37] and are not easily converted to solutions as the one presented in [45]. The tactile inversion problem is due to the addition of elastic layers on tactile sensing structures and consists on computing the changes on the surface of these elastic layers from the sensed data gathered through the elastic medium at the sensing points [2].

The proposed module encompasses a MEMs barometer embedded in a compliant structure (described in detail in the next section) that tackles the tactile inversion problem by conducting forces applied to shallow sensors to the ventilation window (Fig. 5a). This component of the tactile module reproduces the functions of Pacinian corpuscles in sensing deep pressure and pressure changes (Table 5-1).

5.4.3 Study of the Compliant Structure Behavior

The richness of biological tactile sensors (e.g. human skin) relies on the mechanoreceptors placement in layers, their redundant relationship and the fact that such sensors seat on top of a highly compliant layer (e.g. human flesh). The design proposed in this module is bio-inspired and tries to accommodate such aspects.

However, the behavior of compliant structures underlying tactile sensors is not entirely understood due to the challenges that arise from such structures, including sensor placements, the tactile inversion problem, and the difficult task of tracking changes in the topology of such structures while interacting with objects through touch.

The structure proposed in the tactile module is shown in Figure 5-2.3. It is composed of a base encasing the deep pressure sensor (barometer) and a funnel-like part supporting the shallow sensors. The funnel is connected to the base encasing in a circular indentation concentric, along the z-axis, to the barometer ventilation window. The main goal of this structure is to conduct forces applied to the shallow sensors to the deep pressure sensor. This structure and the sensors placement allow the module to conform to the surface of objects while tackling the tactile inversion problem.

In order to evaluate the sensor placement and the behavior of the compliant structure while conducting forces applied to shallow sensors, two scenarios are simulated. The first one evaluates the sensor placement effectiveness when forces resulting from contact are concentrated in a region aligned to the center of the face that supports the shallow sensors (Figure 5-3).

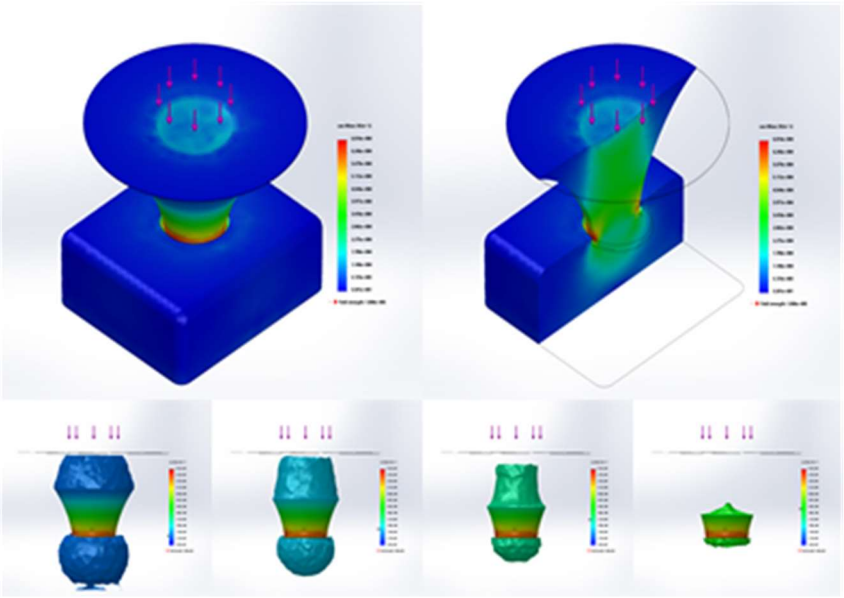

Figure 5-3 Force applied to the region on the center module's surface.

The second one shows the sensor structure response to forces acting in an off-centered area of the supporting face (Figure 5-4). The simulations were carried out using the SolidWorks© Simulation package. In the simulations, the material used for the compliant structure is assumed to be isotropic, linear elastic with an elastic modulus of 1.8e+5 N/m2, a Poisson's ratio of 0.49 and a density of 1123 kg/m3. These properties are believed to provide a good approximation of the polyurethane rubber used in the sensor's fabrication. Figure 3 shows the levels of stress along the structure while subjected to a load of 7N in a circular region (6mm of diameter) concentric to the face that supports the shallow sensors. In the figure, the highest stress (von Mises stress) level is 6.8e+4 N/m2, in red, while blue represents the lowest stress level of 5.58e+1 N/m2. Figure 5-4 shows the levels of stress along the structure while conforming to a load of 7N in a circular region (6mm of diameter) off the center of the surface that supports the shallow sensors. The highest stress level is in this case 5.2e+5 N/m2, shown in red, while the lowest stress level,

shown in blue, is of 6.3e+1 N/m2. The miniatures on Figure 5-3 and Figure 5-4 show different cutoff stress levels. Based on these, it was decided to place the pressure sensor on the bottom of the mid-lower stress level region, below the circular indentation that connects the funnel and the base.

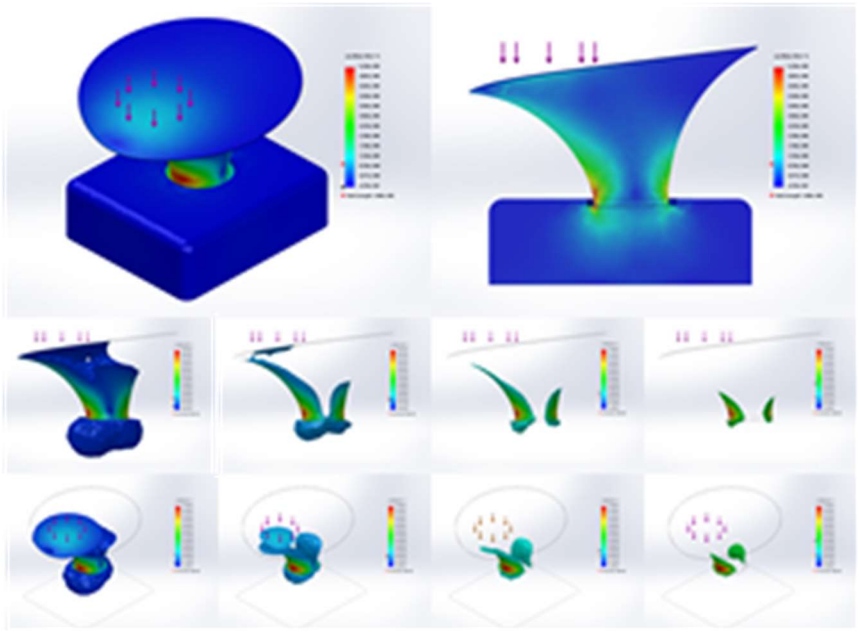

Figure 5-4 Force applied to the region out of the center module's surface.

As one can notice, in both cases, the higher stress levels are present above the barometer's ventilation window, at the indentation that connects the funnel to the base. The placement of the deep pressure sensor at this location allows it to measure forces from the surface in a range between 270 gf when the sensor is being compressed to 330 gf when the sensor is being stretched, as validated experimentally in section 5.7 of the paper (Figure 5-10).

Dahiya et al. [9] state that tactile modules are expected to be mechanically flexible in order to be able to conform to arbitrarily curved surfaces. However, the compliance due to embedding sensors in flexible structures brings challenges such as blurring or spatial filtering, and positional uncertainty in locating the contact point. The proposed module not only conforms to surfaces being touched, but also reduces the blurring by conducting forces to the deep pressure sensor and makes use of the shallow sensors to determine contact points.

5.4.4 Comparison with Other Sensors from the Literature

Table 5-2 summarizes the features of the proposed tactile sensing module in comparison with the closest solutions available in the literature. Unlike our module, the module from [264] relies solely on magnetic sensors. It adds a compliant structure, but still lacks support for a tactile array and the means to calculate the orientation of the surface in contact to objects, e.g. in twisting motions. The work presented in [113], proposes a tactile cell that uses accelerometers to calculate the orientation of a hexagonal module, while attractive, this approach lacks a second source of information invariant to accelerations due to impacts in early stages of touch. For example, if the orientation of a module is estimated based only on the gravity vector, the estimate will be corrupted when external accelerations are applied to the module. The addition of a 3-axis gyroscope, a 3-axis magnetometer, the support for a tactile array, and the compliant structure presented here mitigate such disadvantage.

Table 5-2 Sensing Modules comparison

	S. Youssefian *et. al.*, [264]	**Mittendorfer, [113]**	**Proposed Module**
Size (mm^2)	9.5mm of radius	510mm	15mm of diameter
Optical		✓	
Tactile Array			✓
Temperature		✓	✓
Accelerations		✓	✓
Angular Velocities			✓
Magnetic	✓		✓
Strain	✓		✓
Compliant Structure	✓		✓

The size of the tactile module is 15x18x18mm^3 and is in line with the existing solutions in the literature. The density of sensors is one pressure sensor with one embedded thermometer in the deep level plus a 9DOF MARG system with another embedded thermometer and a 32 piezo-resistive taxels tactile array in the shallow level. These add up to 12 sensors and 32 taxels in a volume of 15x18x18mm^3, without counting the structure engineered to conduct forces to the deep pressure sensor. The total volume of the module could be reduced by placing the capacitors

and pull-up resistors required by the TWI (two wire interface) and RC low pass power supply filter off the sensor's PCBs. Reallocating these components out of the module is however an engineering trade-off between the PCB footprint and the noise added to a system by having these filters far from the sensors. However, this issue and the one of the module's miniaturization are out of the scope of this article.

5.5 Sensing Module fabrication (Prototyping)

The module prototype was fabricated using a 3D printed molding and polyurethane casting process, as shown in Figure 5-5. The process can be divided into three steps: (1) casting of the deep pressure sensor and compliant structure Figure 5-5a-c, (2) casting of the MARG system and bonding to the compliant structure Figure 5-5d-f, and (3) finishing and tactile array attachment Figure 5-5g-i.

The first step is to cast the deep pressure sensor, Figure 5-5a-c. The mold for the base and the funnel is 3D printed (Figure 5-5a, light blue) and fixed around the barometer printed circuit board (PCB) (Figure 5-5, dark blue). Liquid polyurethane is poured into the mold. Due to the superficial resistance and the gases in the liquid, the polyurethane cannot fill up the casing through the narrow ventilation window. After degassing in a vacuum chamber for 4 minutes under 27 inHg of pressure air, bubbles in the liquid and the gap surrounding the barometer are removed. The polyurethane is cured at room temperature for 16 hours, but higher temperatures could accelerate the process. The second step is to cast and bond the MARG system to the compliant structure. The casting uses a positioning mold (shown in light blue in Figure 5-5d-f) and is done in a similar fashion as the one previously described, with the difference that the MARG system is bond to the compliant structure before curing. Figure 5-5f shows the MARG system and compliant structure bond. The mold for the compliant structure is removed prior to this point. In the third and final step, the positioning mold for the MARG system is removed (Figure 5-5g), the resulting gaps are filled up (Figure 5-5h) and the tactile array is attached on the top of the sensor (Figure 5-5i).

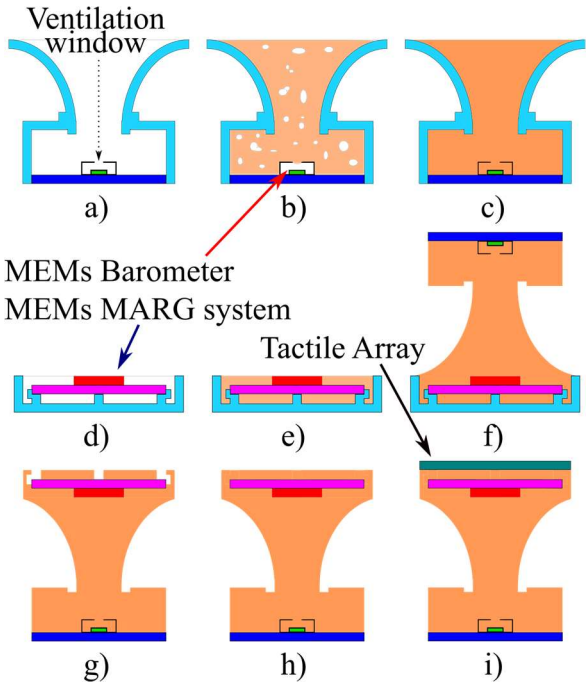

Figure 5-5 Fabrication process: a) The barometer PCB is connected to a 3D printed mold (light blue); b) polyurethane (shown in orange) is cast into the mold; c) structure after degassing; d) MARG system is placed on the 3D printed mold; e) polyurethane is cast around MARG system; f) the barometer and the compliant structure are connected to the MARG system; g, h) the 3D printed mold is removed and positioning gaps are filled; i) tactile array added to the module.

The casting material is polyurethane rubber (Vitaflex 20 Shore A from SmoothOn). It was chosen for its high durability, stretchability (elongation at break: 1000%) and the possibility of casting at room temperature. The mixed viscosity of 1000 cps also allows for the filling of the features of the molds and barometer. The barometer used was the Freescale MPL115A2 with dimensions 5x3x1 mm^3, mounted on a PCB of 15x18mm^2. The MARG system is the STMicroelectronics LSM9DS0 with dimensions 4x4x1 mm^3 mounted on a round PCB with 15 mm of diameter. The tactile array has 32 sensing elements and was custom-made from conductive thread and piezoresistive plastic (Velostat), similar to the one in [162].

The prototype resulting from the process is shown in Figure 5-6. Even though this prototype was built around specific MEMs sensors, the latter do not represent a constraint. The module could be built using sensors from other manufacturers.

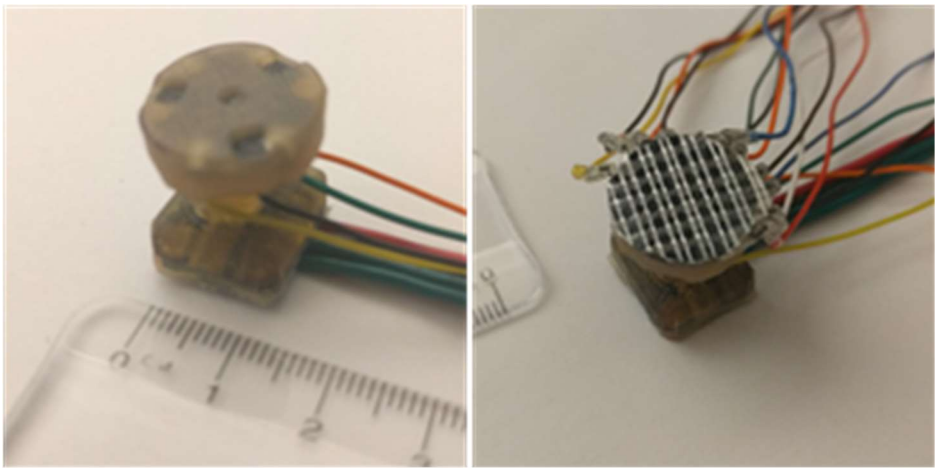

a) b)

Figure 5-6 a) *Integration of the pressure sensor and MARG system; and* b) *tactile array added to the module.*

5.6 System Components

The interface between the tactile tensing module and the computing system is achieved by integrating the module in a dedicated electronic circuitry using three 32-bit ARM MK20DX256VLH7 Microcontroller Units (MCU) from Freescale Semiconductor, denoted as MCU A, B and O in Figure 5-7. The system employs 3 MCUs to take full advantage of the sensors. The use of dedicated MCUs enables the system to take advantage of the highest sampling rates for each group of sensors. The MCUs run embedded versions of the Robotic Operating System (ROS) rosserial nodes.

MCU A measures the resistance across rows and columns of the tactile array using one multiplexer assigned to the rows and other to the columns (not shown in Figure 5-7 for sake of simplicity). This MCU uses 16-bit analog to digital converters (ADCs). MCU B collects temperature and pressure measurements from the barometer. MCU O gathers temperature, angular velocities, accelerations, and magnetic field measurements form the shallow sensors. MCUs B and O communicate with the sensing units through I^2C protocols. All MCUs run at 96MHz and communicate to the computer through USB/serial connections at 256000 bauds. Multiplexers could be added between microcontroller units and sensors to add several modules in a network.

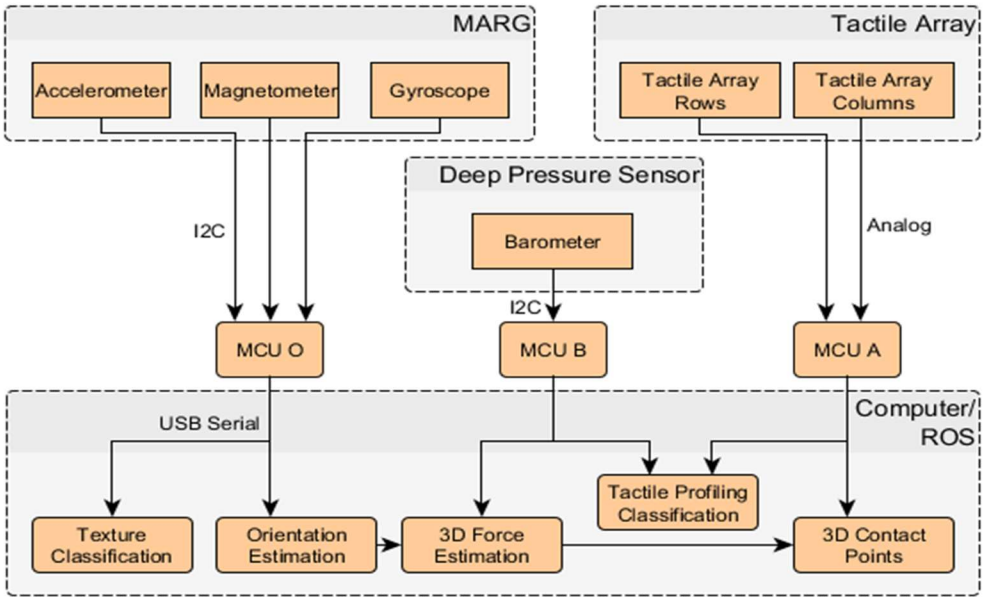

Figure 5-7 System components and examples of applications.

The module is designed to enable various tasks that require tactile information (lower part of Figure 5-7), for example, object recognition through tactile profile or texture classification. Such tasks make use of tactile images and sequential tactile data.

Tactile profiling classification consists on identifying objects through tactile profiles gathered by arrays of sensing elements organized in a structured topology that resembles digital images. Such tactile images can be filtered and then classified by a combination of neural networks as we demonstrate in [16].

Texture classification consists on analyzing the signals that arise from sliding motions while tactile sensors are exploring surfaces. The changes in accelerations, angular velocities and orientations carry features that can be extracted and classified from these signals. In [14], [16], we demonstrate how the signals from a MARG system can have their dimensionality reduced by Principal Component Analysis (PCA) and be classified by a multilayer perceptron neural network in order to discriminate among a group of textures .

These are the reasons why the module encompasses a tactile array and the other shallow sensors onto a compliant structure that conforms to the surface of the objects and allows vibrations.

The module also considers control tasks that require information about how the surface of a compliant substrate deforms due to touch forces. As in the human skin, the level of detail required depends on the task to be performed, from orientation estimation of the shallow sensors to 3D force and 3D contact vectors estimation. To calculate 3D forces and 3D contact points it is necessary to compute the orientation of shallow sensors. The base of all control tasks that the module enables is the orientation estimation. The authors of [277], [278] and [279] present alternative solutions to estimate the orientation of MARG systems.

5.6.1 Orientation Estimation

The orientation estimation method employed here follows the concepts of [278] and [279], starting with the classical prediction of the orientation from the numerical integration of the angular velocity from [277]:

$$ {}^{G}_{L}\dot{\boldsymbol{q}}_{\omega,t_k} = \frac{1}{2}\, {}^{G}_{L}\widehat{\boldsymbol{q}}_{t_{k-1}} \otimes {}^{L}\boldsymbol{\omega}_{q,t_k} \qquad (1) $$

$$ {}^{L}_{G}\boldsymbol{q}_{\omega,t_k} = {}^{L}_{G}\widehat{\boldsymbol{q}}_{t_{k-1}} + {}^{L}_{G}\dot{\boldsymbol{q}}_{\omega,t_k}\boldsymbol{\Delta}t \qquad (2) $$

where ${}^{L}_{G}\boldsymbol{q}_{\omega,t_k}$ is the quaternion that represents the orientation of the shallow sensors frame (L) relative to earth frame (G), estimated based on the angular velocity; ${}^{L}\boldsymbol{\omega}_{q,t_k}$ is the angular velocity in vector format; ${}^{L}_{G}\widehat{\boldsymbol{q}}_{t_{k-1}}$ is the normalized quaternion estimate at time t_{k-1} and $\boldsymbol{\Delta}t$ is the sampling period; and $\otimes$ is the quaternion product.

The initial estimate of the orientation of the shallow sensors based on the angular velocity is important in the tactile realm because it is robust against changes in acceleration due to impact or touch when compared to gravity-only based solutions [113], or magnetic-only solutions subjected to unwanted magnetic flux when handling ferromagnetic objects [264]. On the other hand, due to the imperfections (e.g. manufacturing process) on gyroscopes and to the errors introduced by the numerical integration, the orientation estimate has to be corrected by the measurements of the gravity and magnetic fields when they are not subjected to high non-gravitational accelerations or magnetic disturbances.

The correction of the orientation estimation based on angular rate is achieved using a double correction given by:

$$ {}^{L}_{G}\boldsymbol{q} = {}^{L}_{G}\boldsymbol{q}_{\omega} \otimes \widehat{\boldsymbol{\Delta q}}_{acc} \otimes \widehat{\boldsymbol{\Delta q}}_{mag} \tag{3} $$

where the correction based on gravitational field $\widehat{\boldsymbol{\Delta q}}_{acc}$ is the tilt quaternion that corrects the estimate on the roll and pitch angles calculated based on the following assumption:

$$ \boldsymbol{R}({}^{G}_{L}\boldsymbol{q}_{\omega})\,{}^{L}\boldsymbol{a} = {}^{G}\boldsymbol{g}_{p} \tag{4} $$

where the predicted gravity ${}^{G}\boldsymbol{g}_{p}$ is the measured acceleration ${}^{L}\boldsymbol{a}$ rotated by the predicted quaternion ${}^{G}_{L}\boldsymbol{q}_{\omega}$. $\boldsymbol{\Delta q}_{acc}$ is the delta quaternion that represents the small deviation between the predicted gravity and the real gravity vector, and is calculated based on the ${}^{G}\boldsymbol{g}_{p}$ and the assumption that the real gravity vector ${}^{G}\boldsymbol{g}$ points down.

$$ \begin{aligned} &\left(\boldsymbol{R}(\boldsymbol{\Delta q}_{acc})\,{}^{G}\boldsymbol{g} = {}^{G}\boldsymbol{g}_{p}\right) \Rightarrow \\ &\boldsymbol{R}(\boldsymbol{\Delta q}_{acc})[0 \quad 0 \quad 1]^{T} = [g_x \quad g_y \quad g_z]^{T} \end{aligned} \tag{5} $$

The authors of [279] algebraically determine that $\boldsymbol{\Delta q}_{acc}$ has no influence on the yaw correction, thus its correspondent component is equal to 0.

$$ \boldsymbol{\Delta q}_{acc} = \begin{bmatrix} \sqrt{\dfrac{g_z + 1}{2}} & -\dfrac{g_y}{\sqrt{2(g_z+1)}} & \dfrac{g_x}{\sqrt{2(g_z+1)}} & 0 \end{bmatrix}^{T} \tag{6} $$

The correction based on $\boldsymbol{\Delta q}_{acc}$ is then filtered by a complementary filter:

$$ \overline{\boldsymbol{\Delta q}_{acc}} = (1-\alpha)\boldsymbol{q}_{\boldsymbol{I}} + \alpha\boldsymbol{\Delta q}_{acc} \tag{7} $$

where $\alpha \in [0,1]$ is the filter adaptive gain that characterizes the cut-off frequency, while α is adjusted according to the presence and magnitude of non-gravitational accelerations [279]. The filtered correction is then normalized:

$$ \widehat{\boldsymbol{\Delta q}}_{acc} = \frac{\overline{\boldsymbol{\Delta q}_{acc}}}{||\overline{\boldsymbol{\Delta q}_{acc}}||} \tag{8} $$

The correction based on the magnetic field measurement follows the same idea but starts with the partially corrected orientation ${}^{L}_{G}\boldsymbol{q}'$:

$$ ({}^{L}_{G}\boldsymbol{q}' = {}^{L}_{G}\boldsymbol{q}_{\omega} \otimes \widehat{\boldsymbol{\Delta q}}_{acc}) \Rightarrow \boldsymbol{R}({}^{G}_{L}\boldsymbol{q}')\,{}^{L}\boldsymbol{m} = \boldsymbol{l} \tag{9} $$

here ${}^{L}\boldsymbol{m}$ is the magnetic field observed by the sensor and $\boldsymbol{l}$ is the observation rotated by ${}^{G}_{L}\boldsymbol{q}'$. The assumption to find the yaw correction is to align the *x*-axis to magnetic north:

$$\boldsymbol{R}(\boldsymbol{\Delta q}_{mag})\boldsymbol{l} = {}^{G}\boldsymbol{\Pi}_{zx^+} \Rightarrow$$
$$\boldsymbol{R}(\boldsymbol{\Delta q}_{mag})[l_x \quad l_y \quad l_z]^T = [\sqrt{\Gamma} \quad 0 \quad l_z]^T, \Gamma = l_x^2 + l_y^2 \tag{10}$$

Eq. 10 can be algebraically solved to find the yaw correction quaternion $\boldsymbol{\Delta q}_{mag}$ based on the magnetic observation [279].

$$\boldsymbol{\Delta q}_{mag} = \left[\frac{\sqrt{\Gamma + l_x\sqrt{\Gamma}}}{2\sqrt{\Gamma}} \quad 0 \quad 0 \quad \frac{l_y}{\sqrt{2(\Gamma + l_x\sqrt{\Gamma})}}\right]^T \tag{11}$$

To find $\widehat{\boldsymbol{\Delta q}}_{mag}$, $\boldsymbol{\Delta q}_{mag}$ is filtered and normalized as in Eq. 7 and 8 respectively.

5.6.2 3D Force and Contact Points Estimation

The components of the 3D forces acting on the deep and shallow pressure sensors are calculated using ${}^{G}_{L}\boldsymbol{q}$ from Eq. 3 and the scalar measurements of the barometer and tactile array f'_{Bz} and $f'_{(ij)Az}$ respectively (illustrated in Figure 5-8).

$$\boldsymbol{R}({}^{G}_{L}\boldsymbol{q})[0 \quad 0 \quad f'_{Bz}]^T = {}^{G}[f_{Bx} \quad f_{By} \quad f_{Bz}]^T \tag{12}$$

$$\boldsymbol{R}({}^{G}_{L}\boldsymbol{q})[i \quad j \quad f'_{Az}]^T = {}^{G}[f_{Ax} \quad f_{Ay} \quad f_{Az}]^T \tag{13}$$

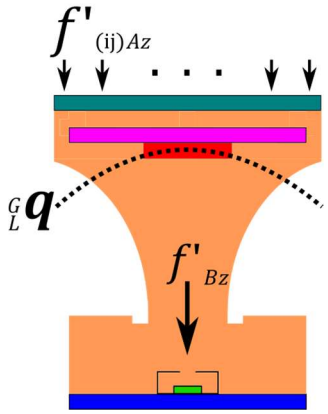

Figure 5-8 Tactile module forces and orientation, f'_{Bz} denotes the scalar component of the force applied on the deep pressure sensor; ${}^{G}_{L}\boldsymbol{q}$ is the orientation estimation along the (compliance hemisphere) curvature path (dashed line); $f'_{(ij)Az}$ is the force exerted on the taxel at row i *column* j.

5.7 Sensing Module Calibration

Regarding the shallow sensors, the calibration of the MARG system follows the ellipsoid fitting method as described in [280]. The MARG system had its measurement range configured to ±6g (0.183 mg/LSB - least significant bit) for the linear acceleration, ±8Gs (gauss) (0.32 mgauss/LSB) for the magnetic field range and ±500dps (degrees per second) (17.50 mdps/digit) for the angular velocity sensor. The linear acceleration sensitivity change vs. temperature is ±1.5% from -40 °C to +85 °C, the magnetic sensitivity change vs. temperature is ±3% from -40 °C to +85 °C, the angular rate sensitivity change vs. temperature is ±2% from -40 °C to +85 °C. As stated in the datasheet provided by the manufacturer [257] the MEMs is calibrated for 3.0V, the same voltage supplied in all the experiments in this article. Before initializing the orientation estimation, the sensors collect raw data for 5 seconds and a bias is calculated for each axis of the MARG system, after that the bias is removed and the orientation estimation filter is applied.

In order to calibrate the deep pressure sensor, we have used the experimental setup from *Figure 5-9*. The experiments consisted in vertically pushing the module against a reference load cell, as illustrated *Figure 5-9*b. Figure 5-10 shows, in red, the relationship between the forces observed by the load cell and the raw sensor output while the linear actuator is compressing the module against the load cell, the shallow sensors face down and touch the load cell compressing the compliant structure.

To calibrate the tensile response, the module's shallow sensors were attached to another reference load cell and the linear actuator pulled the shallow sensor stretching the module's compliant structure, as shown in *Figure 5-9*c.

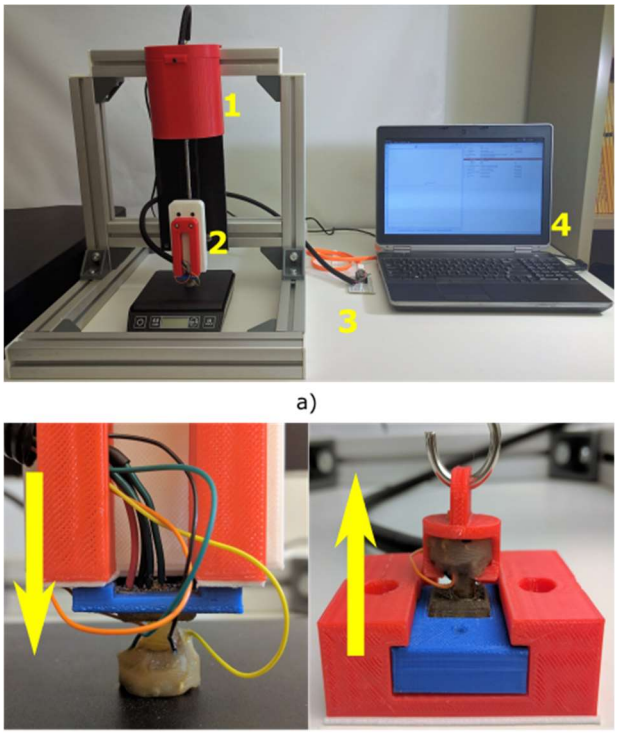

Figure 5-9 Calibration setup, a) consisting of (1) a linear actuator; (2) a carriage; (3) a microcontroller; and (4) a computer. Module b) under compression and c) under tension.

Figure 5-10 shows, in blue, the relationship between the force observed by the load cell and the raw sensor output. The deep pressure sensor is sensitive to pressure in the interval 0.5gf to 270gf. The sensor is also sensitive to tension from 4gf to 330gf (red line in Figure 5-10).

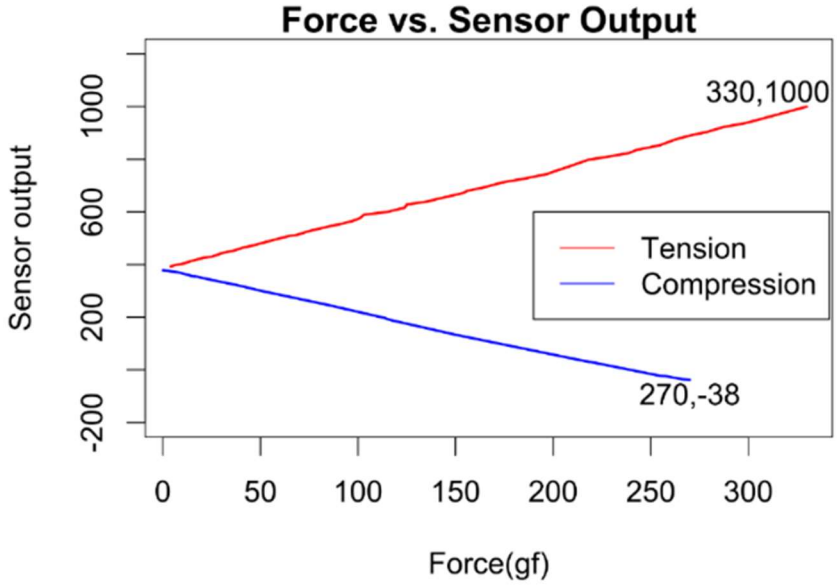

Figure 5-10 Force vs. sensor output.

The calibration of the piezo-resistive tactile array employed in this work follows the one presented in [162].

5.8 Module Characterization and Examples of Applications

Several tests were performed to validate the capabilities of the proposed tactile module. The plots presented in Figure 5-11 show the dynamic behavior of the module's deep pressure sensor. Three experiments have been performed. The first plot, Figure 5-11a, shows the deep pressure sensor response for stimulations of increasing forces, when each stimulation step lasted 10 seconds and was followed (intercalated) by an interval of 10 seconds of no stimulation. The setup used in this experiment is shown in Figure 5-9b. The carriage of the linear motion slide stimulates the sensor by travelling multiples of 0.1mm and receding to its initial position in-between each two stimulations. In Figure 5-9b, the force acting on the sensor was about 0.3N in the first stimulation and 0.7N in the last. Figure 5-11b shows the sensor being stimulated at a faster rate, 0.5 seconds of stimulations followed by 0.5 seconds of no stimulation. The carriage of the linear motion slide traveled 1.7mm and receded to its initial position in-between each two stimulations; each stimulation reached 2.5N. Figure 5-11c shows the sensor being stimulated for steps of 3 seconds each with increasing forces ranging from 0.3N in the first step to 2.4N in the last. The sharp spikes shown in Figure 5-11 are due to the 1-step response of the stepper motor that moves the linear slide. As expected, the sensor measurements display elastic hysteresis due to the compliant structure. This can be observed by the curves that follow the spikes in the three plots. Even though the sensor presents such a hysteresis, it still responds constantly to fast stimuli as those shown in Figure 5-11b. All plots in Figure 5-11 show raw data as recuperated by the sensor.

Figure 5-12 shows the tactile module's deformation and the orientation estimate for several inclined planes with different slopes. The results from Figure 5-12 show the estimates orientation when different 3D-printed inclined planes are pressed against the tactile module. The 1st and 3rd rows of Figure 5-12 show the inclined planes and the deformed tactile module, where the vectors in yellow represent the horizontal plane. The inclined plane is aligned to the y-axis of the sensing module. These vectors are normal to the x-axis of the sensing module (as shown in Figure 5-2).

The plots from the 2nd and 4th rows show the effects that the contact between the inclined planes and the modules has on the measurements. These results are achieved by converting the quaternion ${}^{L}_{G}\boldsymbol{q}$ from Eq. 3 to ϕ (roll), θ (pitch), ψ (yaw), [281]:

$$\begin{bmatrix}\phi\\ \theta\\ \psi\end{bmatrix} = \begin{bmatrix}\tan^{-1}\dfrac{2(q_0q_1+q_2q_3)}{1-2(q_1^2+q_2^2)}\\ \sin^{-1}2(q_0q_3-q_2q_1)\\ \tan^{-1}\dfrac{2(q_0q_3+q_1q_2)}{1-2(q_2^2+q_3^2)}\end{bmatrix} \tag{14}$$

where q_{i} is the *i-th* component of the quaternion ${}^{L}_{G}\boldsymbol{q}$.

The initial orientation of the shallow sensors is around 147 pitch, 0.5 yaw and 180 (more precisely 179.4 to -179.3) roll. When the inclined planes touch the tactile module, the roll angle increases, and this leads to the sharp transitions from positive borderline roll to the negative roll corresponding to the estimate of the slope angle of the inclined plane. This behavior can be observed in the plots in Figure 5-12. The plots show that the module with its current MARG configuration is able to estimate, through the orientation estimation filter, the orientation of the shallow sensors with little crosstalk effect, mostly evident in the Figure 5-12a case. For example, in Figure 5-12d the inclined plane had a slope of 10° while the estimate was of 12.826°, therefore the errors were in the range of ±3°. The errors found in the estimates can be due to the 3D-printed inclined planes imperfections, sensors axis misalignment or prototyping approximations.

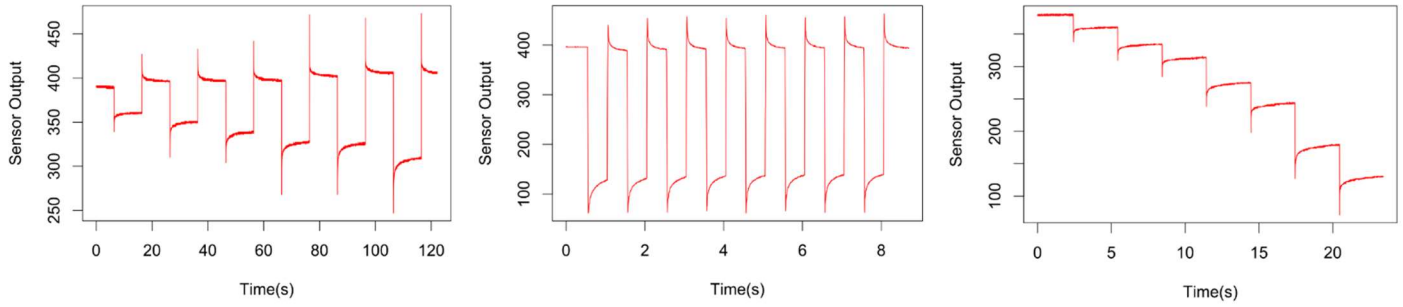

a) b) c)

Figure 5-11 Consecutive stimulations of the deep pressure sensor with different normal forces: a) intercalated sequence of 10 second stimulations; b) intercalated 0.5 second stimulations; c) increasing 3 second stimulations.

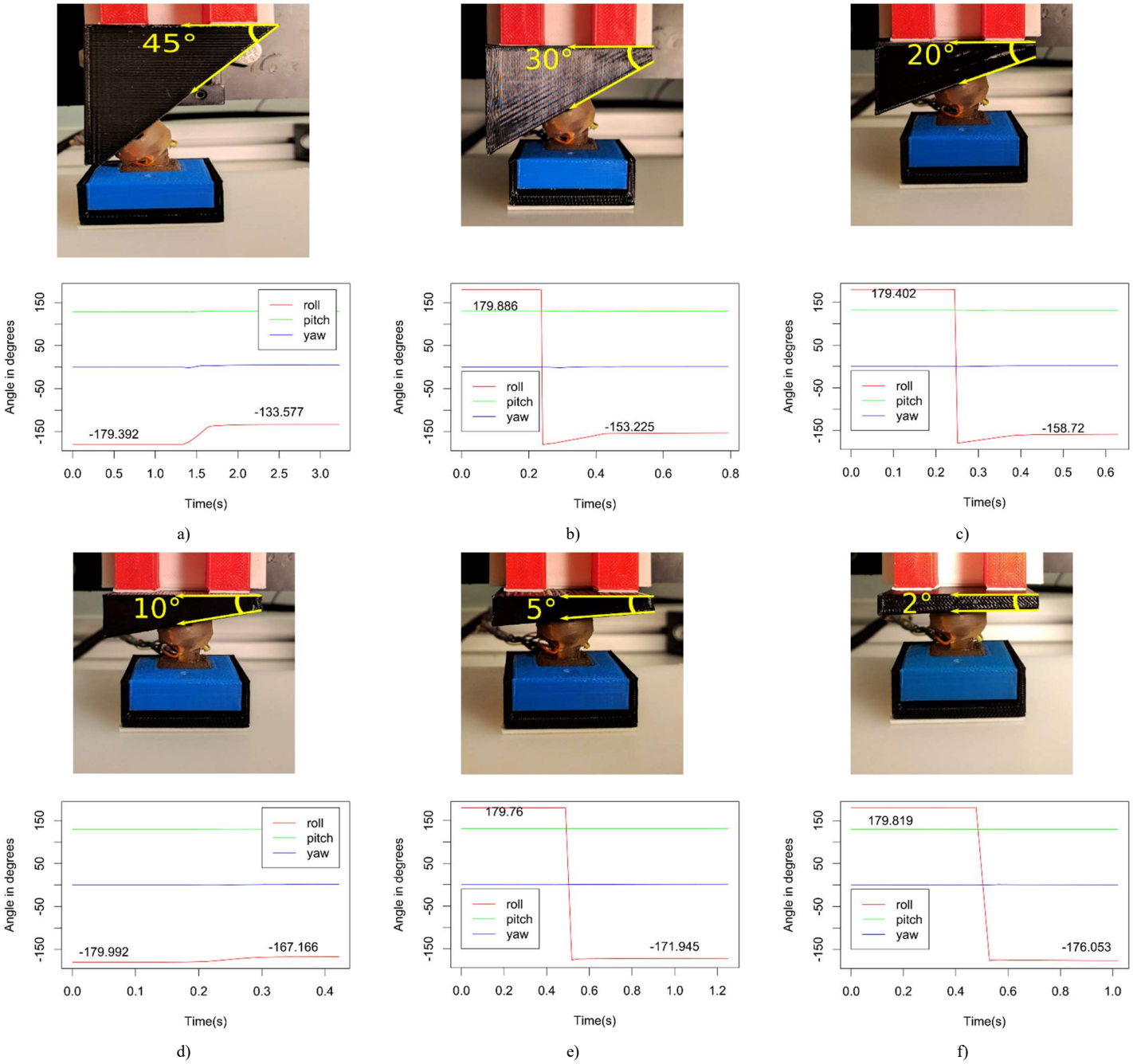

Figure 5-12 Deformation of the sensor module due to the contact of inclined planes with different slopes and its estimated slope angles: a) 45°; b) 30°; c) 20°; d) 10°; e) 5° and f) 2°.

The proposed tactile module has also many possible applications, for example, for orientation estimation of surfaces (see Figure 5-12), for tactile profile recognition ([14]) and for object recognition ([16]). As another example, Figure 5-13 shows the sensors' response for 2 scenarios, tapping impact and the measurement of the carotid pulse. The left column of the figure illustrates

the sensors' response for 3 impacts of an object on the shallow sensors. Impacts can be used to identify early stages of touch. Impacts are also an important safety aspect when robots perform in non-structured environments. They are clearly identified as spikes in pressure, angular velocity and acceleration measurements. The right column of the figure shows the sensors' response for the carotid pulse for a healthy 28-year-old male. During this experiment the sensor was placed over the skin area covering the carotid artery. This experiment shows the sensors' response while the module is kept in stable touch over the carotid artery. The pulse variations are mainly present on the output of the deep pressure sensor while the other sensors present little to no response. In both cases, the response of the magnetic field sensor shows the orientation of the module.

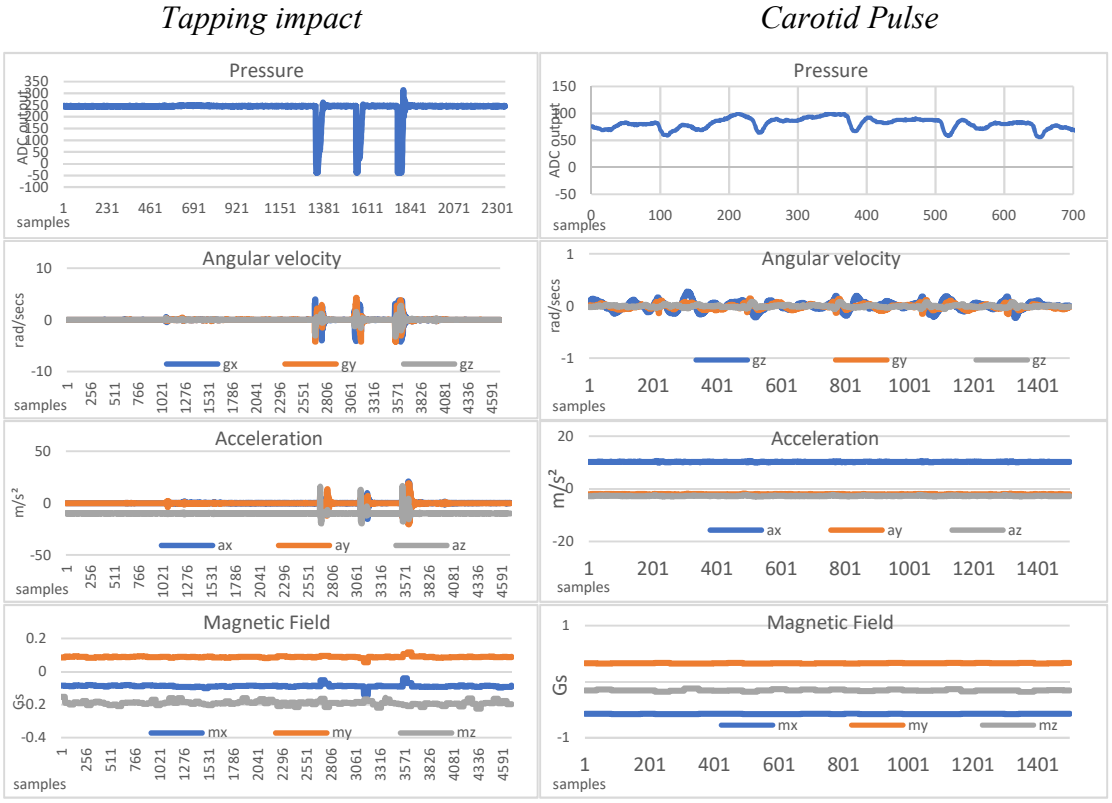

Figure 5-13 Left column shows the sensors response to tapping impact; the right column shows the sensors response when the module is in contact with the human skin over the carotid artery.

5.9 Conclusions

This paper presented the design and hardware implementation of an original bio-inspired multimodal tactile sensing module. The module's compliant structure and sensor placement are

inspired by the function, type and organization of mechanoreceptors in humans' glabrous skin. Mimicking deep and shallow sensors and their relationship through a compliant structure that resembles the Pacinian receptive field, the module provides the data necessary to overcome the problem of estimating non-normal forces acting on the surface of the module without excluding modalities of tactile sensors well developed in the literature, such as tactile arrays.

Beyond the inclusion of more sensing modalities in order to cope with the weaknesses of each sensor used by itself, our contribution to the field of tactile sensing is the description of how to place sensors of different modalities in a compliant structure without losing information about non-normal forces due to the tactile inversion problem and the spatial filtering imposed by the elastic layer. The proposed module is not a blind attempt to mimic biological tactile sensors, it combines well-established engineering solutions for tactile sensors (e.g. tactile arrays) with new bio-inspired concepts.

Future improvements will focus on optimizing the microcontroller code, reducing the printed circuit boards footprints and integrating the module with computational intelligence solutions in order to enable advance tasks of tactile recognition and manipulation.

5.10 Complementary results: End-effector approach flexibilization in a surface approximation task using a bioinspired tactile sensing module

5.10.1 Introduction

As robots advance towards applications in unstructured everyday scenarios, it becomes clear that tactile sensors are the last frontier to robots that can handle everyday objects and interact with humans through contact. Robots are expected to recognize the properties of objects in order to handle them safely and efficiently in a variety of applications, such as health and elder care, manufacturing, or high-risk environments. To be effective, such sensing devices have to sense the geometry of touched surfaces and objects, as well as any other relevant information for their tasks, such as forces, vibrations, and temperature, that allow them to safely and securely interact within an environment [9].

Given the capability of humans to easily capture and interpret tactile data, one promising direction in order to produce enhanced robotic tactile systems is to explore and imitate the human tactile sensing capabilities [5]. These capabilities include the ability to describe surfaces and their inclinations by touch. In [206], points from tactile readings are fit to super-quadric surfaces to reconstruct them based on predefined models. In a similar way, the authors of paper [207] present simulations of a polyhedral model-based method for the recovery of object shapes based on the locations of contact points. The authors demonstrate the importance of surface normal estimations and their impact on the reconstruction of shapes. In [208]–[210], curvatures are described through polynomial fitting of contact points; in [211], the estimation of nonparametric shapes is demonstrated using binary sensing (contact and no contact) and ergodic exploration. These methods require a large number of points and estimate local normals on the surface based on contact points that require remarkably precise robots. The utilization of contact only methods can be time-consuming due to the significant number of contacts required for recognizing or reconstructing the global shape of objects. In [213], the actuator positions of robot fingers and force values from embedded barometer sensors form the feature space to classify object classes using random forests with data acquired during a single and unplanned grasp.

Tasks like the one presented in [213] show the importance of collecting as much information as possible using fewer probing contacts

In this context, this section presents an application of a bio-inspired tactile sensing module [17] for the task of exploring the inclination of a surface and its variation along a path. This task exemplifies the importance of compliant structures for the flexibilization of the approach angle of robotic end-effectors or other parts when touching unknown surfaces or suffering unexpected contact. While with rigid sensors the approach angle has to be normal to the surface of the object being explored, the proposed sensing module removes this constraint with the benefit of estimating the surface inclination. The estimation is performed using data from a MARG (Magnetic, Angular Rate, Gravity) unit located over a barometer, both embedded in polyurethane. The pressure and position of the module is used to approximate the curve of a surface using linear and cubic interpolation. The orientation of the module is used to calculate the normal and the tangent to surface. The intersection point between two tangent lines extracted from neighbor contacts is used as a control point to a Bézier curve [282], thus linking the two probing positions. The experimental results show that the approach using Bézier curves is more robust when approximating the surface using a reduced number of probing contacts.

5.10.2 Experimental Apparatus and Procedure

5.10.2.1 Sensing Module

The sensing apparatus used in this section is a version of the module presented in [17] and shown in *Figure 5-2*. It draws inspiration from the type, functionality, and organization of cutaneous tactile elements, it determines the placement of two shallow sensors, namely, an array and a nine DOF magnetic, angular rate, and gravity system, a flexible compliant structure, and a deep pressure sensor placed in a structure similar to the receptive field of the Pacinian mechanoreceptor from the human skin.

The module employed here doesn't make use of the tactile array shown in *Figure 5-2*(1). In this publication, the inclination of an object surface is considered a global feature independent of the fine details. In our application, the compliant structure *Figure 5-2*(3) adapts to the surfaces that the module makes contact with and guides forces applied to the shallow sensors from *Figure 5-2*(2)

to the deep pressure sensor in *Figure 5-2*(4). More details about the sensing module its bioinspired aspects and design insights can be found in [17].

The 9-DOF MARG system used for the implementation of the sensing module was the STMicroelectronics© LSM9DS0 composed of a triple-axis accelerometer, a triple-axis gyroscope, and a triple-axis magnetometer. The deep pressure sensor sitting on the bottom of the compliant structure was the MPL115A2 from Freescale Semiconductor©. The flexible polyurethane from which the compliant structure is made of VytaFlex© Shore 20 A hardness from Smooth-On©. Table 5-3 shows the MARG unit settings specifying measurement and selected ranges, operating frequency range and selected frequency as well as the resulting sensors resolution.

Table 5-3 MARG Sensors Configuration

	Magnetic Sensor	***Gravity Sensor***	***Angular Rate Sensor***
Measurement range	±2 – ±12 Gs	±2 – ±16 g	±245 – ±2000 dps
Selected range	±2 Gs	±2 g	±245 dps
Frequency range	3.125 – 100 Hz	3.125 – 1600 Hz	3.125 – 1600 Hz
Selected frequency	100 Hz	800 Hz	800 Hz
Resolution	0.08 mG	0.061 mg	8.75 mdps

5.10.2.2 Experimental Setup

The experimental setup and the object of study are shown in Figure 5-14. The 3D printed surface being explored is presented on the bottom part of the figure. The sensing module is carried by the end-effector of the robotic manipulator, represented by the blue-collar base housing the sensor. The 3DOF manipulator employed to bring the module into contact along the surface is comprised of three Robotis Dynamixel AX-12A robot actuators. The right side of Figure 5-14 also shows the kinematic model associated with the robot, in which the pose of the end effector and the sensing module displayed in the experiment are referenced by the base_link frame.

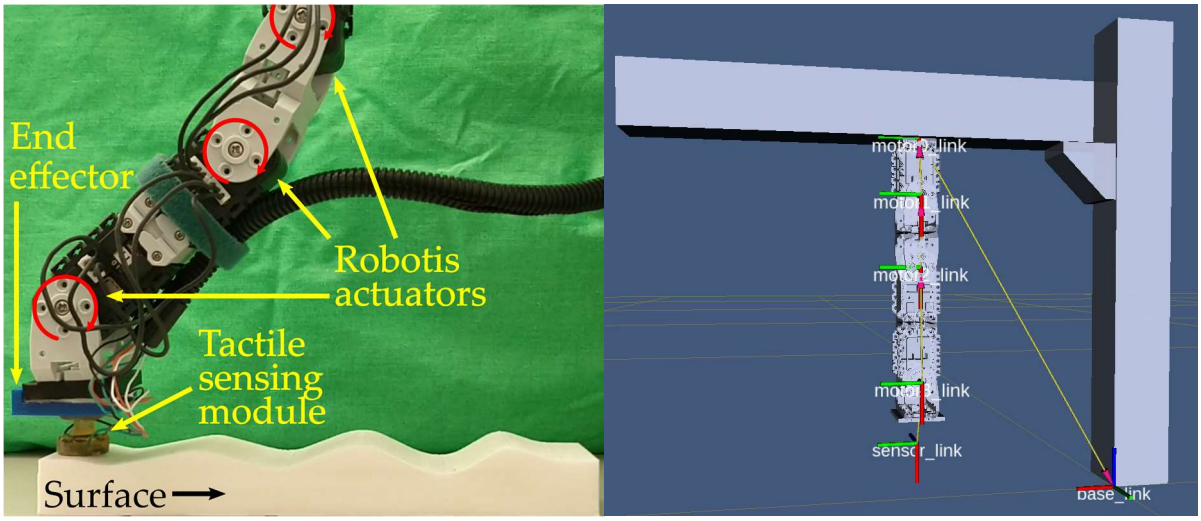

Figure 5-14 Experimental Setup: robotic manipulator, sensing module and explored surface.

5.10.2.3 Data Acquisition and Interpretation

The interface between the computer that collects and analyzes the data from the sensors is a microcontroller MK20DX256VLH7 Cortex-M4 at 72M Hz from Freescale Semiconductor©. The connection between sensors and microcontroller is implemented through a two-wire interface (TWI) at 400 KHz. The link between microcontroller and computer is established using a USB Serial interface. The data acquisition software is developed using the Robotic Operating System (ROS) and *Moveit!* framework. The computer running ROS acquires data from the sensors through the interface microcontroller at 440 Hz.

From this data, the pitch of the end-effector base is calculated through the forward kinematic chain. On the other hand, the pitch of the shallow sensors is estimated using a complementary filter [17], [277]–[279] to combine the information from the magnetic field, angular rate and gravity into a quaternion representation ${}^{L}_{G}\boldsymbol{q}$:

$$ {}^{L}_{G}\boldsymbol{q} = {}^{L}_{G}\boldsymbol{q}_{\omega} \otimes \widehat{\boldsymbol{\Delta q}}_{acc} \otimes \widehat{\boldsymbol{\Delta q}}_{mag} \qquad (15) $$

where ${}^{L}_{G}\boldsymbol{q}_{\omega}$ is the initial estimate given the integration of the angular rate and $\widehat{\boldsymbol{\Delta q}}_{acc}$ and $\widehat{\boldsymbol{\Delta q}}_{mag}$ are the corrections related to the gravity and magnetic fields respectively.

To facilitate analysis and the comparison and between the end-effector pitch and the surface pitch, both orientations are represented in terms of Euler angles with the quaternion ${}^{L}_{G}\boldsymbol{q}$ from Eq. 15 being transformed into ϕ (roll), θ (pitch), ψ (yaw), [281]:

$$\begin{bmatrix}\phi\\ \theta\\ \psi\end{bmatrix} = \begin{bmatrix}\tan^{-1}\dfrac{2(q_0q_1 + q_2q_3)}{1 - 2(q_1^2 + q_2^2)}\\ \sin^{-1}2(q_0q_3 - q_2q_1)\\ \tan^{-1}\dfrac{2(q_0q_3 + q_1q_2)}{1 - 2(q_2^2 + q_3^2)}\end{bmatrix} \qquad (16)$$

where q_{i} is the *i-th* component of the quaternion ${}^{L}_{G}\boldsymbol{q}$.

5.10.3 Experimental Results and Discussion

The acceleration, angular rate, magnetic field, and pressure from the sensing module are acquired along with the kinematic information (angular position of each actuator) of the robot while the finger has its end-effector successively retracted and brought into contact along the 3D printed surface. It is worth noting that the pitch of the end-effector is kept around 0 (zero) degrees throughout the exploration task, with some small variations due to backlash on the robot joints and actuation inaccuracies.

Figure 5-15 displays the deformation of the module during the surface exploration and the approximate inclination of the surface at the respective areas of touch. The graph in Figure 5-16

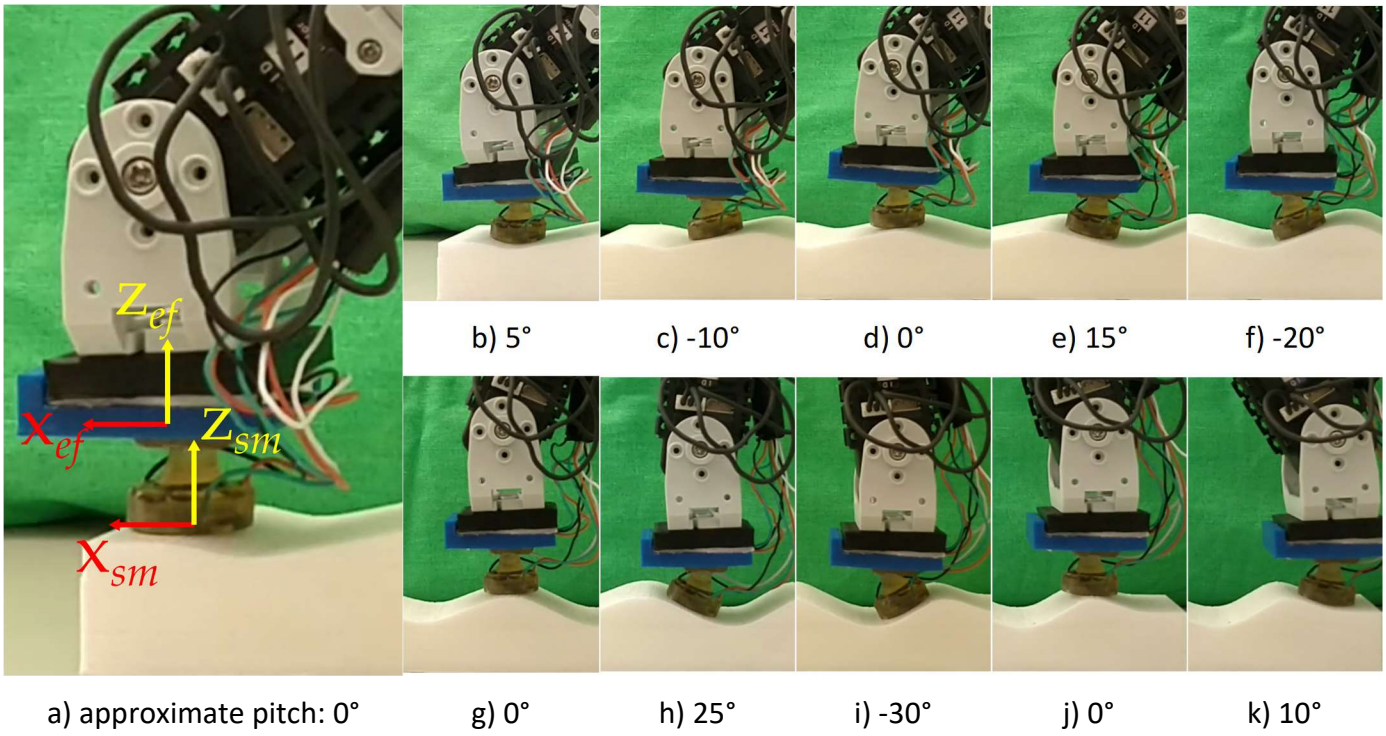

Figure 5-15 End-effector and deformation of the tactile sensing module along the surface. z_{ef} and x_{ef} are the axis for the reference frame of the end effector, z_{sm} and x_{sm} are the axis for the reference frame of the sensing module; both relative to the base_link frame from Figure 5-14.

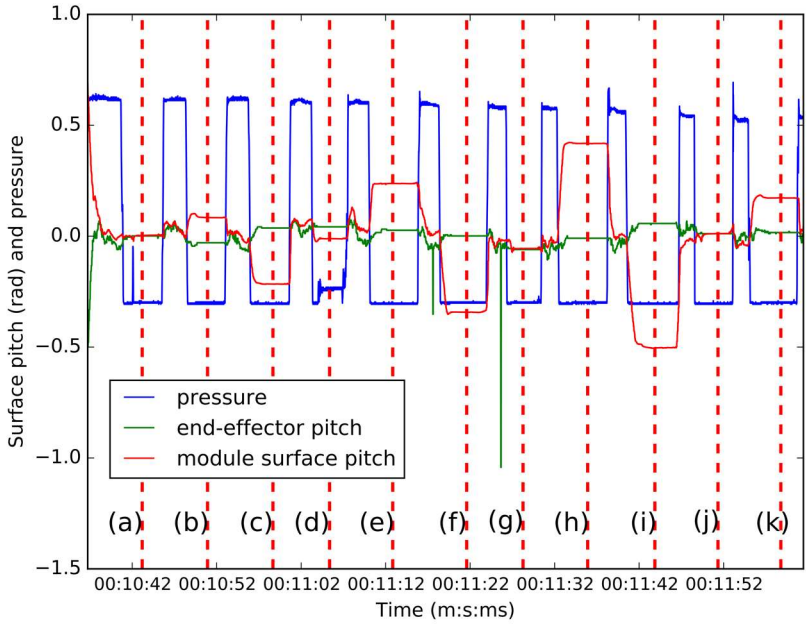

Figure 5-16 Normalized pressure output and corresponding surface and end-effector inclination. The letters from (a) – (k) represent the stimuli shown in Figure 5-15.

shows the normalized pressure signal in blue, the calculated end effector pitch in green, and the estimated surface pitch from the sensing module in red (i.e. the continuous red line). As

expected, the pressure signal dips when the sensor is forced against the surface. The end effector pitch signal varies around 0, while the estimated surface pitch shows the inclination angle of the sensor.

Table 5-4 shows the expected and estimated surface pitch θ_{sm}, as well as the end effector pitch θ_{ef}; the contact location corresponds to the subfigures of Figure 5-15. Figure 5-17 shows the position of the end effector during exploration of the surface. In Figure 5-16 and Figure 5-17 the red vertical dashed lines represent the timestamps in which data was considered for further analysis.

Table 5-4 Surface orientation by touch location

Contact location	a)	b)	c)	d)	e)	f)	g)	h)	i)	j)	k)
θ_{ef}	0.04	-1.78	2.02	2.3	1.43	-0.04	-3.56	-0.61	3.19	0.54	0.84
θ_{sm}	0.49	5.07	-12.08	-0.31	13.94	-19.37	-2.88	24.27	-28.6	0.93	10.14
Expected surface θ	0	5	-10	0	15	-20	0	25	-30	0	10

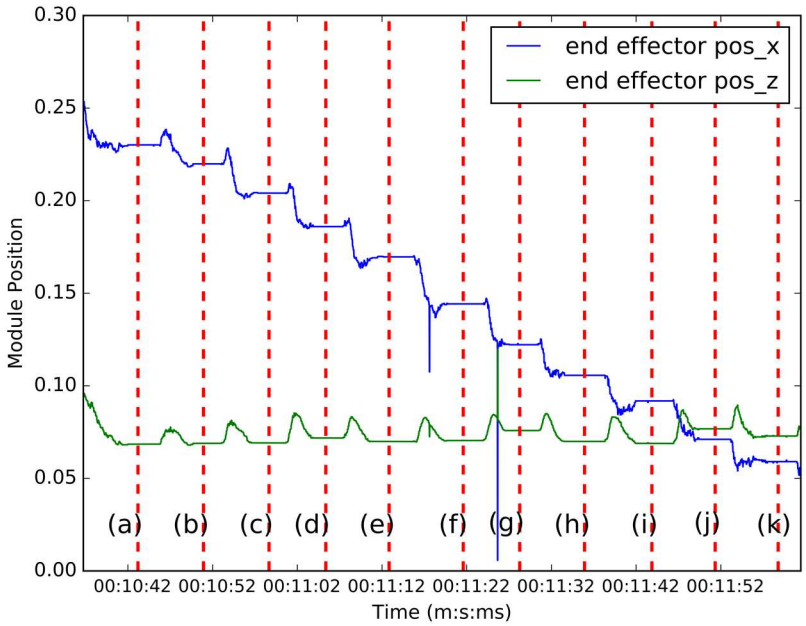

Figure 5-17 Position of the end effector during exploration.

5.10.3.1 Surface approximation

Figure 5-18 displays the points of contact corresponding to the probing positions from Figure 5-15 at the time stamps represented by the red vertical dashed lines shown in Figure 5-16 and

Figure 5-17. The blue vectors are normal to the surface and are calculated using the using the module pitch from Figure 5-16. The red vectors are perpendicular to the normal vectors and represent tangents of the surface. The cyan dots represent control points for the Bézier curves determined by the intersection between two neighbor tangents and given by the equation:

$$\left(P_x, P_y\right) = \left(\begin{array}{c} \frac{(x_1y_2 - y_1x_2)(x_3 - x_4) - (x_1 - x_2)(x_3y_4 - y_3x_4)}{(x_1 - x_2)(y_3 - y_4) - (y_1 - y_2)(x_3 - x_4)}, \\ \frac{(x_1y_2 - y_1x_2)(y_3 - y_4) - (y_1 - y_2)(x_3y_4 - y_3x_4)}{(x_1 - x_2)(y_3 - y_4) - (y_1 - y_2)(x_3 - x_4)} \end{array} \right) \quad (17)$$

where $(x_1, y_1), (x_2, y_2)$ are points of the first tangent and $(x_3, y_3), (x_4, y_4)$ are the points of the second one.

Figure 5-19 shows the linear and cubic interpolations of the contact points as well as Bézier curves based on contact points and control points. The Bézier curves in this article were implemented using the De Casteljau's algorithm [282].

Control points that lay beyond one of either of the contact (i.e. points I_{ab} AND I_{jk} in Figure 5-18) in the x direction cause Bézier curves to curl under or over the contact points used as beginning and end of a curve. Points with this characteristic may indicate that more probing should be performed between the two contact points. The elimination of such control points using probing actions is topic for a future work. Meanwhile, curves with this characteristic will be substituted with linear segments.

In Figure 5-19, the cubic interpolation passes through all eleven probing points and approximates the surface satisfactorily. It is comparable to the Bézier curves based on the contact points and control points calculated from intersecting tangents. The cubic interpolation is an adequate approximation of a surface if the sensing device probing the surface is from the point-like modality [93] and only a limited amount of probing actions is available. If an unlimited number of probing actions is possible, such devices may be used to collect large quantity of points to estimate normal vectors, as in [208]–[210], and from these normal vectors approximate a surface.

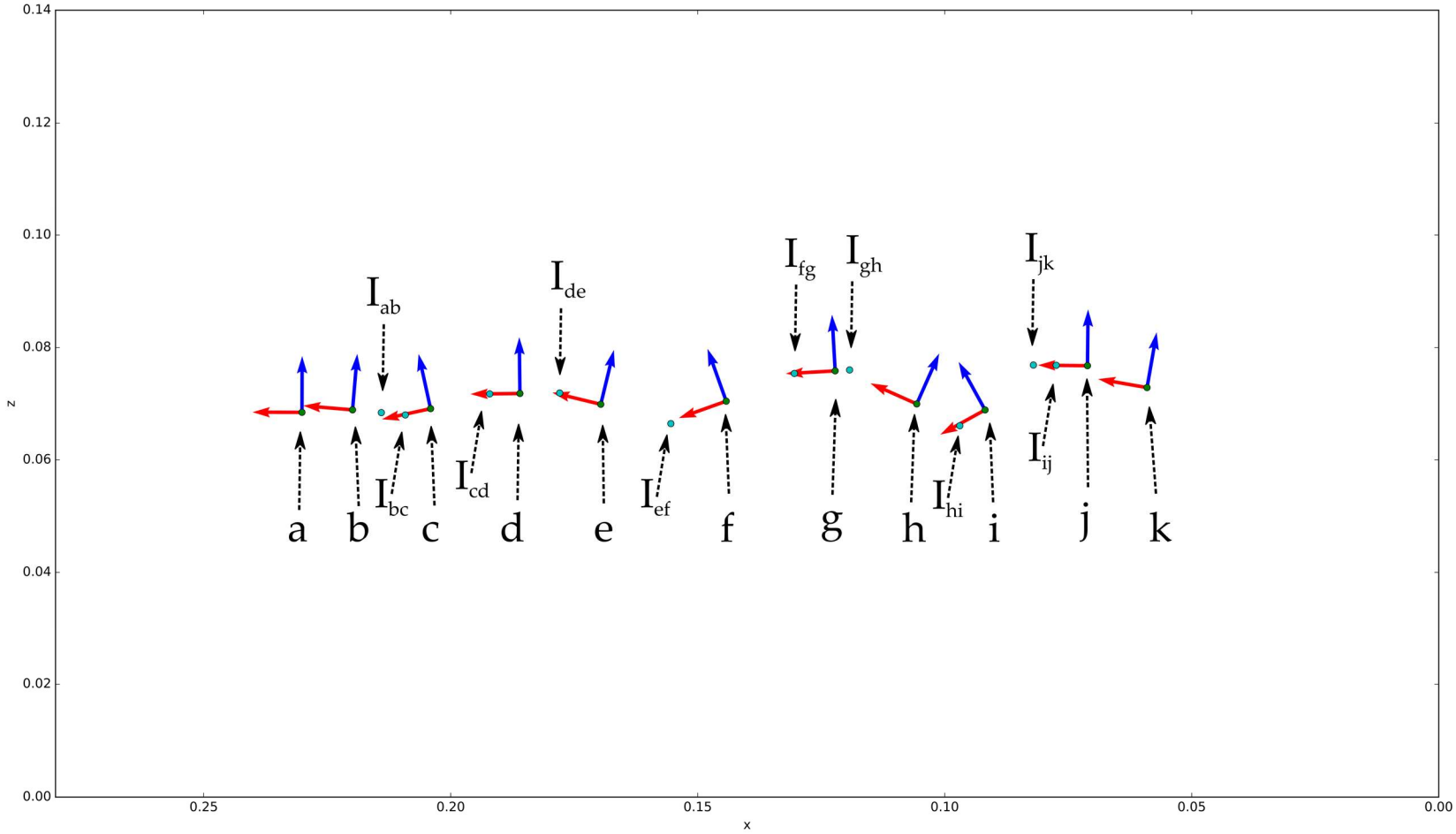

Figure 5-18 Normal (in blue) and tangent (in red) vectors calculated from the pitch and contact points (green dots) at the timestamps shown in Figure 5-15 and Figure 5-16. The letters from (a) – (k) represent the stimuli shown in Figure 5-15.

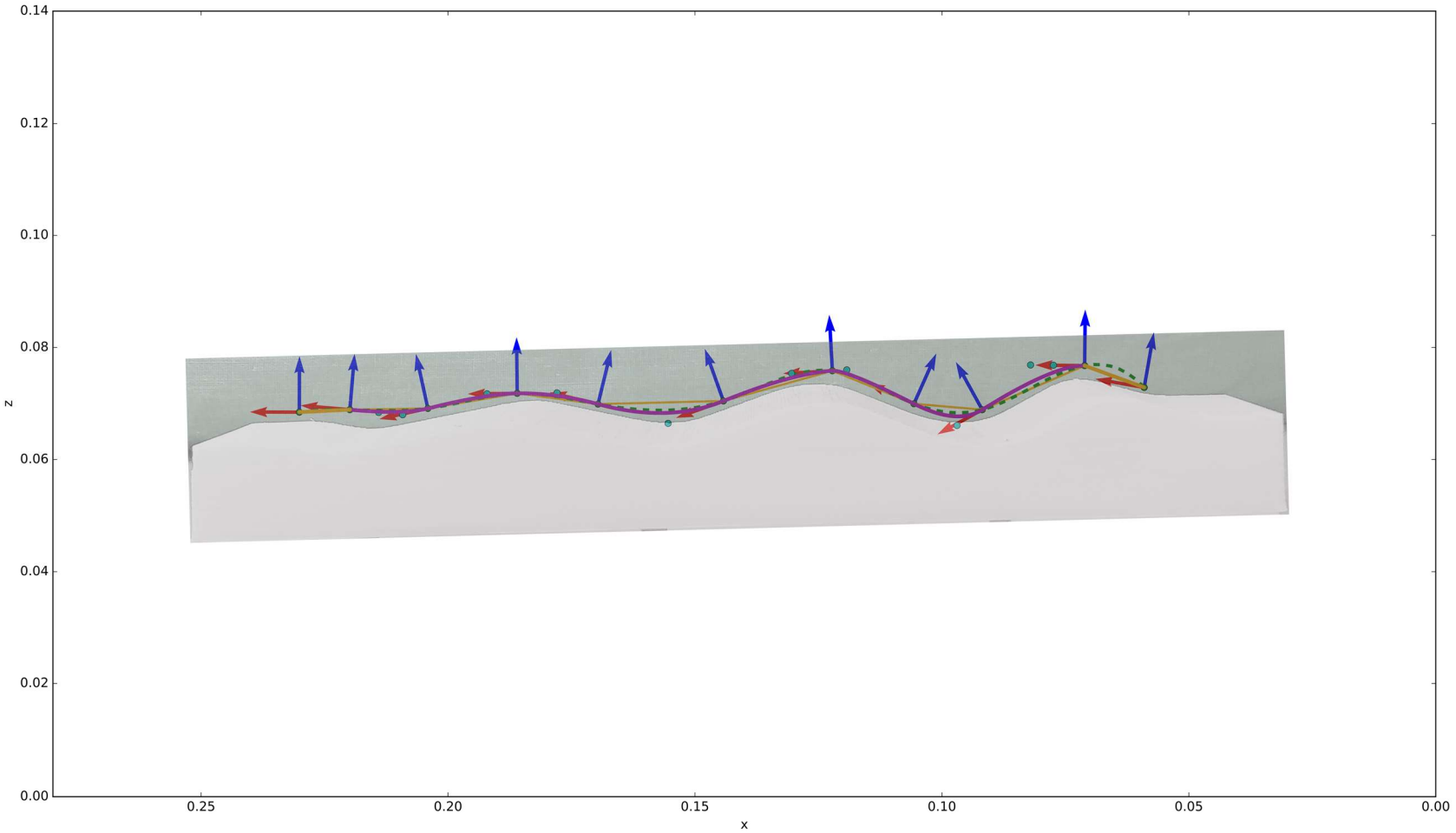

Figure 5-19 Surface approximated using data from all 11 probing points. The green dashed line and orange segments show the cubic and linear interpolations respectively. The magenta line shows the Bézier curves that approximate the curve.

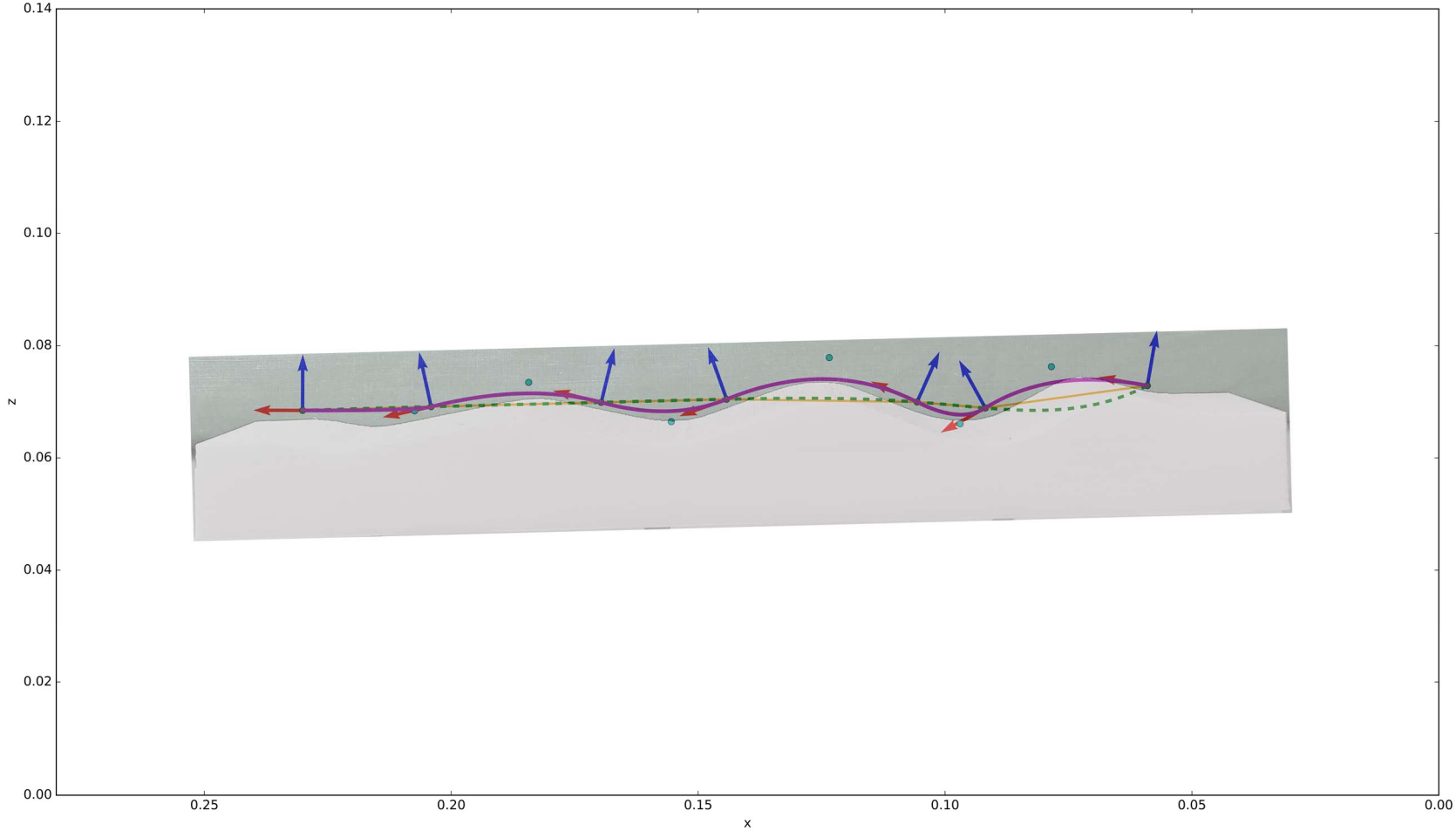

Figure 5-20 Surface approximated using data from 7 probing points, (points b, d, f and j were not considered in this scenario). The green dashed line and orange segments show the cubic and linear interpolations respectively. The magenta line shows the Bézier curves that approximate the curve.

The sensing module used in this article has the advantage of estimating the local normal of an unknown surface from its structure and its sensor placement as evidenced in Figure 5-20 where 4 (b, d, f, j) of the 11 probing actions are not considered when reconstructing the surface. In Figure 5-20 the interpolation method flattens out while the Bézier curves calculated with the pitch information still resembles the surface.

5.10.4 Conclusion and Perspectives

This paper builds upon [17], demonstrating the use of its bioinspired tactile sensing module in a task where a robotic manipulator approaches a surface bringing the module to contact and pressing the module against it. This procedure allows estimating the surface inclination even though the end effector orientation is kept around zero not following the surface pitch. The module used in this task tries to follow recommendations from the principal surveys of the field [5], [9] and adds bioinspired concepts analogous to the mechanoreceptors and receptive fields of the human skin, as well as the compliance of the flesh supporting it.

The scenario exemplified here may occur in a variety of applications where robots acting in unstructured environments cannot control their approach vector to unknown objects or surfaces and handle unexpected contacts. In robots with positioning inaccuracies or imprecisions, the module's compliance can help alleviate alignment errors. For robots with high stiffness, the module may include the compliance needed to approach unknown or fragile objects.

The advantage of the module used here is in the fact that it does not require multiple exploratory actions to estimate a normal to a surface under contact. The normals estimated with the module come from its structure and sensor placement. For each contact with a surface, not only pressure but also a normal vector is calculated without the need for the collection of a large number of points as in [208]–[210]. The surface

approximation performed here is also more robust due to the control points calculated from the tangents to the surfaces.

Future work may concentrate on the use of a network of these modules to generate models of surfaces and objects. Applying the module to 3D surfaces is also an interesting perspective to be explored in the future.

Chapter 6 Conclusion

There are mainly two approaches to contribute to the effective utilization of tactile of tactile sensing: (1) the development of new sensing devices and (2) tactile data interpretation techniques. This thesis mainly focuses on the development of a new tactile sensing module that incorporates bioinspired aspects to satisfy recommendations from main surveys of the field [5], [9].

The most recent design presented in [17], is the result of the expansion of the works presented in [13]–[16]. This design is suitable for tactile tasks in structured and unstructured environments and objects. The module can be used in sliding dynamic tasks where the vibration of the embedded sensors in the unit can be used to extract information from the data collected over the contact surfaces. To maximize the usefulness of such data, it is necessary to constraint the orientation of the module related to surface being explored, as in other works in the literature. To constrain the orientation of the module, it is necessary to determine the surface contour or inclination. The module presented in [17] enables this estimation through the fusion of the data from the MARG system and the deformation of the compliant structure that houses the sensors. The determination of a surface contour or inclination is a static task where the compliant structure is essential to reduce the constraint of the approach angle of an end-effector performing an exploration.

The realization of the multimodal module capable of performing static and dynamic tasks was possible thanks to its bioinspired approach and the appreciation of the importance of the coordination between the vestibular system and tactile/motor systems in humans. This aspect has not been explored in the literature and is essential to describe changes in the topology of the human skin even when it is supported by sometimes thick compliant layers of muscles and fat.

This thesis does not claim for the module developed to be a substitute for vision-based approaches or actuators with passive adjustable compliance or controllable stiffness

for robotic applications. The module is thought to be an addition to such systems serving as an interface between the envelope of robots and their surroundings.

6.1 Contributions

Aiming at complementing the success of the application of tactile arrays in static tasks, this thesis start exploring how MEMs MARG systems can be used in a dynamic tactile profile classification task. The same sensors and a MEMs barometer were then embedded in a soft fingertip and tested for both dynamic grating characterization and for the previous classification task. The fingertip has the same hardness as the human skin and flesh, and the region of contact is intended to emulate the intersection of receptive fields from the mechanoreceptors present in the human skin. The grating characterization followed the same conditions as most works in the literature; it slides the fingertip over the grating patterns with constant linear velocity and orientation. The profile classification task, on the other hand, unlike similar publications, did not constrain the velocity, acceleration or orientation of the fingertip; it followed a prerecorded trajectory repeated to bring the fingertip into contact with the different profiles.

The fingertip presented in Chapter 4 is capable of achieving the same performance as other tactile sensors in the grating characterization task with sensors embedded in a compliant structure and can be used in a profile classification task. The fingertip, however, does not present a straightforward and robust manner to approximate the geometry a surface to be probed using only data from the robot and fingertip itself.

Approximating the geometry of surfaces from tactile data extracted in static probing actions is essential for dynamic tasks where robots may plan and perform motions with sensors or tools being kept in a specific orientation and velocity from the surface.

The sensing module presented in Chapter 5, attempts to use the same sensors from the fingertip proposed in Chapter 4 to enable the robotic systems carrying the module

to estimate the pressure and orientation of sensors in a different compliant structure with the support for a tactile array. The new compliant structure does not invalidate the applications presented in Chapter 4; the module can be used for dynamic tasks if slid tilted related to a surface subject to the movement. The compliant structure in the final design emulates the Pacinian corpuscle receptive field as it covers a large area and encompasses the receptive fields of the other mechanoreceptors. It guides forces applied on the surface of the module to the pressure sensor deep in the structure. The data of the shallow sensors, namely the MARG system, is fused using a complementary filter to deliver a quaternion representing the orientation of the module's when deformed due to contact.

The second part of Chapter 5, section 5.10, demonstrates the importance of including the orientation of a sensing device in the solution for the tactile inversion problem when approximating the geometry of a surface. The data on the position of the end-effector, namely the pressure and the pitch of the module, are used to approximate the geometry of a surface using linear and cubic interpolations as well as Bézier curves. The data points considered for the approximation were collected in a static manner with the pitch of the end-effector kept around zero degrees. Keeping the end-effector pitch around zero is possible due to the module's compliant structure that enables the flexibilization of constraints related to the orientation of end-effectors or other parts carrying the module, i.e., the orientation of these parts does not have to be kept normal to external surfaces when probing them. The results show that for a reduced number of probing points approximations using linear and cubic interpolations collapse while Bezier curves using control points determined by the intersection of two neighboring vectors tangent to the surface and calculated from the pitch of the module still resemble the surface.

The main contributions of this thesis are in the conception, design, and implementation of the bioinspired tactile sensing module, the discrimination of the sensors and their

placement, and the proposal of a compliant structure to tackle the tactile inversion problem and to decrease the constraints on end-effectors exploring unknown surfaces through the adaptability of the module to inclinations and contours of objects, as well as the surface approximation using Bézier curves with control points calculated based on the orientation of the shallow sensors present in the module. More specifically:

1) The development of a general-purpose tactile sensing module capable of measuring forces, vibrations, and deformations due to contact, following recommendations from the principal surveys of the field [5], [9], and adding bioinspired concepts analogous to the mechanoreceptors and receptive fields of the human skin. The design also takes into account the compliance of the flesh supporting the skin, without disregarding the advances in the tactile sensing field when it comes to rigid planar force sensitive arrays;

2) The tactile sensing module presented in this thesis incorporates elements from all three modalities [93]: single-point, tactile arrays, and large area sensors. It makes use of a deep pressure sensor that can act as a single-point contact sensor in case of a failure of the other sensors. In particular, it considers the integration of a tactile array on the top of the compliant structure and several modules can be interconnected to cover a large area;

3) The demonstration of how the multimodality of sensors in the module can be used to characterize surfaces in dynamic tasks matching the performance of other noncompliant sensors present in the literature and classifying tactile profiles using the data of the several sensors (angular velocities, acceleration, magnetic and pressure) as input to a system using principal component analysis and a multilayer feedforward neural network;

4) The module capability of performing static touch tasks on unknown surfaces tackling the tactile inversion problem through the placement of sensors in a

compliant structure that guides deforming forces from its surface to the deep pressure sensor while keeping track of the deformation of the structure using the shallow sensors data fused in a quaternion using a complementary filter;

5) Demonstrate how a robot carrying a sensing module on its end-effector can approach a surface without significant orientation changes to its end-effector and estimate the surface orientation around the contact point in one probing action, i.e., the flexibilization of orientation constraints of end-effectors or other robotic parts carrying the modules to make contact with surfaces of unknown objects;

6) The approximation of the contour of a surface using Bézier curves using the De Casteljau's algorithm with intermediate control points determined based on the intersection of tangent vectors calculated from the pitch estimated by the sensing module and the demonstration that such approximation is more robust with respect to the number of contact points considered when compared to the cubic and linear interpolations.

This research also led to a number of publications, including three journal papers [15]–[17], four conference papers [13], [14], [18], [283], and received the IEEE Award (2016) and 1st place award in the category Electrical and Computer Engineering (2016) at the Engineering and Computer Science and Graduate Poster Competition held at the University of Ottawa.

6.2 Future Work

The artificial skin module presented in this thesis bridges the gap between traditional planar tactile sensing arrays supported by rigid assemblies and compliant sensing setups. This is achieved with an engineered structure that guides forces from the surface of the module to a deep pressure sensor while estimating the orientation of its shallow sensors.

Many opportunities remain open both in terms of applications, as well as in the integration of skin modules in robots. One of the efforts being carried out in the *BioIn Robotics Lab* at the *University of Ottawa* is the miniaturization of the module. Smaller modules could be embedded in robot areas used to acquire fine surface details, for example robot fingers and hands. Larger modules could be used to cover limbs and the torso of robots.

Embedding hundreds of modules in a robot envelope to compose its skin will rise issues regarding the network of modules, and its mechanics and bandwidth. Such networks may solve their bandwidth implementing a parallel and distributed attention model in which the data of modules covering a robot part used to perform a task or stimulated by the environment is given priority of transmission and analysis while the data of dormant parts is suppressed. To implement such functionality, local processing units would have to be added to each module or small set of modules to evaluate if the data collected by the respective modules represents stimuli worth passing to higher level computational nodes. These local processing units would also be responsible to estimate the orientation of the modules and their health.

Networks of modules would also be a fertile field for the application of deep learning techniques specially in dynamic tasks with everyday objects due to the amount of data that arises from these setups.

Another direction in which the use of the module can be expanded is in the development of integrated dynamic and static exploration strategies. In this case, a robot carrying the module would estimate the inclination of small parts of surfaces and with this information dynamically explore these parts sweeping the module at different orientations to collect vibrations with several contact parameters without using data from cameras.

The miniaturization and networking of modules proposed in this thesis will make a robotic skin suitable to in-hand manipulation tasks such as the classification of objects

and estimation of their poses. These operations could be achieved taking advantage from both from the raw sensor data as well as tactile cloud points generated from the position and orientation of the module.

References

[1] R. L. Klatzky and S. J. Lederman, “Object Recognition by Touch,” *Blind. Brain Plast. Navig. Object Recognit.*, pp. 185–205, 2008.

[2] M. . Lee and H. . Nicholls, “Review Article Tactile sensing for mechatronics—a state of the art survey,” *Mechatronics*, vol. 9, no. 1, pp. 1–31, Feb. 1999.

[3] E. R. Kandel, J. H. Schwartz, T. M. Jessell, S. A. Siegelbaum, and A. J. Hudspeth, *Principles of Neural Science*, 5th ed. McGraw-Hill Education, 2012.

[4] J. M. Wolfe *et al.*, *Sensation & Perception*. Sinauer Associates Incorporated, 2014.

[5] R. S. Dahiya, G. Metta, M. Valle, and G. Sandini, “Tactile Sensing—From Humans to Humanoids,” *IEEE Trans. Robot.*, vol. 26, no. 1, pp. 1–20, Feb. 2010.

[6] D. Purves, G. J. Augustine, D. Fitzpatrick, W. C. Hall, A.-S. LaMantia, and L. E. White, *Neuroscience*, 5th ed. Sunderland, Massachusetts U.S.A.: Sinauer Associates, Inc, 2011.

[7] G. A. Bekey and R. C. Arkin, *Autonomous Robots: From Biological Inspiration to Implementation and Control*. MIT Press, 2005.

[8] R. Pfeifer, M. Lungarella, and F. Iida, “Self-Organization, Embodiment, and Biologically Inspired Robotics,” *Science (80-.).*, vol. 318, no. 5853, pp. 1088–1093, Nov. 2007.

[9] R. S. Dahiya, P. Mittendorfer, M. Valle, G. Cheng, and V. J. Lumelsky, “Directions Toward Effective Utilization of Tactile Skin: A Review,” *IEEE Sens. J.*, vol. 13, no. 11, pp. 4121–4138, Nov. 2013.

[10] “Bioinspired,” *Merriam-Webster dictionary*, 2018. [Online]. Available: https://www.merriam-webster.com/dictionary/bioinspired.

[11] I. Darian-Smith and L. E. Oke, “Peripheral neural representation of the spatial frequency of a grating moving across the monkey’s finger pad.,” *J. Physiol.*, vol.

309, no. 1, pp. 117–133, Dec. 1980.

[12] C. M. Oddo, L. Beccai, M. Felder, F. Giovacchini, and M. C. Carrozza, “Artificial roughness encoding with a bio-inspired MEMS- Based tactile sensor array,” *Sensors*, vol. 9, no. 5, pp. 3161–3183, 2009.

[13] T. E. A. de Oliveira, V. Prado da Fonseca, E. Huluta, P. F. F. Rosa, and E. M. Petriu, “Data-driven analysis of kinaesthetic and tactile information for shape classification,” in *2015 IEEE International Conference on Computational Intelligence and Virtual Environments for Measurement Systems and Applications (CIVEMSA)*, 2015, pp. 1–5.

[14] T. E. Alves de Oliveira, B. M. Rocha Lima, A. Cretu, and E. Petriu, “Tactile profile classification using a multimodal MEMs-based sensing module,” in *Proceedings of 3rd International Electronic Conference on Sensors and Applications*, 2016, vol. 3, no. November, p. E007.

[15] T. E. Alves de Oliveira, A.-M. Cretu, and E. M. Petriu, “Multimodal Bio-Inspired Tactile Sensing Module for Surface Characterization,” *Sensors*, vol. 17, no. 6, pp. 1–19, May 2017.

[16] T. E. A. De Oliveira, A. M. Cretu, V. P. Da Fonseca, and E. M. Petriu, “Touch sensing for humanoid robots,” *IEEE Instrum. Meas. Mag.*, vol. 18, no. 5, pp. 13–19, 2015.

[17] T. E. Alves de Oliveira, A.-M. Cretu, and E. M. Petriu, “Multimodal bio-inspired tactile sensing module,” *IEEE Sens. J.*, vol. 17, no. 11, p. 13, Jun. 2017.

[18] T. E. Alves de Oliveira, V. P. da Fonseca, B. M. Rocha Lima, A.-M. Cretu, and E. M. Petriu, “End-effector approach flexibilization in a surface approximation task using a bioinspired tactile sensing module,” in *[submitted] To appear in the 2019 IEEE International Symposium on RObotic and SEnsors Environments (ROSE)*, 2019.

[19] M. R. Cutkosky, R. D. Howe, and W. R. Provancher, “Force and Tactile Sensors,” in *Springer Handbook of Robotics*, B. Siciliano and O. Khatib, Eds. Berlin,

Heidelberg: Springer Berlin Heidelberg, 2008, pp. 455–476.

[20] H. R. Nicholls and M. H. Lee, “A Survey of Robot Tactile Sensing Technology,” *Int. J. Rob. Res.*, vol. 8, no. 3, pp. 3–30, Jun. 1989.

[21] A. D. Berger and P. K. Khosla, “Using Tactile Data for Real-Time Feedback,” *Int. J. Rob. Res.*, vol. 10, no. 2, pp. 88–102, 1991.

[22] R. D. Howe and M. R. Cutkosky, “Integrating Tactile Sensing with control for Dextrous Manipulation,” in *Proceedings of the IEEE International Workshop on Intelligent Motion Control*, 1990, vol. 1, pp. 369–374.

[23] Z. Li, P. Hsu, and S. Sastry, “Grasping and Coordinated Manipulation by a Multifingered Robot Hand,” *Int. J. Rob. Res.*, vol. 8, no. 4, pp. 33–50, 1989.

[24] H. Yousef, M. Boukallel, and K. Althoefer, “Tactile sensing for dexterous in-hand manipulation in robotics—A review,” *Sensors Actuators A Phys.*, vol. 167, no. 2, pp. 171–187, Jun. 2011.

[25] R. S. Fearing, “Tactile Sensing Mechanisms,” *Int. J. Rob. Res.*, vol. 9, no. 3, pp. 3–23, Jun. 1990.

[26] A. Bicchi, J. K. Salisbury, and P. Dario, “Augmentation of grasp robustness using intrinsic tactile sensing,” in *Proceedings, 1989 International Conference on Robotics and Automation*, 1989, pp. 302–307.

[27] H. Dang, J. Weisz, and P. K. Allen, “Blind grasping: Stable robotic grasping using tactile feedback and hand kinematics,” in *2011 IEEE International Conference on Robotics and Automation*, 2011, pp. 5917–5922.

[28] R. M. Murray, Z. Li, and S. S. Sastry, *A Mathematical Introduction to Robotic Manipulation*, vol. 29. 1994.

[29] D. De Rossi, G. Canepa, G. Magenes, F. Germagnoli, A. Caiti, and T. Parisini, “Skin-like tactile sensor arrays for contact stress field extraction,” *Mater. Sci. Eng. C*, vol. 1, no. 1, pp. 23–36, May 1993.

[30] C. Domenici, D. De Rossi, A. Bacci, and S. Bennati, “Shear stress detection in an elastic layer by a piezoelectric polymer tactile sensor,” *IEEE Trans. Electr. Insul.*,

vol. 24, no. 6, pp. 1077–1081, 1989.

[31] S. L. L. Ricker and R. E. E. Ellis, “2-D finite-element models of tactile sensors,” in *[1993] Proceedings IEEE International Conference on Robotics and Automation*, 1993, pp. 941–947.

[32] R. E. Ellis and M. Qin, “Singular-value and finite-element analysis of tactile shape recognition,” in *Proceedings of the 1994 IEEE International Conference on Robotics and Automation*, 1994, pp. 2529–2535.

[33] J. L. Novak, “Initial design and analysis of a capacitive sensor for shear and normal force measurement,” in *Proceedings, 1989 International Conference on Robotics and Automation*, pp. 137–144.

[34] R. S. Fearing and T. O. Binford, “Using a cylindrical tactile sensor for determining curvature,” *IEEE Trans. Robot. Autom.*, vol. 7, no. 6, pp. 806–817, 1991.

[35] R. A. Russell and S. Parkinson, “Sensing surface shape by touch,” in *[1993] Proceedings IEEE International Conference on Robotics and Automation*, 1993, pp. 423–428.

[36] M. Charlebois, K. Gupta, and S. Payandeh, “On estimating local shape using contact sensing,” *J. Robot. Syst.*, vol. 17, no. 12, pp. 643–658, Dec. 2000.

[37] M. Shikida, T. Shimizu, K. Sato, and K. Itoigawa, “Active tactile sensor for detecting contact force and hardness of an object,” in *Sensors and Actuators, A: Physical*, 2003, vol. 103, no. 1–2, pp. 213–218.

[38] J. I. Yuji and C. Sonoda, “A PVDF tactile sensor for static contact force and contact temperature,” in *Proceedings of IEEE Sensors*, 2006, pp. 738–741.

[39] V. Maheshwari, “High-Resolution Thin-Film Device to Sense Texture by Touch,” *Science (80-.).*, vol. 312, no. 5779, pp. 1501–1504, Jun. 2006.

[40] R. Crowder, “APPLIED PHYSICS: Toward Robots That Can Sense Texture by Touch,” *Science (80-.).*, vol. 312, no. 5779, pp. 1478–1479, Jun. 2006.

[41] P. Payeur, C. Pasca, A.-M. Cretu, and E. M. Petriu, “Intelligent Haptic Sensor System for Robotic Manipulation,” *IEEE Trans. Instrum. Meas.*, vol. 54, no. 4, pp.

1583–1592, Aug. 2005.

[42] R. S. Dahiya and M. Valle, *Robotic Tactile Sensing: Technologies and System*. 2013.

[43] Hong Zhang and E. So, “Hybrid resistive tactile sensing,” *IEEE Trans. Syst. Man Cybern. Part B*, vol. 32, no. 1, pp. 57–65, Feb. 2002.

[44] F. S. R. Sensors, “http://www.interlinkelectronics.com/.” 2014.

[45] S. K. Yeung, E. M. Petriu, W. S. McMath, and D. C. Petriu, “High Sampling Resolution Tactile Sensor for Object Recognition,” *IEEE Trans. Instrum. Meas.*, vol. 43, no. 2, pp. 277–282, Apr. 1994.

[46] E. M. Petriu, S. K. S. Yeung, S. R. Das, A. M. Cretu, and H. J. W. Spoelder, “Robotic tactile recognition of pseudorandom encoded objects,” *IEEE Trans. Instrum. Meas.*, vol. 53, no. 5, pp. 1425–1432, 2004.

[47] D. Goger, N. Gorges, and H. Worn, “Tactile sensing for an anthropomorphic robotic hand: Hardware and signal processing,” in *2009 IEEE International Conference on Robotics and Automation*, 2009, pp. 895–901.

[48] M. A. Diftler, C. J. Culbert, R. O. Ambrose, R. Platt, and W. J. Bluethmann, “Evolution of the NASA/DARPA Robonaut control system,” in *2003 IEEE International Conference on Robotics and Automation (Cat. No.03CH37422)*, pp. 2543–2548.

[49] D. J. Beebe, A. S. Hsieh, D. D. Denton, and R. G. Radwin, “A silicon force sensor for robotics and medicine,” *Sensors Actuators A Phys.*, vol. 50, no. 1–2, pp. 55–65, Aug. 1995.

[50] M. R. Wolffenbuttel and P. P. L. Regtien, “Polysilicon bridges for the realization of tactile sensors,” *Sensors Actuators A Phys.*, vol. 26, no. 1–3, pp. 257–264, Mar. 1991.

[51] “Pressure Sensitive Ink, Tekscan.” [Online]. Available: https://www.tekscan.com/product-group/test-measurement/pressure-mapping?tab=products-solutions. [Accessed: 01-Jan-2018].

[52] V. M. Donaghue and A. Veves, “Foot pressure measurement,” *Orthop. Phys. Ther. Clin. North Am.*, vol. 6, pp. 1–16, 1997.

[53] “QTC Single-Point Sensors, Paratech.” [Online]. Available: https://www.peratech.com/qtc-single-point-sensors/. [Accessed: 01-Jan-2018].

[54] D. Bloor, A. Graham, E. J. Williams, P. J. Laughlin, and D. Lussey, “Metal–polymer composite with nanostructured filler particles and amplified physical properties,” *Appl. Phys. Lett.*, vol. 88, no. 10, p. 102103, Mar. 2006.

[55] Shadow Robot Company, “Developments in dextrous hands for advanced robotic applications,” *Autom. Congr. 2004. Proceedings. World*, vol. 15, pp. 123–128, 2004.

[56] B. L. Gray and R. S. Fearing, “A surface micromachined microtactile sensor array,” in *Proceedings of IEEE International Conference on Robotics and Automation*, 1996, vol. 1, pp. 1–6.

[57] P. A. Schmidt, E. Maël, and R. P. Würtz, “A sensor for dynamic tactile information with applications in human-robot interaction and object exploration,” *Rob. Auton. Syst.*, vol. 54, no. 12, pp. 1005–1014, 2006.

[58] M. Maggiali, G. Cannata, P. Maiolino, G. Metta, M. Randazzo, and G. Sandini, “Embedded Distributed Capacitive Tactile Sensor,” *11th Mechatronics Forum Bienn. Int. Conf.*, no. 039, pp. 1–5, 2008.

[59] Z. Chu, P. M. Sarro, and S. Middelhoek, “Silicon three-axial tactile sensor,” *Sensors Actuators A Phys.*, vol. 54, no. 1–3, pp. 505–510, Jun. 1996.

[60] R. J. De Souza, R. J. De Souza, and K. D. Wise, “A very high density bulk micromachined capacitive tactile imager,” in *Proceedings of International Solid State Sensors and Actuators Conference (Transducers ’97)*, 1997, vol. 2, pp. 1473–1476 vol.2.

[61] J. S. Heo, J. H. Chung, and J. J. Lee, “Tactile sensor arrays using fiber Bragg grating sensors,” *SENSORS AND ACTUATORS A-PHYSICAL*, vol. 126, no. 2, pp. 312–327, Feb. 2006.

[62] M. Ohka, H. Kobayashi, J. Takata, and Y. Mitsuya, “Sensing precision of an optical three-axis tactile sensor for a robotic finger,” in *Proceedings - IEEE International Workshop on Robot and Human Interactive Communication*, 2006, pp. 214–219.

[63] Y. Ohmura, Y. Kuniyoshi, and A. Nagakubo, “Conformable and scalable tactile sensor skin for curved surfaces,” *Proc. 2006 IEEE Int. Conf. Robot. Autom. 2006. ICRA 2006.*, vol. 2006, no. May, pp. 1348–1353, 2006.

[64] E. Cheung and V. Lumelsky, “A sensitive skin system for motion control of robot arm manipulators,” *Rob. Auton. Syst.*, vol. 10, no. 1, pp. 9–32, 1992.

[65] H. Maekawa, K. Tanie, K. Komoriya, M. Kaneko, C. Horiguchi, and T. Sugawara, “Development of a finger-shaped tactile sensor and its evaluation by active touch,” *Proc. 1992 IEEE Int. Conf. Robot. Autom.*, pp. 1327–1334, 1992.

[66] G. Milighetti, T. Emter, H. B. Kuntze, D. Bechler, and K. Kroschel, “Combined visual-acoustic grasping for humanoid robots,” in *IEEE International Conference on Multisensor Fusion and Integration for Intelligent Systems*, 2006, pp. 1–6.

[67] N. Roy, G. Dudek, and P. Freedman, “Surface sensing and classification for efficient mobile robot navigation,” in *Proceedings of IEEE International Conference on Robotics and Automation*, 1996, vol. 2, no. April, pp. 1224–1228.

[68] J. Edwards, J. Lawry, J. Rossiter, and C. Melhuish, “Extracting textural features from tactile sensors,” *Bioinspir. Biomim.*, vol. 3, no. 3, p. 035002, Sep. 2008.

[69] H. Shinoda and S. Ando, “A tactile sensor with 5-D deformation sensing element,” in *Robotics and Automation, 1996. Proceedings., 1996 IEEE International Conference on*, 1996, vol. 1, pp. 7–12.

[70] B. L. Hutchings, A. R. Grahn, and R. J. Petersen, “Multiple-layer cross-field ultrasonic tactile sensor,” in *Robotics and Automation, 1994. Proceedings., 1994 IEEE International Conference on*, 1994, pp. 2522–2528.

[71] A. S. Shinoda H. Uehara M., “A tactile sensor using 3-dimensional structure,” in *Robotics and Automation, 1993. Proceedings., 1993 IEEE International Conference on*, 1993, pp. 435–441.

[72] E. Torres-Jara, I. Vasilescu, and R. Coral, “A soft touch: Compliant tactile sensors for sensitive manipulation,” CSAIL, Massachusetts Institute of Technology,Tech. Report., 2006.

[73] L. Jamone, G. Metta, F. Nori, and G. Sandini, “James: A Humanoid Robot Acting over an Unstructured World,” in *2006 6th IEEE-RAS International Conference on Humanoid Robots*, 2006, pp. 143–150.

[74] T. J. NELSON, R. B. VANDOVER, S. JIN, S. HACKWOOD, and G. BENI, “SHEAR-SENSITIVE MAGNETORESISTIVE ROBOTIC TACTILE SENSOR,” *IEEE Trans. Magn.*, vol. 22, no. 5, pp. 394–396, Sep. 1986.

[75] D. Li and K. Shida, “Monostructure touch sensor with multifunction for discrimination of material properties,” *Electr. Eng. Japan*, vol. 117, no. 3, pp. 68–75, 1996.

[76] Y. Yamada, K. Shin, N. Tsuchida, and M. Komai, “A tactile sensor system for universal joint sections of manipulators,” *Robot. Autom. IEEE Trans.*, vol. 9, no. 4, pp. 512–517, 1993.

[77] P. DARIO and D. DEROSSI, “TACTILE SENSORS AND THE GRIPPING CHALLENGE,” *IEEE Spectr.*, vol. 22, no. 8, pp. 46–52, 1985.

[78] E. S. Kolesar, C. S. Dyson, R. R. Reston, R. C. Fitch, D. G. Ford, and S. D. Nelms, “Tactile integrated circuit sensor realized with a piezoelectric polymer,” in *EIGHTH ANNUAL IEEE INTERNATIONAL CONFERENCE ON INNOVATIVE SYSTEMS IN SILICON, 1996 PROCEEDINGS*, 1996, pp. 372–381.

[79] S. ANDO, “ULTRASONIC EMISSION TACTILE SENSING,” *IEEE Control Syst. Mag.*, vol. 15, no. 1, pp. 61–69, Feb. 1995.

[80] S. Ando, H. Shinoda, A. Yonenaga, and J. Terao, “Ultrasonic six-axis deformation sensing,” *IEEE Trans. Ultrason. Ferroelectr. Freq. Control*, vol. 48, no. 4, pp. 1031–1045, Jul. 2001.

[81] R. D. Howe and M. R. Cutkosky, “Dynamic tactile sensing: Perception of fine surface features with stress rate sensing,” *Robot. Autom. IEEE Trans.*, vol. 9, no.

2, pp. 140–151, 1993.

[82] R. D. Howe, “Tactile sensing and control of robotic manipulation,” *Adv. Robot.*, vol. 8, no. 3, pp. 245–261, Jan. 1993.

[83] J. Rossiter and T. Mukai, “An LED-based Tactile Sensor for Multi-sensing over Large Areas,” in *2006 5th IEEE Conference on Sensors*, 2006, pp. 835–838.

[84] S. Omata, Y. Murayama, and C. E. Constantinou, “Real time robotic tactile sensor system for the determination of the physical properties of biomaterials,” *Sensors Actuators A Phys.*, vol. 112, no. 2–3, pp. 278–285, May 2004.

[85] K. B. SHIMOGA and A. A. GOLDENBERG, “SOFT MATERIALS FOR ROBOTIC FINGERS,” in *1992 IEEE INTERNATIONAL CONF ON ROBOTICS AND AUTOMATION : PROCEEDINGS, VOLS 1-3*, 1992, pp. 1300–1305.

[86] T. Someya, T. Sekitani, S. Iba, Y. Kato, H. Kawaguchi, and T. Sakurai, “A large-area, flexible pressure sensor matrix with organic field-effect transistors for artificial skin applications,” *Proc. Natl. Acad. Sci. U. S. A.*, vol. 101, no. 27, pp. 9966–9970, Jul. 2004.

[87] M. Shimojo, A. Namiki, M. Ishikawa, R. Makino, and K. Mabuchi, “A tactile sensor sheet using pressure conductive rubber with electrical-wires stitched method,” *IEEE Sens. J.*, vol. 4, no. 5, pp. 589–596, 2004.

[88] R. Kageyama, S. Kagami, M. Inaba, and H. Inoue, “Development of soft and distributed tactile sensors and the application to a humanoid robot,” in *IEEE SMC’99 Conference Proceedings. 1999 IEEE International Conference on Systems, Man, and Cybernetics (Cat. No.99CH37028)*, vol. 2, pp. 981–986.

[89] R. M. Voyles, G. Fedder, and P. K. Khosla, “Design of a modular tactile sensor and actuator based on an electrorheological gel,” in *Proceedings of IEEE International Conference on Robotics and Automation*, 1996, vol. 1, no. April, pp. 13–17.

[90] K. Sawahata, J. P. Gong, and Y. Osada, “Soft and wet touch-sensing system made of hydrogel,” *Macromol. Rapid Commun.*, vol. 16, no. 10, pp. 713–716, 1995.

[91] R. Koiva, M. Zenker, C. Schuermann, R. Haschke, and H. J. Ritter, “A highly sensitive 3D-shaped tactile sensor,” in *2013 IEEE/ASME INTERNATIONAL CONFERENCE ON ADVANCED INTELLIGENT MECHATRONICS (AIM): MECHATRONICS FOR HUMAN WELLBEING*, 2013, pp. 1084–1089.

[92] G. H. Buescher, R. Koiva, C. Schuermann, R. Haschke, and H. J. Ritter, “Flexible and stretchable fabric-based tactile sensor,” *Rob. Auton. Syst.*, vol. 63, no. 3, SI, pp. 244–252, Jan. 2015.

[93] S. Luo, J. Bimbo, R. Dahiya, and H. Liu, “Robotic tactile perception of object properties: A review,” *Mechatronics*, vol. 48, no. December, pp. 54–67, 2017.

[94] O. Kroemer, C. H. Lampert, and J. Peters, “Learning Dynamic Tactile Sensing With Robust Vision-Based Training,” *IEEE Trans. Robot.*, vol. 27, no. 3, pp. 545–557, Jun. 2011.

[95] C. Fox, M. Evans, M. Pearson, and T. Prescott, “Tactile SLAM with a biomimetic whiskered robot,” in *2012 IEEE International Conference on Robotics and Automation*, 2012, pp. 4925–4930.

[96] K. J. Kuchenbecker, J. Fiene, and G. Niemeyer, “Improving contact realism through event-based haptic feedback,” *IEEE Trans. Vis. Comput. Graph.*, vol. 12, no. 2, pp. 219–230, 2006.

[97] B. Mitchinson, M. J. Pearson, A. G. Pipe, and T. J. Prescott, “Biomimetic tactile target acquisition, tracking and capture,” *Rob. Auton. Syst.*, vol. 62, no. 3, SI, pp. 366–375, Mar. 2014.

[98] L. A. Huet, J. W. Rudnicki, and M. J. Z. Hartmann, “Tactile Sensing with Whiskers of Various Shapes: Determining the Three-Dimensional Location of Object Contact Based on Mechanical Signals at the Whisker Base,” *SOFT Robot.*, vol. 4, no. 2, pp. 88–102, Jun. 2017.

[99] Z. Kappassov, J.-A. Corrales, and V. Perdereau, “Tactile sensing in dexterous robot hands - Review,” *Rob. Auton. Syst.*, vol. 74, no. A, pp. 195–220, Dec. 2015.

[100] H. Xie, H. Liu, S. Luo, L. D. Seneviratne, and K. Althoefer, “Fiber Optics Tactile

Array Probe for Tissue Palpation during Minimally Invasive Surgery," in *2013 IEEE/RSJ INTERNATIONAL CONFERENCE ON INTELLIGENT ROBOTS AND SYSTEMS (IROS)*, 2013, pp. 2539–2544.

[101] Y. Tenzer, L. P. Jentoft, and R. D. Howe, "The Feel of MEMS Barometers: Inexpensive and Easily Customized Tactile Array Sensors," *IEEE Robot. Autom. Mag.*, vol. 21, no. 3, pp. 89–95, Sep. 2014.

[102] C. Chorley, C. Melhuish, T. Pipe, and J. Rossiter, "Development of a tactile sensor based on biologically inspired edge encoding," *2009 Int. Conf. Adv. Robot.*, 2009.

[103] K. Sato, K. Kamiyama, N. Kawakami, and S. Tachi, "Finger-Shaped GelForce: Sensor for Measuring Surface Traction Fields for Robotic Hand," *IEEE Trans. Haptics*, vol. 3, no. 1, pp. 37–47, 2010.

[104] M. K. Johnson, F. Cole, A. Raj, and E. H. Adelson, "Microgeometry Capture using an Elastomeric Sensor," *ACM Trans. Graph.*, vol. 30, no. 4, Jul. 2011.

[105] A. Yamaguchi and C. G. Atkeson, "Combining Finger Vision and Optical Tactile Sensing: Reducing and Handling Errors While Cutting Vegetables," in *2016 IEEE-RAS 16TH INTERNATIONAL CONFERENCE ON HUMANOID ROBOTS (HUMANOIDS)*, 2016, pp. 1045–1051.

[106] "Pressure Profile Systems." [Online]. Available: https://pressureprofile.com/. [Accessed: 01-Jan-2018].

[107] "Weiss Robotics." [Online]. Available: www.weiss-robotics.com/en/produkte/tactile-sensing/wts-en/. [Accessed: 01-Jan-2018].

[108] "SynTouch." [Online]. Available: www.syntouchinc.com/. [Accessed: 01-Jan-2018].

[109] M. Kaltenbrunner *et al.*, "An ultra-lightweight design for imperceptible plastic electronics," *Nature*, vol. 499, no. 7459, p. 458+, Jul. 2013.

[110] E. O. Polat, O. Balci, N. Kakenov, H. B. Uzlu, C. Kocabas, and R. Dahiya, "Synthesis of Large Area Graphene for High Performance in Flexible Optoelectronic Devices," *Sci. Rep.*, vol. 5, Nov. 2015.

[111] M. Hoffmann, Z. Straka, I. Farkas, M. Vavrecka, and G. Metta, “Robotic homunculus: Learning of artificial skin representation in a humanoid robot motivated by primary somatosensory cortex,” *IEEE Trans. Cogn. Dev. Syst.*, pp. 1–1, 2017.

[112] L. Muscari, L. Seminara, F. Mastrogiovanni, M. Valle, M. Capurro, and G. Cannata, “Real-Time Reconstruction of Contact Shapes for Large Area Robot Skin,” in *2013 IEEE INTERNATIONAL CONFERENCE ON ROBOTICS AND AUTOMATION (ICRA)*, 2013, pp. 2360–2366.

[113] P. Mittendorfer and G. Cheng, “Humanoid Multimodal Tactile-Sensing Modules,” *IEEE Trans. Robot.*, vol. 27, no. 3, pp. 401–410, Jun. 2011.

[114] C. Bartolozzi, L. Natale, F. Nori, and G. Metta, “Robots with a sense of touch,” *Nat. Mater.*, vol. 15, no. 9, pp. 921–925, Sep. 2016.

[115] M. Kaboli, A. Long, and G. Cheng, “Humanoids learn touch modalities identification via multi-modal robotic skin and robust tactile descriptors,” *Adv. Robot.*, vol. 29, no. 21, SI, pp. 1411–1425, Nov. 2015.

[116] S. Khan, L. Lorenzelli, and R. S. Dahiya, “Technologies for Printing Sensors and Electronics Over Large Flexible Substrates: A Review,” *IEEE Sens. J.*, vol. 15, no. 6, pp. 3164–3185, Jun. 2015.

[117] H. Heidari, N. Wacker, and R. Dahiya, “Bending induced electrical response variations in ultra-thin flexible chips and device modeling,” *Appl. Phys. Rev.*, vol. 4, no. 3, Sep. 2017.

[118] W. Dang, V. Vinciguerra, L. Lorenzelli, and R. Dahiya, “Printable stretchable interconnects,” *Flex. Print. Electron.*, vol. 2, no. 1, p. 013003, Mar. 2017.

[119] A. Schneider, J. J. Sturm, C. Stachniss, M. Reisert, H. Burkhardt, and W. Burgard, “Object identification with tactile sensors using bag-of-features,” *2009 IEEE/RSJ Int. Conf. Intell. Robot. Syst.*, pp. 243–248, Oct. 2009.

[120] Z. Pezzementi, E. Plaku, C. Reyda, and G. D. Hager, “Tactile-Object Recognition From Appearance Information,” *IEEE Trans. Robot.*, vol. 27, no. 3, pp. 473–487,

Jun. 2011.

[121] G. Cannata, S. Denei, and F. Mastrogiovanni, “A Framework for Representing Interaction Tasks based on Tactile Data,” in *2010 IEEE RO-MAN*, 2010, pp. 698–703.

[122] G. Heidemann and M. Schopfer, “Dynamic tactile sensing for object identification,” in *2004 IEEE INTERNATIONAL CONFERENCE ON ROBOTICS AND AUTOMATION, VOLS 1- 5, PROCEEDINGS*, 2004, pp. 813–818.

[123] H. Liu, X. Song, T. Nanayakkara, L. D. Seneviratne, and K. Althoefer, “A Computationally Fast Algorithm for Local Contact Shape and Pose Classification using a Tactile Array Sensor,” in *2012 IEEE INTERNATIONAL CONFERENCE ON ROBOTICS AND AUTOMATION (ICRA)*, 2012, pp. 1410–1415.

[124] J. Tegin, S. Ekvall, D. Kragic, J. Wikander, and B. Iliev, “Demonstration-based learning and control for automatic grasping,” *Intell. Serv. Robot.*, vol. 2, no. 1, pp. 23–30, Jan. 2009.

[125] X. Song, H. Liu, K. Althoefer, T. Nanayakkara, and L. D. Seneviratne, “Efficient Break-Away Friction Ratio and Slip Prediction Based on Haptic Surface Exploration,” *IEEE Trans. Robot.*, vol. 30, no. 1, pp. 203–219, Feb. 2014.

[126] Y. Bekiroglu, J. Laaksonen, J. A. Jorgensen, V. Kyrki, and D. Kragic, “Assessing Grasp Stability Based on Learning and Haptic Data,” *IEEE Trans. Robot.*, vol. 27, no. 3, pp. 616–629, Jun. 2011.

[127] M. Li, S. Luo, T. Nanayakkara, L. D. Seneviratne, P. Dasgupta, and K. Althoefer, “Multi-fingered haptic palpation using pneumatic feedback actuators,” *SENSORS AND ACTUATORS A-PHYSICAL*, vol. 218, pp. 132–141, Oct. 2014.

[128] M. Benali-Khoudja, M. Hafez, J. M. Alexandre, and A. Kheddar, “Tactile Interfaces: a state-of-the-art survey ,” *Isr*, no. January 2004, pp. 1–9, 2004.

[129] T. R. Coles, D. Meglan, and N. W. John, “The Role of Haptics in Medical Training Simulators: A Survey of the State of the Art,” *IEEE Trans. Haptics*, vol. 4, no. 1, pp. 51–66, 2011.

[130] A. Aggarwal and F. Kirchner, “Object Recognition and Localization: The Role of Tactile Sensors,” *SENSORS*, vol. 14, no. 2, pp. 3227–3266, Feb. 2014.

[131] W. C. Nowlin, “Experimental results on Bayesian algorithms for interpreting compliant tactile sensing data,” in *Robotics and Automation, 1991. Proceedings., 1991 IEEE International Conference on*, 1991, pp. 378–383.

[132] J. Jockusch, J. Walter, and H. Ritter, “A tactile sensor system for a three-fingered robot manipulator,” in *Proceedings of International Conference on Robotics and Automation*, 1997, vol. 4, no. April, pp. 3080–3086.

[133] R. E. Saad, A. Bonen, K. C. Smith, and B. Benhabib, “Distributed-force recovery for a planar photoelastic tactile sensor,” *Instrum. Meas. IEEE Trans.*, vol. 45, no. 2, pp. 541–546, 1996.

[134] C. Liu, L. Sharan, E. H. Adelson, and R. Rosenholtz, “Exploring Features in a Bayesian Framework for Material Recognition,” in *2010 IEEE CONFERENCE ON COMPUTER VISION AND PATTERN RECOGNITION (CVPR)*, 2010, pp. 239–246.

[135] L. Sharan, C. Liu, R. Rosenholtz, and E. H. Adelson, “Recognizing Materials Using Perceptually Inspired Features,” *Int. J. Comput. Vis.*, vol. 103, no. 3, pp. 348–371, Jul. 2013.

[136] L. Sun, S. Rogers, G. Aragon-Camarasa, and J. P. Siebert, “Recognising the Clothing Categories from Free-Configuration using Gaussian-Process-Based Interactive Perception,” in *2016 IEEE INTERNATIONAL CONFERENCE ON ROBOTICS AND AUTOMATION (ICRA)*, 2016, pp. 2464–2470.

[137] S. J. LEDERMAN and R. L. KLATZKY, “HAPTIC CLASSIFICATION OF COMMON OBJECTS - KNOWLEDGE-DRIVEN EXPLORATION,” *Cogn. Psychol.*, vol. 22, no. 4, pp. 421–459, Oct. 1990.

[138] W. M. B. Tiest, “Tactual perception of material properties,” *Vision Res.*, vol. 50, no. 24, SI, pp. 2775–2782, Dec. 2010.

[139] S. Luo, L. Zhu, K. Althoefer, and H. Liu, “Knock-Knock: Acoustic object recognition by using stacked denoising autoencoders,” *Neurocomputing*, vol. 267, pp. 18–

24, Dec. 2017.

[140] M. Johnsson and C. Balkenius, “Sense of Touch in Robots With Self-Organizing Maps,” *IEEE Trans. Robot.*, vol. 27, no. 3, pp. 498–507, Jun. 2011.

[141] N. Jamali and C. Sammut, “Material Classification by Tactile Sensing using Surface Textures,” *2010 IEEE Int. Conf. Robot. Autom.*, vol. 27, no. 3, pp. 2336–2341, May 2010.

[142] H. Liu, X. Song, J. Bimbo, L. Seneviratne, and K. Althoefer, “Surface material recognition through haptic exploration using an intelligent contact sensing finger,” in *2012 IEEE/RSJ International Conference on Intelligent Robots and Systems*, 2012, pp. 52–57.

[143] V. A. Ho, T. Araki, M. Makikawa, and S. Hirai, “Experimental Investigation of Surface Identification Ability of a Low-Profile Fabric Tactile Sensor,” in *2012 IEEE/RSJ INTERNATIONAL CONFERENCE ON INTELLIGENT ROBOTS AND SYSTEMS (IROS)*, 2012, pp. 4497–4504.

[144] P. Dallaire, P. Giguère, D. Émond, and B. Chaib-draa, “Autonomous tactile perception: A combined improved sensing and Bayesian nonparametric approach,” *Rob. Auton. Syst.*, vol. 62, no. 4, pp. 422–435, Apr. 2014.

[145] P. Giguere and G. Dudek, “A Simple Tactile Probe for Surface Identification by Mobile Robots,” *IEEE Trans. Robot.*, vol. 27, no. 3, pp. 534–544, Jun. 2011.

[146] J. Sinapov, V. Sukhoy, R. Sahai, and A. Stoytchev, “Vibrotactile Recognition and Categorization of Surfaces by a Humanoid Robot,” *IEEE Trans. Robot.*, vol. 27, no. 3, pp. 488–497, Jun. 2011.

[147] J. M. Romano and K. J. Kuchenbecker, “Methods for Robotic Tool-Mediated Haptic Surface Recognition,” in *2014 IEEE HAPTICS SYMPOSIUM (HAPTICS)*, 2014, pp. 49–56.

[148] M. Kaboli, P. Mittendorfer, V. Hugel, and G. Cheng, “Humanoids Learn Object Properties From Robust Tactile Feature Descriptors via Multi-Modal Artificial Skin,” in *2014 14th IEEE-RAS International Conference on Humanoid Robots*

(Humanoids), 2014, pp. 187–192.

[149] M. Tanaka, J. L. Leveque, H. Tagami, K. Kikuchi, and S. Chonan, “The ``Haptic Finger{''} - a new device for monitoring skin condition,” *Ski. Res. Technol.*, vol. 9, no. 2, pp. 131–136, May 2003.

[150] C. M. Oddo, M. Controzzi, L. Beccai, C. Cipriani, and M. C. Carrozza, “Roughness Encoding for Discrimination of Surfaces in Artificial Active-Touch,” *IEEE Trans. Robot.*, vol. 27, no. 3, pp. 522–533, Jun. 2011.

[151] D. Xu, G. E. Loeb, and J. A. Fishel, “Tactile identification of objects using Bayesian exploration,” in *2013 IEEE International Conference on Robotics and Automation*, 2013, pp. 3056–3061.

[152] R. Li and E. H. Adelson, “Sensing and Recognizing Surface Textures Using a GelSight Sensor,” in *2013 IEEE CONFERENCE ON COMPUTER VISION AND PATTERN RECOGNITION (CVPR)*, 2013, pp. 1241–1247.

[153] B. Winstone, G. Griffiths, T. Pipe, C. Melhuish, and J. Rossiter, “TACTIP - Tactile Fingertip Device, Texture Analysis through Optical Tracking of Skin Features,” 2013, pp. 323–334.

[154] S.-H. Kim, J. Engel, C. Liu, and D. L. Jones, “Texture classification using a polymer-based MEMS tactile sensor,” *J. Micromechanics Microengineering*, vol. 15, no. 5, pp. 912–920, May 2005.

[155] J. J. Shill, E. G. Collins Jr., E. Coyle, and J. Clark, “Tactile surface classification for limbed robots using a pressure sensitive robot skin,” *Bioinspir. Biomim.*, vol. 10, no. 1, Feb. 2015.

[156] T. Nanayakkara, A. Jiang, M. del R. A. Fernandez, H. Liu, K. Althoefer, and J. Bimbo, “Stable Grip Control on Soft Objects With Time-Varying Stiffness,” *IEEE Trans. Robot.*, vol. 32, no. 3, pp. 626–637, Jun. 2016.

[157] Z. Su, J. A. Fishel, T. Yamamoto, and G. E. Loeb, “Use of tactile feedback to control exploratory movements to characterize object compliance,” *Front. Neurorobot.*, vol. 6, 2012.

[158] J. Hoelscher, J. Peters, and T. Hermans, “Evaluation of Tactile Feature Extraction for Interactive Object Recognition,” in *2015 IEEE-RAS 15TH INTERNATIONAL CONFERENCE ON HUMANOID ROBOTS (HUMANOIDS)*, 2015, pp. 310–317.

[159] V. Chu *et al.*, “Using Robotic Exploratory Procedures to Learn the Meaning of Haptic Adjectives,” in *2013 IEEE INTERNATIONAL CONFERENCE ON ROBOTICS AND AUTOMATION (ICRA)*, 2013, pp. 3048–3055.

[160] W. Yuan, M. A. Srinivasan, and E. H. Adelson, “Estimating Object Hardness with a GelSight Touch Sensor,” in *2016 IEEE/RSJ INTERNATIONAL CONFERENCE ON INTELLIGENT ROBOTS AND SYSTEMS (IROS 2016)*, 2016, pp. 208–215.

[161] W. Yuan, C. Zhu, A. Owens, M. A. Srinivasan, and E. H. Adelson, “Shape-independent hardness estimation using deep learning and a GelSight tactile sensor,” in *2017 IEEE International Conference on Robotics and Automation (ICRA)*, 2017, pp. 951–958.

[162] A. Drimus, G. Kootstra, A. Bilberg, and D. Kragic, “Design of a flexible tactile sensor for classification of rigid and deformable objects,” *Rob. Auton. Syst.*, vol. 62, no. 1, pp. 3–15, Jan. 2014.

[163] K. Sangpradit, H. Liu, P. Dasgupta, K. Althoefer, and L. D. Seneviratne, “Finite-Element Modeling of Soft Tissue Rolling Indentation,” *IEEE Trans. Biomed. Eng.*, vol. 58, no. 12, 1, pp. 3319–3327, Dec. 2011.

[164] A. Faragasso, A. Stilli, J. Bimbo, H. A. Wurdemann, and K. Althoefer, “Multi-axis Stiffness Sensing Device for Medical Palpation,” in *2015 IEEE/RSJ INTERNATIONAL CONFERENCE ON INTELLIGENT ROBOTS AND SYSTEMS (IROS)*, 2015, pp. 2711–2716.

[165] D. G. Lowe, “Object recognition from local scale-invariant features,” in *Computer Vision, 1999. The Proceedings of the Seventh IEEE International Conference on*, 1999, vol. 2, pp. 1150–1157 vol.2.

[166] P. F. Felzenszwalb and D. P. Huttenlocher, “Pictorial structures for object recognition,” *Int. J. Comput. Vis.*, vol. 61, no. 1, pp. 55–79, Jan. 2005.

[167] T. Corradi, P. Hall, and P. Iravani, “Bayesian Tactile Object Recognition: learning and recognising objects using a new inexpensive tactile sensor,” in *2015 IEEE INTERNATIONAL CONFERENCE ON ROBOTICS AND AUTOMATION (ICRA)*, 2015, pp. 3909–3914.

[168] N. Jamali and C. Sammut, “Majority Voting: Material Classification by Tactile Sensing Using Surface Texture,” *IEEE Trans. Robot.*, vol. 27, no. 3, SI, pp. 508–521, Jun. 2011.

[169] A. R. Jimenez, A. S. Soembagijo, D. Reynaerts, H. VanBrussel, R. Ceres, and J. L. Pons, “Featureless classification of tactile contacts in a gripper using neural networks,” *SENSORS AND ACTUATORS A-PHYSICAL*, vol. 62, no. 1–3, pp. 488–491, Jul. 1997.

[170] H. Liu, J. Greco, X. Song, J. Bimbo, L. Seneviratne, and K. Althoefer, “Tactile image based contact shape recognition using neural network,” in *2012 IEEE International Conference on Multisensor Fusion and Integration for Intelligent Systems (MFI)*, 2012, pp. 138–143.

[171] U. Martinez-Hernandez, T. J. Dodd, L. Natale, G. Metta, T. J. Prescott, and N. F. Lepora, “Active contour following to explore object shape with robot touch,” in *2013 WORLD HAPTICS CONFERENCE (WHC)*, 2013, pp. 341–346.

[172] M. Schopfer, M. Pardowitz, and H. Ritter, “Using entropy for dimension reduction of tactile data,” *Int. Conf. Adv. Robot.*, pp. 1–6, 2009.

[173] D. Silvera Tawil, D. Rye, and M. Velonaki, “Touch modality interpretation for an EIT-based sensitive skin,” in *2011 IEEE International Conference on Robotics and Automation*, 2011, pp. 3770–3776.

[174] S. Chitta, J. Sturm, M. Piccoli, and W. Burgard, “Tactile Sensing for Mobile Manipulation,” *IEEE Trans. Robot.*, vol. 27, no. 3, pp. 558–568, Jun. 2011.

[175] R. Russell, “Object recognition by a ‘smart’ tactile sensor,” *Proc. Aust. Conf. Robot.*, pp. 93–98, 2000.

[176] A. J. Schmid, N. Gorges, D. Goeger, and H. Woern, “Opening a door with a

humanoid robot using multi-sensory tactile feedback," in *2008 IEEE INTERNATIONAL CONFERENCE ON ROBOTICS AND AUTOMATION, VOLS 1-9*, 2008, pp. 285–291.

[177] Y. Bekiroglu, R. Detry, and D. Kragic, "Learning Tactile Characterizations Of Object- And Pose-specific Grasps," in *2011 IEEE/RSJ INTERNATIONAL CONFERENCE ON INTELLIGENT ROBOTS AND SYSTEMS*, 2011, pp. 1554–1560.

[178] C. Schurmann, R. K~oiva, R. Haschke, and H. Ritter, "A modular high-speed tactile sensor for human manipulation research," in *2011 IEEE World Haptics Conference*, 2011, pp. 339–344.

[179] Q. Li, C. Sch, R. Haschke, and H. Ritter, "A control framework for tactile servoing," *Rss2013*, no. June, 2013.

[180] Y. Bekiroglu, D. Song, L. Wang, and D. Kragic, "A Probabilistic Framework for Task-Oriented Grasp Stability Assessment," in *2013 IEEE INTERNATIONAL CONFERENCE ON ROBOTICS AND AUTOMATION (ICRA)*, 2013, pp. 3040–3047.

[181] A. Khasnobish, G. Singh, A. Jati, A. Konar, and D. N. Tibarewala, "Object-shape recognition and 3D reconstruction from tactile sensor images," *Med. Biol. Eng. Comput.*, vol. 52, no. 4, pp. 353–362, Apr. 2014.

[182] S. Luo, X. Liu, K. Althoefer, and H. Liu, "Tactile Object Recognition with Semi-supervised Learning," in *INTELLIGENT ROBOTICS AND APPLICATIONS (ICIRA 2015), PT II*, 2015, vol. 9245, pp. 15–26.

[183] S. Luo, W. Mou, K. Althoefer, and H. Liu, "Novel Tactile-SIFT Descriptor for Object Shape Recognition," *IEEE Sens. J.*, vol. 15, no. 9, pp. 5001–5009, Sep. 2015.

[184] Shan Luo, Wenxuan Mou, Min Li, K. Althoefer, and Hongbin Liu, "Rotation and translation invariant object recognition with a tactile sensor," in *IEEE SENSORS 2014 Proceedings*, 2014, pp. 1030–1033.

[185] S. Belongie, J. Malik, and J. Puzicha, "Shape matching and object recognition using shape contexts," *IEEE Trans. Pattern Anal. Mach. Intell.*, vol. 24, no. 4, pp. 509–522, Apr. 2002.

[186] H. Bay, A. Ess, T. Tuytelaars, and L. Van Gool, “Speeded-Up Robust Features (SURF),” *Comput. Vis. Image Underst.*, vol. 110, no. 3, pp. 346–359, Jun. 2008.

[187] F. Tombari, S. Salti, and L. Di Stefano, “Unique Signatures of Histograms for Local Surface Description,” in *COMPUTER VISION-ECCV 2010, PT III*, 2010, vol. 6313, no. III, pp. 356–369.

[188] Z. Ji, F. Amirabdollahian, D. Polani, and K. Dautenhahn, “Histogram based classification of tactile patterns on periodically distributed skin sensors for a humanoid robot,” in *2011 RO-MAN*, 2011, pp. 433–440.

[189] R. Li *et al.*, “Localization and Manipulation of Small Parts Using GelSight Tactile Sensing,” in *2014 IEEE/RSJ INTERNATIONAL CONFERENCE ON INTELLIGENT ROBOTS AND SYSTEMS (IROS 2014)*, 2014, pp. 3988–3993.

[190] Y.-H. Liu, Y.-T. Hsiao, W.-T. Cheng, Y.-C. Liu, and J.-Y. Su, “Low-Resolution Tactile Image Recognition for Automated Robotic Assembly Using Kernel PCA-Based Feature Fusion and Multiple Kernel Learning-Based Support Vector Machine,” *Math. Probl. Eng.*, vol. 2014, pp. 1–11, 2014.

[191] M. Li, Y. Bekiroglu, D. Kragic, and A. Billard, “Learning of Grasp Adaptation through Experience and Tactile Sensing,” in *2014 IEEE/RSJ INTERNATIONAL CONFERENCE ON INTELLIGENT ROBOTS AND SYSTEMS (IROS 2014)*, 2014, pp. 3339–3346.

[192] M. Schoepfer, H. Ritter, and G. Heidemann, “Acquisition and application of a tactile database,” in *PROCEEDINGS OF THE 2007 IEEE INTERNATIONAL CONFERENCE ON ROBOTICS AND AUTOMATION, VOLS 1-10*, 2007, p. 1517+.

[193] J. Bimbo, S. Luo, K. Althoefer, and H. Liu, “In-Hand Object Pose Estimation Using Covariance-Based Tactile To Geometry Matching,” *IEEE Robot. Autom. Lett.*, vol. 1, no. 1, pp. 570–577, Jan. 2016.

[194] M. Madry, L. Bo, D. Kragic, and D. Fox, “ST-HMP: Unsupervised Spatio-Temporal Feature Learning for Tactile Data,” in *2014 IEEE INTERNATIONAL CONFERENCE ON ROBOTICS AND AUTOMATION (ICRA)*, 2014, pp. 2262–2269.

[195] H. Soh, Y. Su, and Y. Demiris, “Online spatio-temporal Gaussian process experts with application to tactile classification,” in *2012 IEEE/RSJ International Conference on Intelligent Robots and Systems*, 2012, pp. 4489–4496.

[196] H. Soh and Y. Demiris, “Incrementally Learning Objects by Touch: Online Discriminative and Generative Models for Tactile-Based Recognition,” *IEEE Trans. Haptics*, vol. 7, no. 4, pp. 512–525, 2014.

[197] A. Molchanov, O. Kroemer, Z. Su, and G. S. Sukhatme, “Contact Localization on Grasped Objects using Tactile Sensing,” in *2016 IEEE/RSJ INTERNATIONAL CONFERENCE ON INTELLIGENT ROBOTS AND SYSTEMS (IROS 2016)*, 2016, pp. 216–222.

[198] A. Schmitz, Y. Bansho, K. Noda, H. Iwata, T. Ogata, and S. Sugano, “Tactile Object Recognition using Deep Learning and Dropout,” in *2014 14th IEEE-RAS International Conference on Humanoid Robots (Humanoids)*, 2014, pp. 1044–1050.

[199] L. Cao, R. Kotagiri, F. Sun, H. Liu, W. Huang, and Z. M. M. . Aye, “Efficient spatio-temporal tactile object recognition with randomized tiling convolutional networks in a hierarchical fusion strategy,” *30th AAAI Conf. Artif. Intell. AAAI 2016*, pp. 3337–3345, 2016.

[200] H. Liu, D. Guo, and F. Sun, “Object Recognition Using Tactile Measurements: Kernel Sparse Coding Methods,” *IEEE Trans. Instrum. Meas.*, vol. 65, no. 3, pp. 656–665, Mar. 2016.

[201] Y. Bengio, A. Courville, and P. Vincent, “Representation Learning: A Review and New Perspectives,” *IEEE Trans. Pattern Anal. Mach. Intell.*, vol. 35, no. 8, pp. 1798–1828, Aug. 2013.

[202] E. Hyttinen, D. Kragic, and R. Detry, “Learning the Tactile Signatures of Prototypical Object Parts for Robust Part-based Grasping of Novel Objects,” in *2015 IEEE INTERNATIONAL CONFERENCE ON ROBOTICS AND AUTOMATION (ICRA)*, 2015, pp. 4927–4932.

[203] J. A. Stork, C. H. Ek, Y. Bekiroglu, and D. Kragic, “Learning Predictive State Representation for In-Hand Manipulation,” in *2015 IEEE INTERNATIONAL CONFERENCE ON ROBOTICS AND AUTOMATION (ICRA)*, 2015, pp. 3207–3214.

[204] A. M. Okamura and M. R. Cutkosky, “Feature Detection for Haptic Exploration with Robotic Fingers,” *Int. J. Rob. Res.*, vol. 20, no. 12, pp. 925–938, Dec. 2001.

[205] M. Charlebois, K. Gupta, and S. Payandeh, “Shape description of curved surfaces from contact sensing using surface normals,” *Int. J. Rob. Res.*, vol. 18, no. 8, pp. 779–787, Aug. 1999.

[206] P. K. Allen and K. S. Roberts, “Haptic object recognition using a multi-fingered dextrous hand,” in *Proceedings, 1989 International Conference on Robotics and Automation*, 1989, pp. 342–347.

[207] S. Casselli, C. Magnanini, and F. Zanichelli, “On the robustness of haptic object recognition based on polyhedral shape representations,” in *Proceedings 1995 IEEE/RSJ International Conference on Intelligent Robots and Systems. Human Robot Interaction and Cooperative Robots*, 1995, vol. 2, pp. 200–206.

[208] Y.-B. Jia and J. Tian, “Surface Patch Reconstruction From One-Dimensional Tactile Data,” *IEEE Trans. Autom. Sci. Eng.*, vol. 7, no. 2, pp. 400–407, Apr. 2010.

[209] Yan-Bin Jia, Liangchuan Mi, and Jiang Tian, “Surface patch reconstruction via curve sampling,” in *Proceedings 2006 IEEE International Conference on Robotics and Automation, 2006. ICRA 2006.*, 2006, pp. 1371–1377.

[210] R. Ibrayev and Y. B. Jia, “Semidifferential invariants for tactile recognition of algebraic curves,” *Int. J. Rob. Res.*, vol. 24, no. 11, pp. 951–969, Nov. 2005.

[211] I. Abraham, A. Prabhakar, M. J. Z. Hartmann, and T. D. Murphey, “Ergodic Exploration Using Binary Sensing for Nonparametric Shape Estimation,” *IEEE Robot. Autom. Lett.*, vol. 2, no. 2, pp. 827–834, Apr. 2017.

[212] M. Meier, M. Schopfer, R. Haschke, and H. Ritter, “A Probabilistic Approach to Tactile Shape Reconstruction,” *IEEE Trans. Robot.*, vol. 27, no. 3, pp. 630–635, Jun. 2011.

[213] A. J. Spiers, M. V Liarokapis, B. Calli, and A. M. Dollar, “Single-Grasp Object Classification and Feature Extraction with Simple Robot Hands and Tactile Sensors,” *IEEE Trans. Haptics*, vol. 9, no. 2, pp. 207–220, 2016.

[214] E. M. Petriu, W. S. McMath, S. S. K. Yeung, and N. Trif, “Active tactile perception of object surface geometric profiles,” *IEEE Trans. Instrum. Meas.*, vol. 41, no. 1, pp. 87–92, Feb. 1992.

[215] W. S. McMath, S. K. Yeung, E. Petriu, and N. Trif, “Tactile sensor for geometric profile perception,” in *Proceedings IECON ’91: 1991 International Conference on Industrial Electronics, Control and Instrumentation*, pp. 893–897.

[216] S. Luo, W. Mou, K. Althoefer, and H. Liu, “Iterative Closest Labeled Point for tactile object shape recognition,” in *2016 IEEE/RSJ International Conference on Intelligent Robots and Systems (IROS)*, 2016, pp. 3137–3142.

[217] K. Hertkorn, M. A. Roa, and C. Borst, “Planning in-hand object manipulation with multifingered hands considering task constraints,” in *2013 IEEE International Conference on Robotics and Automation*, 2013, pp. 617–624.

[218] D. M. Siegel, “Finding the pose of an object in a hand,” in *Proceedings. 1991 IEEE International Conference on Robotics and Automation*, pp. 406–411.

[219] C. Corcoran and R. Platt, “A measurement model for tracking hand-object state during dexterous manipulation,” in *2010 IEEE International Conference on Robotics and Automation*, 2010, pp. 4302–4308.

[220] R. Platt, F. Permenter, and J. Pfeiffer, “Using Bayesian Filtering to Localize Flexible Materials During Manipulation,” *IEEE Trans. Robot.*, vol. 27, no. 3, pp. 586–598, Jun. 2011.

[221] A. Petrovskaya and O. Khatib, “Global Localization of Objects via Touch,” *IEEE Trans. Robot.*, vol. 27, no. 3, pp. 569–585, Jun. 2011.

[222] A. Petrovskaya, O. Khatib, S. Thrun, and A. Y. Ng, “Touch Based Perception for Object Manipulation,” *Robot. Sci. Syst. Robot Manip. Work.*, no. February, pp. 2–7, 2007.

[223] A. Petrovskaya, O. Khatib, S. Thrun, and A. Y. Ng, “Bayesian estimation for autonomous object manipulation based on tactile sensors,” in *Proceedings 2006 IEEE International Conference on Robotics and Automation, 2006. ICRA 2006.*, 2006, pp. 707–714.

[224] J. Bimbo, P. Kormushev, K. Althoefer, and H. Liu, “Global estimation of an object’s pose using tactile sensing,” *Adv. Robot.*, vol. 29, no. 5, SI, pp. 363–374, Mar. 2015.

[225] S. J. S. Lederman and D. T. Pawluk, “Lessons From the Study of Biological Touch for Robotic Tactile Sensing,” in *Adv. Tactile Sens. Robot*, 1992, pp. 151–192.

[226] J. Dargahi and S. Najarian, “Human tactile perception as a standard for artificial tactile sensing - a review,” *Int. J. Med. Robot. Comput. Assist. Surg.*, vol. 1, no. 1, pp. 23–35, Jun. 2004.

[227] R. Fearing and J. Hollerbach, “Basic solid mechanics for tactile sensing,” in *Proceedings. 1984 IEEE International Conference on Robotics and Automation*, vol. 1, pp. 266–275.

[228] R. S. Dahiya and M. Gori, “Probing With and Into Fingerprints,” *J. Neurophysiol.*, vol. 104, no. 1, pp. 1–3, Jul. 2010.

[229] P. Mittendorfer and G. Cheng, “Integrating discrete force cells into multi-modal artificial skin,” in *Humanoid Robots (Humanoids), 2012 12th IEEE-RAS International Conference on*, 2012, pp. 847–852.

[230] H. Alirezaei, A. Nagakubo, and Y. Kuniyoshi, “A highly stretchable tactile distribution sensor for smooth surfaced humanoids,” in *Humanoid Robots, 2007 7th IEEE-RAS International Conference on*, 2007, pp. 167–173.

[231] T. Mukai, M. Onishi, T. Odashima, S. Hirano, and Z. Luo, “Development of the tactile sensor system of a human-interactive robot ‘RI-MAN,’” *IEEE Trans. Robot.*, vol. 24, no. 2, pp. 505–512, 2008.

[232] R. S. Dahiya and M. Valle, *Robotic Tactile Sensing: Technologies and System*. 2012.

[233] B. Zitova and J. Flusser, “Image registration methods: a survey,” *Image Vis. Comput.*, vol. 21, no. 11, pp. 977–1000, 2003.

[234] D. J. Van Den Heever, K. Schreve, and C. Scheffer, “Tactile sensing using force sensing resistors and a super-resolution algorithm,” *Sensors Journal, IEEE*, vol. 9, no. 1, pp. 29–35, 2009.

[235] R. Sekuler and R. Blake, *Perception*, no. v. 1. McGraw-Hill, 2002.

[236] H. C. Elliott, *The shape of intelligence: the evolution of the human brain*. Scribner, 1969.

[237] M. P. McKinley and V. D. O’Loughlin, *Human Anatomy*. McGraw-Hill Higher Education, 2007.

[238] S. Ballesteros, J. M. Reales, L. P. De Leon, and B. Garcia, “The perception of ecological textures by touch: Does the perceptual space change under bimodal visual and haptic exploration?,” *Proc. - 1st Jt. Eurohaptics Conf. Symp. Haptic Interfaces Virtual Environ. Teleoperator Syst. World Haptics Conf. WHC 2005*, no. 1, pp. 635–638, 2005.

[239] A.-M. M. Cretu, T. E. A. De Oliveira, V. Prado Da Fonseca, B. Tawbe, E. M. Petriu, and V. Z. Groza, “Computational intelligence and mechatronics solutions for robotic tactile object recognition,” in *2015 IEEE 9th International Symposium on Intelligent Signal Processing (WISP) Proceedings*, 2015, no. 2, pp. 1–6.

[240] G. Spigler, C. M. Oddo, and M. C. Carrozza, “Soft-neuromorphic artificial touch for applications in neuro-robotics,” *Proc. IEEE RAS EMBS Int. Conf. Biomed. Robot. Biomechatronics*, pp. 1913–1918, 2012.

[241] F. de Boissieu, C. Godin, B. Guilhamat, D. David, C. Serviere, and D. Baudois, “Tactile Texture Recognition with a 3-Axial Force MEMS integrated Artificial Finger,” in *Robotics: Science and Systems*, 2009, pp. 49–56.

[242] P. Dallaire, D. Emond, P. Giguere, and B. Chaib-Draa, “Artificial tactile perception for surface identification using a triple axis accelerometer probe,” in *2011 IEEE International Symposium on Robotic and Sensors Environments (ROSE)*, 2011,

pp. 101–106.

[243] P. Giguere and G. Dudek, “Surface identification using simple contact dynamics for mobile robots,” in *2009 IEEE International Conference on Robotics and Automation*, 2009, pp. 3301–3306.

[244] G. De Maria, C. Natale, and S. Pirozzi, “Force/tactile sensor for robotic applications,” *Sensors Actuators A Phys.*, vol. 175, pp. 60–72, Mar. 2012.

[245] G. De Maria, C. Natale, and S. Pirozzi, “Tactile data modeling and interpretation for stable grasping and manipulation,” *Rob. Auton. Syst.*, vol. 61, no. 9, pp. 1008–1020, Sep. 2013.

[246] G. De Maria, C. Natale, and S. Pirozzi, “Tactile sensor for human-like manipulation,” *2012 4th IEEE RAS EMBS Int. Conf. Biomed. Robot. Biomechatronics*, pp. 1686–1691, Jun. 2012.

[247] T. Assaf, C. Roke, J. Rossiter, T. Pipe, and C. Melhuish, “Seeing by touch: Evaluation of a soft biologically-inspired artificial fingertip in real-time active touch,” *Sensors (Switzerland)*, vol. 14, no. 2, pp. 2561–2577, 2014.

[248] Y.-L. Park, R. J. Black, B. Moslehi, and M. R. Cutkosky, “Fingertip force control with embedded fiber Bragg grating sensors,” *2008 IEEE Int. Conf. Robot. Autom.*, pp. 3431–3436, May 2008.

[249] M. Johnsson and C. Balkenius, “Recognizing texture and hardness by touch,” *2008 IEEE/RSJ Int. Conf. Intell. Robot. Syst.*, pp. 482–487, Sep. 2008.

[250] D. S. Chathuranga, Z. Wang, V. A. Ho, A. Mitani, and S. Hirai, “A biomimetic soft fingertip applicable to haptic feedback systems for texture identification,” in *HAVE 2013 - 2013 IEEE International Symposium on Haptic Audio-Visual Environments and Games, Proceedings*, 2013, pp. 29–33.

[251] K. V. D. S. Chathuranga, V. A. Ho, and S. Hirai, “A bio-mimetic fingertip that detects force and vibration modalities and its application to surface identification,” *2012 IEEE Int. Conf. Robot. Biomimetics, ROBIO 2012 - Conf. Dig.*, pp. 575–581, 2012.

[252] D. S. Chathuranga, V. A. Ho, and S. Hirai, “Investigation of a biomimetic fingertip’s ability to discriminate fabrics based on surface textures,” *2013 IEEE/ASME Int. Conf. Adv. Intell. Mechatronics Mechatronics Hum. Wellbeing, AIM 2013*, pp. 1667–1674, 2013.

[253] Loomis J. M. and Lederman S., “CHAPTER 31: TACTUAL PERCEPTION,” in *Handbook of Perception and Human Performance, Vol. 2: Cognitive Processes and Performance*, J. P. Thomas, L. Kaufman, and K. R. Boff, Eds. New York, NY: John Wiley & Sons, 1986.

[254] S. Kuroki, H. Kajimoto, H. Nii, N. Kawakami, and S. Tachi, “Proposal of the stretch detection hypothesis of the meissner corpuscle,” *Lect. Notes Comput. Sci. (including Subser. Lect. Notes Artif. Intell. Lect. Notes Bioinformatics)*, vol. 5024 LNCS, pp. 245–254, 2008.

[255] V. Falanga and B. Bucalo, “Use of a durometer to assess skin hardness,” *J. Am. Acad. Dermatol.*, vol. 29, no. 1, pp. 47–51, Jul. 1993.

[256] L. P. Jentoft and R. D. Howe, “Determining object geometry with compliance and simple sensors,” in *2011 IEEE/RSJ International Conference on Intelligent Robots and Systems*, 2011, pp. 3468–3473.

[257] ST-Microelectronics, “LSM9DS0: iNEMO inertial module: 3D accelerometer, 3D gyroscope, 3D magnetometer,” 2013. [Online]. Available: http://www.st.com/st-web-ui/static/active/en/resource/technical/document/datasheet/DM00087365.pdf%5Cnhttp://www.st.com/web/catalog/sense_power/FM89/SC1448/PF258556.

[258] Freescale Semiconductor, “MPL115A2, Miniature I2C Digital Barometer,” pp. 1–17, 2006.

[259] M. Konyo, S. Tadokoro, A. Yoshida, and N. Saiwaki, “A tactile synthesis method using multiple frequency vibrations for representing virtual touch,” in *2005 IEEE/RSJ International Conference on Intelligent Robots and Systems*, 2005, pp. 3965–3971.

[260] J. W. Cooley and J. W. Tukey, “An algorithm for the machine calculation of complex Fourier series,” *Math. Comput.*, vol. 19, no. 90, pp. 297–297, May 1965.

[261] S. G. Mallat, “A Theory for Multiresolution Signal Decomposition: The Wavelet Representation,” *IEEE Trans. Pattern Anal. Mach. Intell.*, vol. 11, no. 7, pp. 674–693, 1989.

[262] R. Bro and A. K. Smilde, “Principal component analysis,” *Anal. Methods*, vol. 6, p. 2812, 2014.

[263] M. F. Møller, “A scaled conjugate gradient algorithm for fast supervised learning,” *Neural Networks*, vol. 6, pp. 525–533, 1993.

[264] S. Youssefian, N. Rahbar, and E. Torres-Jara, “Contact Behavior of Soft Spherical Tactile Sensors,” *IEEE Sens. J.*, vol. 14, no. 5, pp. 1435–1442, May 2014.

[265] L. Jamone, L. Natale, G. Metta, and G. Sandini, “Highly Sensitive Soft Tactile Sensors for an Anthropomorphic Robotic Hand,” *IEEE Sens. J.*, vol. 15, no. 8, pp. 4226–4233, 2015.

[266] T. P. Tomo *et al.*, “Design and characterization of a three-axis hall effect-based soft skin sensor,” *Sensors (Switzerland)*, vol. 16, no. 4, 2016.

[267] M. Zillich and W. Feiten, “A versatile tactile sensor system for covering large and curved surface areas,” *IEEE Int. Conf. Intell. Robot. Syst.*, pp. 20–24, 2012.

[268] T. Bhattacharjee, J. M. Rehg, and C. C. Kemp, “Haptic classification and recognition of objects using a tactile sensing forearm,” *2012 IEEE/RSJ Int. Conf. Intell. Robot. Syst.*, pp. 4090–4097, Oct. 2012.

[269] Y. L. Park, K. Chau, R. J. Black, and M. R. Cutkosky, “Force sensing robot fingers using embedded fiber Bragg grating sensors and shape deposition manufacturing,” in *Proceedings - IEEE International Conference on Robotics and Automation*, 2007, vol. 24, no. 7, pp. 1510–1516.

[270] J. R. Phillips, R. S. Johansson, and K. O. Johnson, “Representation of braille characters in human nerve fibres,” *Exp. Brain Res.*, vol. 81, no. 3, pp. 589–592, 1990.

[271] R. J. Wood, “Design and Fabrication of Soft Artificial Skin Using Embedded Microchannels and Liquid Conductors,” *IEEE Sens. J.*, vol. 12, no. 8, pp. 2711–2718, Aug. 2012.

[272] S. Stassi, V. Cauda, G. Canavese, and C. F. Pirri, “Flexible tactile sensing based on piezoresistive composites: A review,” *Sensors (Switzerland)*, vol. 14, no. 3, pp. 5296–5332, Mar. 2014.

[273] A. M. Shkel, “Type I and Type II Micromachined Vibratory Gyroscopes,” in *2006 IEEE/ION Position, Location, And Navigation Symposium*, 2006, vol. 2006, pp. 586–593.

[274] Y. Michalevsky, D. Boneh, and G. Nakibly, “Gyrophone: Recognizing Speech from Gyroscope Signals,” *23rd USENIX Secur. Symp. (USENIX Secur. 14)*, pp. 1053–1067, 2014.

[275] G. LANGFELDER and A. TOCCHIO, *MEMS integrating motion and displacement sensors*. Woodhead Publishing Limited, 2014.

[276] L. Jentoft and R. Howe, “Compliant fingers make simple sensors smart,” *Proc. 2010 IFToMM/ASME Work. …*, pp. 3–10, 2010.

[277] J. M. Cooke, M. J. Zyda, D. R. Pratt, and R. B. Mcghee, “Npsnet: Flight Simulation Dynamic Modeling Using Quaternions,” *Presence*, vol. 1, no. 4, pp. 404–420, 1994.

[278] S. O. H. Madgwick, A. J. L. Harrison, and R. Vaidyanathan, “Estimation of IMU and MARG orientation using a gradient descent algorithm,” *IEEE Int. Conf. Rehabil. Robot.*, 2011.

[279] R. G. Valenti, I. Dryanovski, and J. Xiao, “Keeping a Good Attitude: A Quaternion-Based Orientation Filter for IMUs and MARGs.,” *Sensors (Basel).*, vol. 15, no. 8, pp. 19302–30, Jan. 2015.

[280] F. Camps, S. Harasse, and A. Monin, “Numerical calibration for 3-axis accelerometers and magnetometers,” in *2009 IEEE International Conference on Electro/Information Technology*, 2009, pp. 217–221.

[281] J. Blanco, “A tutorial on se (3) transformation parameterizations and on-manifold optimization,” *Univ. Malaga, Tech. Rep*, no. 3, 2014.

[282] G. E. Farin and D. Hansford, *The Essentials of CAGD*, 1st ed. Natick, MA, USA: A. K. Peters, Ltd., 2000.

[283] V. Prado da Fonseca, T. E. A. de Oliveira, K. Eyre, and E. M. Petriu, “Stable grasping and object reorientation with a three-fingered robotic hand,” in *2017 IEEE International Symposium on Robotics and Intelligent Sensors (IRIS)*, 2017, pp. 311–317.